Stony Brook University

Constraining Climate Model projections of Change in Clouds and their Radiative Feedback

A Dissertation Presented

by

Parama Mukherjee

to

The Graduate School

In Partial Fulfillment of the

Requirements

for the Degree of

Doctor of Philosophy

in

Marine and Atmospheric Sciences

Stony Brook University

December 2015

Stony Brook University

The Graduate School

Parama Mukherjee

We, the dissertation committee for the above candidate for the
Doctor of Philosophy degree, hereby recommend
acceptance of this dissertation.

Minghua Zhang – Dissertation Advisor
Professor, Marine and Atmospheric Science

Sultan Hameed - Chairperson of Defense
Professor, Marine and Atmospheric Science

Marat Khairoutdinov
Associate Professor, Marine and Atmospheric Science

Wuyin Lin
Associate Scientist, Brookhaven National Laboratory

Shaocheng Xie
Research Scientist, Lawrence Livermore National Laboratory

This dissertation is accepted by the Graduate School

Charles Taber

Dean of the Graduate School

Abstract of the Dissertation

Constraining Climate Model projections of Change in Clouds and their Radiative Feedback

by

Parama Mukherjee

Doctor of Philosophy

in

Marine and Atmospheric Sciences

Stony Brook University

2015

Climate Change is among the most important problems challenging today's scientific community with far reaching impact for the world at large. Numerous efforts have been directed towards designing state of the art climate models which can simulate a realistic projection of the future climate and provide a true picture of the changing environment in the coming years. Despite decades of effort on the part of the climate modeling community, models still differ greatly in their prognosis of future climate change. However, they are all in agreement that clouds and their radiative feedback are the key players responsible for the divergence in model projections. Therefore, constraining the climate changes in clouds and their radiative forcing in the models could in effect constrain the wide range of climate sensitivity exhibited by them.

The present dissertation investigates the possibility of constraining the future cloud changes simulated by the models by using short term climate phenomenon. It was found that in the mid-latitudinal belt, seasonal changes in cloud properties, from cold to warm season, correlated well with their long term changes due to climate warming. Observational estimates of seasonal changes from satellite data were used to assess current model performance and detect possible biases that could translate into their climate projections.

In the tropical belt, a different approach was formulated whereby the mean surface temperature in the tropics was used to classify warm and cold years and then the difference in cloud properties between them was computed to represent transition from cold to warm climate. Such a temporal shift in temperature resulted in cloud evolution that correlated reasonably well with their long term climate change counterparts.

In the last part of this dissertation, model spread in cloud radiative forcing and possibilities of constraining it with observational data have been analyzed.

Table of Contents

Abstract……..……iii

Table of Contents……v

List of Figures…….……...…….vi

List of Tables…….……..……..…xvi

List of Abbreviations…….……..…xvii

Acknowledgement ……..…….....xix

1. Introduction and Motivation 1
   1.1. Objectives 4
2. Data and Model Description 6
   2.1. CMIP5 6
   2.2. C3M 8
   2.3. ECMWF 9
   2.4. ISCCP 10
   2.5. Obs4MIPs 10
3. Seasonal Change in Mid-Latitudinal Cloud Fraction and its covariance with Climate Change 12
   3.1. Data and Models 12
   3.2. Mean Cloud Fraction 14
   3.3. Seasonal variability of Clouds 15
   3.4. Climatological change in Clouds 16
   3.5. Co-variability of Seasonal and Climatological Cloud changes 17
   3.6. Summary 23

4. Co-variability of Seasonal and Climatological Change in Mid-Latitudinal Cloud Hydrometeors 40
4.1. Data and Models 40
4.2. Mean and Seasonal difference profiles of Cloud Hydrometeors 41
4.3. Climatological changes in Cloud Hydrometeors 43
4.4. Co-variability in Cloud Hydrometeors 44
4.4.1. Cloud ICE 45
4.4.2. Cloud Liquid 49
4.4.3.Total Cloud Hydrometeors 52
4.5. Co-variability of area and intensity of hydrometeor change 54
4.6. Summary 54
5. Inter-Annual Variability in Tropical clouds and their relation with Climate Change 76
5.1. Data and Models 76
5.2. Inter-annual variability of clouds and Climate change 77
5.3. Comparison with Observations 80
5.4. Summary 82
6. Constraining Mid-Latitude Cloud Radiative Forcing Change in CMIP5 models 91
6.1. Data and Models 91
6.2. Seasonal and Climatological changes in CRF 92
6.3. Offline radiation model runs with prescribed clouds 95
6.4. Summary 98
7. Conclusions and Future Work 108
7.1. Conclusions 108
7.2. Future work 112
References 118

List of Figures

Figure 3.1: Zonally averaged pressure-latitude section of mean cloud fraction (expressed in %) from July, 2006 – June, 2010 using (a) C3M observation data (b) ensemble mean over RCP8.5 runs of 25 CMIP5 models. 27

Figure 3.2 : Zonally averaged pressure-latitude section of mean cloud fraction (expressed in %) in the following five models : CCSM4, GFDL-CM3, IPSL-CM5A-LR, MIROC5, MRI-CGCM3 from (a)-(e) amip-COSP product (2006-years available) and (f)-(j) RCP8.5 product (2006 – 2009)..... 28

Figure 3.3 : Map of average total column cloud fraction distribution (2006-2009) from (a) CALIPSO-GOCCP observations, (b) C3M observations, (c) Mean over amip-COSP runs (2006-2008) of 5 CMIP5 models (CCSM4, GFDL-CM3, IPSL-CM5A-LR, MIROC5, MRI-CGCM3) and (d) Mean over RCP8.5 runs of the same set of models 29

Figure 3.4 : Zonally averaged pressure-latitude section of seasonal difference (JJA - DJF) between July, 2006 - June, 2010 in cloud fraction (expressed in %) using (a) C3M observations and (b) ensemble model mean over RCP8.5 runs of 25 CMIP5 models. Seasonal differences in SH have been reversed in sign. (c) Zonally averaged pressure-latitude section of climatological difference in cloud fraction from ensemble model mean of 25 CMIP5 models between 2010-19 and 2090-99. 30

Figure 3.5 : Zonally averaged pressure-latitude section of (a) ensemble mean climatological difference in cloud fraction (expressed in %) between 2010-19 and 2090-99 using RCP8.5 runs of 25 CMIP5 models (b) ensemble mean cloud fraction (expressed in %) difference between amip (control) and amip4K (perturbed) runs over 12 models and (c) between amip(control) and amipFuture (perturbed) runs over 11 models between 1990-1999. 31

Figure 3.6 : Scatter plots showing the relationship between Temperature normalized and Mass weighted Seasonal change (y-axis) and Climatological difference (x-axis) in mid-latitudinal cloud fraction (in $kg/m^2/K$) for 25 CMIP5 models (listed with their symbols in the key) in the (a) High-level clouds (440hPa and above), (b) Mid-level clouds (680 hPa -440 hPa) and (c) Low-level clouds (below 680 hPa). Grey solid line is the linear regression fit. Observed values of Seasonal change in cloud fraction are represented by pink horizontal lines. Correlation coefficient values are indicated at the top right corner of each figure. Zero x- and y-axes are included as blue dashed lines..... 32

Figure 3.7 : Scatter plots showing the relationship between mid-latitudinal Mass weighted Temperature normalized Seasonal change in kg/m^2/K (y-axis) and Mass weighted Mean value (x-axis) of cloud fraction in kg/m^2 in the (a) High-level clouds (440hPa and above), (b) Mid-level clouds (680 hPa -440 hPa) and (c) Low-level clouds (below 680 hPa) for 25 CMIP5 models (key in Figure 3.6). Grey solid line is the linear regression fit. Observed values of Mean and Seasonal change in cloud fraction are represented by a pink cross. Correlation coefficient values are indicated at the top right corner of each figure. Zero x- and y-axes are included as blue dashed lines. 33

Figure 3.8 : Zonally averaged pressure-latitude section of mean cloud fraction (expressed in %) for (a) June-July-August and (b) December-January-February months using C3M observation data and (c) JJA and (d) DJF using ensemble mean over RCP8.5 runs of 25 CMIP5 models between 2006-2010..... 34

Figure 3.9 : Scatter plots showing the relationship between mid-latitudinal Temperature normalized Mass weighted Seasonal change (y-axis) in kg/m^2/K and Mass weighted Mean values (x-axis) for JJA months in kg/m^2 of cloud fraction for 25 CMIP5 models (key in Figure 3.6) for (a) Total Column, (b) High Level Clouds, (c) Mid-Level Clouds and (d) Low Level Clouds. Observed values indicated by pink cross. Grey solid lines represent the linear regression fit. Dashed blue lines indicate the zero x- and y-axes while Correlation coefficients are noted at top right corner in each plot..... 35

Figure 3.10 : Scatter plots showing the relationship between mid-latitudinal Temperature normalized Mass weighted Seasonal change (y-axis) in kg/m^2/K and Mass weighted Mean values (x-axis) for DJF months in kg/m^2 of cloud fraction for 25 CMIP5 models (key in Figure 3.6) for (a) Total Column, (b) High Level Clouds, (c) Mid-Level Clouds and (d) Low Level Clouds. Observed values indicated by pink cross. Grey solid lines represent the linear regression fit. Dashed blue lines indicate the zero x- and y-axes while Correlation coefficients are noted at top right corner in each plot..... 36

Figure 3.11 : Scatter plots showing the relationship between mid-latitudinal Mass weighted (a) and (b) Temperature normalized Seasonal change (y-axis) in kg/m^2/K and Mean values (x-axis) in kg/m^2 of cloud fraction for 25 CMIP5 models (key in Figure 3.6) in the layers of Seasonal Cloud reduction and Cloud Increase respectively and (c) and (d) between Mass weighted Temperature normalized Seasonal change (y-axis) and Climatological difference (x-axis) in cloud fraction (kg/m^2/K) in the layers of corresponding Cloud reduction and Cloud Increase respectively. Observed values are indicated by pink cross in (a) and (b) and pink dashed line in (c) and (d). Grey solid

lines represent the linear regression fit. Dashed blue lines indicate the zero x- and y-axes while Correlation coefficients are noted at top right corner in each plot. 37

Figure 3.12 : Scatter plots showing the relationship between NH mid-latitudinal Mass weighted (a) and (b) Temperature normalized Seasonal change (y-axis) in $kg/m^2/K$ and Mean values (x-axis) in kg/m^2 of cloud fraction for 25 CMIP5 models (key in Figure 3.6) in the layers of Seasonal Cloud reduction and Cloud Increase respectively and (c) and (d) between Mass weighted Temperature normalized Seasonal change (y-axis) and Climatological difference (x-axis) in cloud fraction ($kg/m^2/K$) in the layers of corresponding Cloud reduction and Cloud Increase respectively. Observed values are indicated by pink cross in (a) and (b) and pink dashed line in (c) and (d). Grey solid lines represent the linear regression fit. Dashed blue lines indicate the zero x- and y-axes while Correlation coefficients are noted at top right corner in each plot. Spearman's rank correlation coefficient also indicated for (b) in blue. 38

Figure 3.13 : Scatter plots showing the relationship between SH mid-latitudinal Mass weighted (a) and (b) Temperature normalized Seasonal change (y-axis) in $kg/m^2/K$ and Mean values (x-axis) in kg/m^2 of cloud fraction for 25 CMIP5 models (key in Figure 3.6) in the layers of Seasonal Cloud reduction and Cloud Increase respectively and (c) and (d) between Mass weightedTemperature normalized Seasonal change (y-axis) and Climatological difference (x-axis) in cloud fraction ($kg/m^2/K$) in the layers of corresponding Cloud reduction and Cloud Increase respectively. Observed values are indicated by pink cross in (a) and (b) and pink dashed line in (c) and (d). Grey solid lines represent the linear regression fit. Dashed blue lines indicate the zero x- and y-axes while Correlation coefficients are noted at top right corner in each plot. Spearman's rank correlation coefficient also indicated for (b) and (d) in blue. 39

Figure 4.1 : Zonally averaged vertical pressure-latitude section of (a) mean cloud ice, (b) mean cloud liquid and (c) mean cloud hydrometeor (mass fraction percentage in air multiplied by 10^3) from July,2006 to June,2009 using C3M observation dataset. 56

Figure 4.2 : Zonally averaged vertical pressure-latitude section of (a) mean ice cloud fraction and (b) mean liquid cloud fraction from 2006-2010 using CALIPSO-GOCCP dataset. .. 57

Figure 4.3 : Zonally averaged vertical pressure-latitude section of (a) mean cloud ICE, (b) mean cloud LIQ and (c) mean cloud Hydrometeor (mass fraction percentage in air multiplied by 10^3) from July,2006 to June,2009 using ensemble mean over RCP8.5 runs of 25 CMIP5 models. 58

Figure 4.4 : Adapted from Figure 7 from a study by Cesana and Chepfer. The first two columns show the vertical distribution of cloud ice and cloud liquid phase clouds for the months of Jan, Feb and March, in CALIPSO-GOCCP observations(first row), in COSP-Lidar simulator from GCM (second row) and directly from LMDZ GCM (third row)(Cesana and Chepfer, 2013)..... 59

Figure 4.5 : Zonally averaged pressure-latitude section of seasonal difference (JJA - DJF) between July, 2006 - June, 2010 in observed (a) Cloud ICE, (b) Cloud LIQ, and (c) Cloud HYD (mass fraction multiplied by 10^5) and model mean values over RCP8.5 runs of 25 CMIP5 models in (d) Cloud ICE, (e) Cloud LIQ, and (f) Cloud HYD. Seasonal differences in SH have been reversed in sign. 60

Figure 4.6 : Ensemble mean zonally averaged pressure-latitude section of climatological difference (between 2010-19 and 2090-99) in (a) Cloud ICE, (b) Cloud LIQ and (c) Cloud HYD (mass fraction multiplied by 10^5) over RCP8.5 runs of 25 CMIP5 models. 61

Figure 4.7 : Zonally averaged pressure-latitude section of Normalized (a) ensemble mean climatological difference in total cloud Hydrometeors (mass fraction multiplied by 10^5) between 2010-19 and 2090-99 using RCP8.5 runs of 25 CMIP5 models (b) ensemble mean cloud Hydrometeor difference between amip (control) and amip4K (perturbed) runs over 12 models and (c) between amip(control) and amipFuture (perturbed) runs over 11 models between 1990-1999. 62

Figure 4.8 : Scatter plots showing the relationship between Temperature normalized Mass-weighted Seasonal change (y-axis) in kg/m^2/K and Mass-weighted Mean values (x-axis) in kg/m^2 of mid-latitudinal cloud ICE mass fraction (*10^2) for 25 CMIP5 models (key in Figure 3.6) in the (a) Total cloud column, (b) High-level clouds (440hPa and above), (c) Mid-level clouds (680 hPa -440 hPa) and (d) Low-level clouds (below 680 hPa). Grey solid line is the linear regression fit. Observed values of Mean and Seasonal change in cloud ICE are represented by pink crosses. Correlation coefficient values (Black: Pearson; Blue: Spearman) are indicated at the top right corner of each figure. Zero x- and y-axes included as blue dashed lines..... 63

Figure 4.9 : Scatter plots showing the relationship between Mid-latitudinal Temperature normalized Mass-weighted Seasonal change (y-axis) and Climatological difference (x-axis) in kg/m^2/K in cloud ICE mass fraction (multiplied by 100) for 25 CMIP5 models (key in Figure 3.6) in the (a) Total cloud column, (b) High-level clouds (440hPa and above), (c) Mid-level clouds (680 hPa -440 hPa) and (d) Low-level clouds (below 680 hPa). Grey solid line is the linear regression fit. Observed values of Seasonal change in

cloud ICE are represented by pink horizontal lines. Correlation coefficient values are indicated at the top right corner of each figure. Zero x- and y-axes are included as blue dashed lines 64

Figure 4.10 : Scatter plots showing the relationship between Temperature normalized Mass-weighted Seasonal change (y-axis) and Climatological difference (x-axis) in kg/m^2/K in mid-latitudinal cloud ICE mass fraction (multiplied by 100) for 25 CMIP5 models (key in Figure 3.6) in the corresponding layers of (a) Cloud ICE reduction and (b) Cloud ICE Increase respectively, and, between Mass-weighted Mean Cloud ICE mass fraction (x-axis) in kg/m^2 and Seasonal change (y-axis) in the layers of (c) Seasonal Cloud ICE reduction and (b) Seasonal Cloud ICE Increase. Grey solid lines represent the linear regression fit. Dashed blue lines indicate the zero x- and y-axes while Correlation coefficients (Black: Pearson; Blue: Spearman) are noted at top right corner in each plot. Observed CICE indicated by pink dashed line in (a),(b) and pink cross in (c),(d)..... 65

Figure 4.11 : Scatter plots showing the relationship between Temperature normalized Mass-weighted Seasonal change (y-axis) in kg/m^2/K and Mass-weighted Mean values (x-axis) in kg/m^2 of mid-latitudinal cloud LIQ mass fraction (*10^2) for 25 CMIP5 models (key in Figure 3.6) in the (a) Total cloud column, (b) High-level clouds (440hPa and above), (c) Mid-level clouds (680 hPa -440 hPa) and (d) Low-level clouds (below 680 hPa). Grey solid line is the linear regression fit. Observed values of Mean and Seasonal change in cloud LIQ are represented by pink crosses. Correlation coefficient values (Black: Pearson; Blue: Spearman) are indicated at the top right corner of each figure. Zero x- and y-axes included as blue dashed lines. 66

Figure 4.12 : Scatter plots showing the relationship between Mid-latitudinal Temperature normalized Mass-weighted Seasonal change (y-axis) and Climatological difference (x-axis) in kg/m^2/K in cloud LIQ mass fraction (multiplied by 100) for 25 CMIP5 models (key in Figure 3.6) in the (a) Total cloud column, (b) High-level clouds (440hPa and above), (c) Mid-level clouds (680 hPa -440 hPa) and (d) Low-level clouds (below 680 hPa). Grey solid line is the linear regression fit. Observed values of Seasonal change in cloud LIQ are represented by pink horizontal lines. Correlation coefficient values are indicated at the top right corner of each figure (Black: Pearson; Blue: Spearman). Zero x- and y-axes are included as blue dashed lines. 67

Figure 4.13 : Scatter plots showing the relationship between Temperature normalized Mass-weighted Seasonal change (y-axis) and Climatological difference (x-axis) in kg/m^2/K in mid-latitudinal cloud LIQ mass fraction (multiplied by 100) for 25 CMIP5 models

(key in Figure 3.6) in the corresponding layers of (a) Cloud LIQ reduction and (b) Cloud LIQ Increase respectively, and, between Mass-weighted Mean Cloud LIQ mass fraction (x-axis) in kg/m^2 and Seasonal change (y-axis) in the layers of (c) Seasonal Cloud LIQ reduction and (b) Seasonal Cloud LIQ Increase. Grey solid lines represent the linear regression fit. Dashed blue lines indicate the zero x- and y-axes while Correlation coefficients (Black: Pearson; Blue: Spearman) are noted at top right corner in each plot. Observed CLIQ indicated by pink dashed line in (a),(b) and pink cross in (c),(d). 68

Figure 4.14 : Scatter plots showing the relationship between Temperature normalized Mass-weighted Seasonal change (y-axis) and Climatological difference (x-axis) in kg/m^2/K in mid-latitudinal cloud LIQ mass fraction (multiplied by 100) in the corresponding (a) layers of Cloud LIQ reduction and (b) modified Cloud LIQ reduction with small layer of increase at the bottom. Grey solid lines represent the linear regression fit. Dashed blue lines indicate the zero x- and y-axes. Observed CLIQ indicated by pink dashed line while Correlation coefficients (Black: Pearson; Blue: Spearman) are noted at top right corner in each plot. 69

Figure 4.15 : Scatter plots showing the relationship between Temperature normalized Mass-weighted Seasonal change (y-axis) in kg/m^2/K and Mass-weighted Mean values (x-axis) in kg/m^2 of mid-latitudinal cloud HYD mass fraction (*10^2) for 25 CMIP5 models (key in Figure 3.6) in the (a) Total cloud column, (b) High-level clouds (440hPa and above), (c) Mid-level clouds (680 hPa -440 hPa) and (d) Low-level clouds (below 680 hPa). Grey solid line is the linear regression fit. Observed values of Mean and Seasonal change in cloud HYD are represented by pink crosses. Correlation coefficient values are indicated at the top right corner of each figure. Zero x- and y-axes included as blue dashed lines. 70

Figure 4.16 : Scatter plots showing the relationship between Mid-latitudinal Temperature normalized Mass-weighted Seasonal change (y-axis) and Climatological difference (x-axis) in kg/m^2/K in cloud HYD mass fraction (multiplied by 100) for 25 CMIP5 models (key in Figure 3.6) in the (a) Total cloud column, (b) High-level clouds (440hPa and above), (c) Mid-level clouds (680 hPa -440 hPa) and (d) Low-level clouds (below 680 hPa). Grey solid line is the linear regression fit. Observed values of Seasonal change in cloud HYD are represented by pink horizontal lines. Correlation coefficient values are indicated at the top right corner of each figure (Black: Pearson; Blue: Spearman). Zero x- and y-axes are included as blue dashed lines 71

Figure 4.17 : Scatter plots showing the relationship between Temperature normalized Mass-weighted Seasonal change (y-axis) and Climatological difference (x-axis) in kg/m^2/K in mid-latitudinal cloud HYD mass fraction (multiplied by 100) for 25 CMIP5 models (key in Figure 3.6) in the corresponding layers of (a) Cloud HYD reduction and (b) Cloud HYD Increase respectively, and, between Mass-weighted Mean Cloud HYD mass fraction (x-axis) in kg/m^2 and Seasonal change (y-axis) in the layers of (c) Seasonal Cloud HYD reduction and (b) Seasonal Cloud HYD Increase. Grey solid lines represent the linear regression fit. Dashed blue lines indicate the zero x- and y-axes while Correlation coefficients are noted at top right corner in each plot. Observed CHYD indicated by pink dashed line in (a),(b) and pink cross in (c),(d)..... 72

Figure 4.18 : Scatter plots showing the relationship in mid-latitudinal belt between fraction of total number of pressure–latitude grid boxes (expressed in %) with Cloud ICE (a) increase and (b) reduction seasonally (y-axis) and climatologically (x-axis), and average cloud ICE mass fraction (c) increase and (d) reduction in each grid box seasonally (y-axis) and climatologically (x-axis) using 25 CMIP5 models. Solid gray line represents linear regression fit to the data and dashed blue lines indicate the position of zero x-and y-axes. Observation indicated by pink dashed line. Correlation coefficients (Black: Pearson; Blue: Spearman) are noted at top right corner in each plot. Changes in average mass fraction of cloud ICE have been multiplied by 100..... 73

Figure 4.19 : Scatter plots showing the relationship in mid-latitudinal belt between fraction of total number of pressure–latitude grid boxes (expressed in %) with Cloud LIQ (a) increase and (b) reduction seasonally (y-axis) and climatologically (x-axis), and average cloud LIQ mass fraction (c) increase and (d) reduction in each grid box seasonally (y-axis) and climatologically (x-axis) using 25 CMIP5 models. Solid gray line represents linear regression fit to the data and dashed blue lines indicate the position of zero x-and y-axes. Observation indicated by pink dashed line. Correlation coefficients (Black: Pearson; Blue: Spearman) are noted at top right corner in each plot. Changes in average mass fraction of cloud LIQ have been multiplied by 100..... 74

Figure 4.20 : Scatter plots showing the relationship in mid-latitudinal belt between fraction of total number of pressure–latitude grid boxes (expressed in %) with Cloud HYD (a) increase and (b) reduction seasonally (y-axis) and climatologically (x-axis), and average cloud HYD mass fraction (c) increase and (d) reduction in each grid box seasonally (y-axis) and climatologically (x-axis) using 25 CMIP5 models. Solid gray line represents linear regression fit to the data and dashed blue lines indicate the position of zero x-and y-axes. Observation indicated by pink dashed line. Correlation coefficients (Black:

Pearson; Blue: Spearman) are noted at top right corner in each plot. Changes in average mass fraction of cloud HYD have been multiplied by 100..... 75

Figure 5.1 Ensemble mean zonally averaged pressure-latitude sections of (a) Inter-Annual difference in Cloud Fraction (%) and (b) Climatological difference in Cloud Fraction (%) in the tropical belt between 30˚S to 30˚N latitudes..... 83

Figure 5.2 : Ensemble mean zonally averaged pressure-latitude sections of (a) Inter-annual difference and (b) Climatological difference in Cloud ice content (mass fraction in air multiplied by 100) and (c) Inter-annual and (d) Climatological difference in Cloud water content (mass fraction in air multiplied by 100) in the tropical belt between 30˚S to 30˚N latitudes..... 84

Figure 5.3 : Ensemble mean zonally averaged pressure-latitude section of (a) Inter-annual difference and (b) Climatological difference in Cloud Hydrometeor content (mass fraction in air multiplied by 100) in the tropical belt between 30˚S to 30˚N latitudes. 85

Figure 5.4 : Correlation contours representing the correlation coefficient between the values of Inter-annual difference and Climatological difference at each pressure-latitude grid point in (a) Cloud Fraction and (b) Cloud Hydrometeors for 25 CMIP5 models. Hatched lines indicate regions of significant correlation (5% level)..... 86

Figure 5.5 : Scatter plots showing the relationship between Inter-annual Change (x-axis) and Climatological difference (y-axis) in cloud fraction for 25 CMIP5 models (listed with their symbols later in Figure 5-7) summed over (a) Zone-1 (above 400hPa), (b) Zone-2 (between 850-600hPa) and (c) Zone-3 (below 925 hPa). Grey solid line is the linear regression fit. Zero x- and y-axes are included as blue dashed lines..... 87

Figure 5.6 : (a) Correlation map constructed from correlation coefficients between model spread in Total Cloud Inter-annual and Climatological changes. Hatched lines indicate regions of significant correlation (5% level). Mean climatology of (b) Low and (c) High level clouds from C3M observations (2006-2010) in the tropical belt. Rectangular boxes indicate the location of Region-1, 2 and 3 discussed in the text and are marked here as ① ② ③ 88

Figure 5.7 : Scatter plots showing the relationship between Inter-annual (x-axis) and Climatological difference (y-axis) in total cloud fraction for 25 CMIP5 models in (a) Region-1 (3˚S – 1.5˚N; 102˚E – 112˚E), (b) Region-2 (0.5˚N – 10˚N; 240˚E – 280˚E)

and (c) Region-3 (30˚S – 15.5˚S; 278˚E – 290˚E) Grey solid line is the linear regression fit. Observed values of Inter-annual total cloud change from ISCCP represented by pink horizontal lines. Correlation coefficient values indicated at the top left corner of each figure. 89

Figure 5.8 : Ensemble mean zonally averaged pressure-latitude section of Inter-Annual difference in Cloud Fraction (%) between years before and after Mt. Pinatubo eruption in 1991. 90

Figure 6.1 : Seasonal variation (JJA-DJF) of (a) SWCRF, (b) NetCRF, and (c) LWCRF from Obs4MIPS observations and (d) SWCRF, (e) NetCRF and (f) LWCRF from ensemble model mean over 16 CMIP5 models. 100

Figure 6.2 : Correlation maps constructed using the values of correlation coefficient, at each Lat-Lon grid point, between CMIP5 model spread in Seasonal (JJA-DJF) and Climatological Differences in (a) SWCRF, (b) LWCRF and (c) NetCRF). Hatched lines indicate regions of significant Correlation. 101

Figure 6.3 : Scatter plots showing the relationship between Seasonal change (x-axis) and Climatological difference (y-axis) in mid-latitudinal (a) SWCRF, (b) LWCRF and (c) NetCRF in 16 CMIP5 models (listed in the key). Grey solid line is the linear regression fit. Observed values of Seasonal changes in CRF are represented by cyan vertical lines. Correlation coefficient values (Black: Pearson; Blue: Spearman) are indicated at the top right corner of each figure. Zero x- and y-axes are included as blue dashed lines. 102

Figure 6.4 : (a) Summary of the correlations between CMIP5 output and prescribed CESM model run output Seasonal and Climatological differences in SWCRF, LWCRF and NetCRF. Taylor diagram (Taylor, 2000) exhibiting (a) CMIP5 and (b) prescribed CESM-run model spread in climatological projection of change in NetCRF with the ensemble mean values as Reference. 103

Figure 6.5 : Scatter plots showing the relationship between Seasonal change (x-axis) and Climatological difference (y-axis) in mid-latitudinal (a) SWCRF, (b) LWCRF and (c) NetCRF due to total column clouds in 16 CMIP5 models (key in Figure 6.3) from the prescribed CESM runs. Grey solid line is the linear regression fit. Observed values of Seasonal changes in CRF are represented by cyan vertical lines. Correlation coefficient values (Black: Pearson; Blue: Spearman) are noted at the top right corner of each figure. Zero x- and y-axes are included as blue dashed lines. 104

Figure 6.6 : Scatter plots showing the relationship between Seasonal change (x-axis) and Climatological difference (y-axis) in mid-latitudinal SWCRF due to clouds at (a) High- , (b) Mid- and (c) Low-levels in 16 CMIP5 models (key in Figure 6.3) from the prescribed CESM runs. Grey solid line is the linear regression fit. Correlation coefficient values are noted at the top right corner of each figure. Zero x- and y-axes are included as blue dashed lines. 105

Figure 6.7 : Scatter plots showing the relationship between Seasonal change (x-axis) and Climatological difference (y-axis) in mid-latitudinal LWCRF due to clouds at (a) High- , (b) Mid- and (c) Low-levels in 16 CMIP5 models (key in Figure 6.3) from the prescribed CESM runs. Grey solid line is the linear regression fit. Correlation coefficient values are noted at the top right corner of each figure. Zero x- and y-axes are included as blue dashed lines. 106

Figure 6.8 : Scatter plots showing the relationship between Seasonal change (x-axis) and Climatological difference (y-axis) in mid-latitudinal NetCRF due to clouds at (a) High- , (b) Mid- and (c) Low-levels in 16 CMIP5 models (key in Figure 6.3) from the prescribed CESM runs. Grey solid line is the linear regression fit. Correlation coefficient values are noted at the top right corner of each figure. Zero x- and y-axes are included as blue dashed lines. 107

Figure 7.1 : Distribution of high Cloud fraction as a function of surface tempertaure (y-axis) and vertical velocity in the 850-500 hPa pressure level (x-axis) in the (a) ensemble model mean of CMIP5 models and (b) C3M observations. 115

Figure 7.2 : Correlation map showing the contribution of model spread at each lat-lon grid point to the total model spread in NetCRF between 60^{o}N - 60^{o}S latitudes..... 116

Figure 7.3 : Correlation map showing the contribution of model spread at each lat-lon grid point to the total model spread in NetCRF between 60^{o}N - 60^{o}S latitudes..... 117

List of Tables

Table 1: List of CMIP5 models and their modeling centers used in Chapter 3, 4 and 5. 24

Table 2: List of CMIP5 models whose amip, amip4K and amipfuture runs were analyzed. 26

Table 3: List of CMIP5 models used for CRF analysis 99

List of Abbreviations

amip	Atmospheric Model Intercomparison Project
AOGCMs	Atmosphere-Ocean General Circulation Model
C3M	CALIPSO-CloudSat-CERES-MODIS Product
CALIPSO	Cloud-Aerosol Lidar and Infrared Pathfinder Satellite Observations.
CERES-EBAF	Clouds and the Earth's Radiant Energy System – Energy balanced and Filled
CFMIP-2	Cloud Feedback Model Intercomparison Project
CLTOT	Total Cloud Product from CMIP5 models
CMIP5	Coupled Model Intercomparison Project-5
ESGF	Earth System Grid Federation
COSP	CFMIP Observation Simulator Package
CRF	Cloud Radiative Forcing
DJF	December January February (months)
DOE	Department of Energy
ECMWF	European Centre for Medium-range Weather Forecasts
ECS	Equilibrium Climate Sensitivity
EOF	Empirical Orthogonal Function
ESA	European Space Agency
ESM	Earth System Models
GCM	General Circulation Models
GMS	Geostationary Meteorological Satellite
GOCCP	GCM Oriented CALIPSO Cloud Product

GOES-EAST/WEST	Geostationary Operational Environmental Satellite-EAST/ WEST
IFS	Integrated Forecasting System
IPCC-AR4	Intergovernmental Panel on Climate Change Fourth Assessment Report
ISCCP	International Satellite Cloud Climatology Project
ITCZ	Inter Tropical Convergence Zone
JJA	June July August (months)
LMDZ5	Laboratoire de Météorologie Dynamique Zoom 5
LWCRF	Long Wave Cloud Radiative Forcing
METEOSAT	Geostationary Meteorological Satellite operated by EUMESTAT (European Organization for the exploitation of meteorological satellites)
MODIS	Moderate Resolution Imaging Spectroradiometer
NASA	National Aeronautics and Space Administration
NH	Northern Hemisphere
Obs4MIPS	Observations for Climate Model Intercomparison Project
PCMDI	Program for Climate Model Diagnosis and Intercomparison
RCP8.5	Representative Concentration Pathways 8.5
SH	Southern Hemisphere
SST	Sea Surface Temperature
SWCRF	Short Wave Cloud Radiative Forcing
TIROS	Television Infrared Observation Satellites
TOA	Top of the Atmosphere
WCRP	World Climate Research Programme
WGCM	Working Group on Coupled Modelling

Acknowledgements

Firstly, I would like to convey my special gratitude to Prof. Minghua Zhang for his supportive and motivating guidance throughout this research. I would also like to extend my sincere thanks to Dr. Wuyin Lin for his constant suggestions and help at all stages of my work. I am grateful to Prof. Sultan Hameed and Prof. Marat Khairoutdinov for agreeing to be a part of my dissertation committee and providing their valuable advice and comments. Sincere thanks go out to Dr. Shaocheng Xie for considering my request to be the external member of my examination committee.

I am also grateful to Prof. Ping Liu for his constant support in resolving technical and computing issues. I also want to thank all my classmates and groupmates at SOMAS for the many discussions, both academic and non-academic, and for being with me through all the good and rough times in these past few years. Special thanks to Carol Dovi, Gina Gartin and Christina Fink for ensuring that I never had to worry about any paperwork or graduate school deadlines.

I would also like to acknowledge here, the contribution made by all my teachers, throughout my school, college and university, towards my education. Whatever I am today is the sum total of all the knowledge that each of them imparted to me.

The rock solid support system provided by my family cannot be thanked for by using mere words. About them I would just like to say that whatever shortcomings I had, whichever talent I lacked they made up for all that and more and I can honestly say that their efforts towards the completion of this thesis is equal to my own. I dedicate this thesis to them - my dear husband and my parents.

Chapter 1

Introduction and Motivation

Understanding climate change is one of the biggest challenges experienced by the scientific community today (Le Treut et al., 2007). Ever since its inception, numerous researchers have directed their efforts to study and predict its impact on the society. Equilibrium Climate Sensitivity (ECS) is one of the most accepted indices to measure the climate system and models to study climate change. It is defined as the change in global mean surface air temperature in response to a doubling of atmospheric CO_2 from its pre-industrial concentration. However, three dimensional General Circulation Models (GCMs), which are the best means to get a comprehensive picture of the climate change scenario (Cess et al., 1990), have continued to predict a wide range of ECS values. The most recent results from CMIP5 experiments indicate a range of ECS from 2.1-4.7 K (Andrews et al., 2012) which is still not significantly different from the studies using previous generations of models (Webb et al., 2006; Dufresne and Bony, 2008; Randall et al., 2007; Volodin, 2008). In order to achieve a reasonable estimation of the future climate, it is of essence that different GCM's concur in their long term predictions.

It is already a well-established fact that clouds and their radiative feedback are primarily responsible for the spread in model sensitivity ((Soden and Held, 2006; Randall et al., 2007; Bony et al., 2006; CESS et al., 1989). In particular, the subtropical shortwave cloud feedback is assumed to contribute mostly to model discrepancies (Bony and Dufresne, 2005; Zelinka et al., 2011). Alongside the prevalent idea that physics parameterizations in climate models are primarily

responsible for deciding the model response to perturbations there has been another chain of thought that supports the view that the large scale circulation pattern has a greater bearing on cloud amount, their radiative responses and consequently on the projected climate sensitivity (Tomassini et al., 2014; Stevens and Bony, 2013; Sherwood et al., 2014; Su et al., 2014). Some of these studies have even found robust relationships between model predicted ECS and some parameter representative of the large scale state of base climate, like rate of Hadley overturning circulation (Su et al., 2014) or globally averaged surface temperature (Tomassini et al., 2014).

An ideal solution to this problem could be obtained if the cloud feedback in models is constrained is some way by using observational data. This would thus make it possible to constrain the climate change predictions of GCMs, resulting in a narrower spread of ECS values among models. However, observations are currently available only for short periods of time, excluding the possibility of their use in estimating any long term climate change. If on the other hand, a significant relationship can be established between changes in cloud properties in the base climate with long term cloud changes due to anthropogenic warming, short term observations could still be used to restrict model cloud behavior. Once the cloud feedback is confined to a small allowed range, their ECS values would likely converge ((Dessler, 2010; Fasullo and Trenberth, 2012; Shell, 2012).

This concept of emergent constraints, which relates an observable current climate variable directly to climate sensitivity or some related physical quantity using an ensemble of models (Flato et al., 2013; Caldwell et al., 2014), has evolved through several recent works. In the tropics, strong correlation between inter-annual variability of extreme tropical precipitation and its long-term climate counterpart has been observed (O'Gorman, 2012). A robust linear relationship between changes in long term tropical land carbon storage with warming and inter-annual variability of atmospheric CO_2 with temperature has also been introduced (Cox et al., 2013; Wenzel et al., 2014). Radiation pattern indices designed so as to correlate well with ECS have been utilized to rule out the possibility of ECS values lower than 2K (Huber et al., 2010). Earlier (Hall and Qu, 2006), present day seasonal cycle of snow albedo feedback had been used to constrain climate change in northern hemisphere land masses. Other examples include correlation between projected Arctic sea ice cover in September and magnitudes of past sea-ice trend (Boe et al., 2009); polar surface temperature change projection and mean temperature state in present climate (Bracegirdle and

Stephenson, 2012); cloud amount contrast between the tropics and mid-latitudes and ECS (Volodin, 2008) and amplitude of seasonal cycle of surface temperature in high latitudes with ECS (Knutti et al., 2006).

More recently, (Bracegirdle et al., 2015) focused on the Antarctic region and found a reflection of the biases in CMIP5 model simulated historical sea ice onto its projections of net precipitation, temperature and sea ice area. A slightly different approach of constraining model performance on the basis of their skills in simulating paleo climate has also been investigated (Schmidt et al., 2013). Another recent study (Tsushima et al., 2015) attempted to find correlations between cloud properties and their radiative responses in the control climate and a warmer future climate scenario in specific cloud regimes. They investigated liquid water path in clouds as an emergent constraint on cloud feedback in stratocumulus cloud regions. Seasonal variations in marine boundary layer cloud (MBLC) fraction was shown to have strong relationship with ECS by (Zhai et al., 2015). Using these relationships, this study was able to constrain ECS values to 3.9K with a standard deviation of 0.45K. Linking two of the most challenging problems in climate science, (Tian, 2015) were able to demonstrate the presence of an inverse relationship between double ITCZ bias and model projections of ECS. Models with low ITCZ bias were found to exhibit higher climate sensitivity thereby concluding that in general models under predict ECS values. A review of several proposed emergent constraints specifically relating to cloud feedback has been compiled by (Klein and Hall, 2015).

These studies strengthen the concept of emergent constraint as a useful tool for climate change studies. On the other hand, they also document the various challenges of formulating such a constraint including the need for an in-depth physical understanding of the strong correlations seen in these studies, limitations of available observations suitable for constraining model performance and complications of using an emergent constraint that has contributions from multiple independent processes.

1.1. Objectives

The primary objective of this dissertation is to investigate the relationship between the long term climatological changes in cloud patterns with cloud changes occurring over short periods of time. Once such a relationship is established, the available cloud observational data is then used to constrain the long term cloud changes into the future. These goals are summed up in the following questions that this thesis seeks to address:

1. Can the cloud changes on seasonal and interannual time scales in climate models be used to infer the changes in clouds and other related variables in their future projections?

2. Is the short term climate phenomenon in question restricted to particular geographical regions (such as the tropics or mid-latitudes) or to specific heights in the atmospheric column?

3. Can observational data available in the time range of the short term climate variability be used to determine model biases in simulating short term climate change that eventually translates onto their long term projections?

In the course of answering these basic questions, it is hoped that the analysis will also identify the possible sources of model bias, e.g.: different cloud levels, different geographical locations, different cloud properties etc. or the primary contributors to the model spread in simulating cloud changes under different climate phenomenon. Attempt would also be made to extend the observed relationship between cloud variables onto the cloud radiative properties which would finally pave the way to formulate such relationships for cloud feedbacks that have a more direct bearing on the model simulated climate sensitivity.

The organization of this dissertation is as follows: Chapter 2 provides brief descriptions of the various models and observation as well as re-analysis datasets used in the study. In Chapter 3, the relationship between seasonal changes in mid-latitudinal cloud fraction and their long term climatological changes are investigated. This study is further extended to include cloud hydrometeors: both cloud ice and cloud liquid content in Chapter 4. Following the investigation on seasonal changes, the relationship between inter-annual changes in cloud fraction and

hydrometeors with their long term climate change counterparts in the tropical belt are analyzed in Chapter 5. Chapter 6 then presents the study of interrelationship between seasonal and climatological changes in cloud radiative forcing. Lastly, Chapter 7 summarizes the conclusions from this study along with a brief description of the possible directions of future work that have emerged from this study.

Chapter 2

Data and Model Description

In this study, monthly mean climate model data from various CMIP5 experiments have been analyzed. For the purpose of evaluating model performance in simulating the present climate against observation data, model output from historical runs, between 1980-2005, and five initial years, 2006-2010, of RCP8.5 scenario runs have been used. Change in clouds and their radiative properties, due to climate warming, have been computed using both RCP8.5 long term projections as well as the differences between amip and amip4K/amipfuture experiments that will be described in the next section. The inter-annual variability in model data has been calculated using CMIP5 historical runs. To assess the efficacy of model output against observations, C3M satellite data product from NASA has been employed for a comparison of cloud amount and cloud hydrometeor vertical profiles at various pressure levels. This data was supplemented with ECMWF reanalysis surface temperature and surface pressure values wherever required. The study also compares inter-annual variability of total, low, mid and high column cloud amount generated by different models with the analogous ISCCP cloud product. Obs4MIPS radiation data was used for assessing CMIP5 model performance in simulating seasonal variability of cloud radiative forcing. A more detailed description of these data products and their applicability for different sections of this study is given in this chapter.

2.1. CMIP5

CMIP or the Coupled Model Intercomparison Project was established by the Working Group on Coupled Modelling (WGCM) as a part of the World Climate Research Programme (WCRP) in 1995. It was conceived to provide a standard set of protocols for climate model

experiments enabling a coordinated study of coupled atmosphere-ocean general circulation models (AOGCMs). The fifth phase of this project, CMIP5 was designed to address several key scientific questions raised during preparation of the Intergovernmental Panel on Climate Change (IPCC) Fourth Assessment Report (AR4) and saw the coming together of 20 different modeling groups from all over the world to work as a community towards improving climate model projections and reducing inter-model variability in simulating feedback processes (Taylor et al. 2011). The Program for Climate Model Diagnosis and Intercomparison (PCMDI) maintains the state-of-the-art multi-model CMIP5 data archive and provides related technical support.

The objectives behind CMIP5 experimental design were threefold: 1) To gain an understanding of the factors that cause differences in model estimations of cloud and carbon cycle feedback, 2) To evaluate the predictability of climate by models in particular at decadal scales, and 3) To discover why models undergoing the same forcing might produce different responses. To address these issues and several others, a set of specific experiments for the AOGCMs and Earth System Models (ESM) were conducted under the following main categories: 1) long term integrations over centuries, 2) near term or decadal integrations, and 3) atmosphere only time slice experiments for high resolution models or models with involved chemistry modules. CMIP5 builds on the previous versions of inter-model comparison with increased sets of historical and paleo simulations and an expanded set of model outputs. It also features four different future scenario runs thus generating a range of future climate simulations.

For various sections of this dissertation, CMIP5 data from the historical runs, amip, amip4K and amipFuture runs as well as RCP8.5 scenario runs were used. Historical runs (1850-2005) are coupled atmosphere-ocean 20^{th} century runs with all forcing. All amip runs (1979-2008) are atmosphere only runs forced with prescribed SST and sea ice values. For amip4K the SST is artificially increased by 4K everywhere and for amipFuture runs a patterned SST perturbation is superposed on the climatological SST values. The CMIP5 guidelines prescribe four different emission scenarios for the future climate referred to as Representative Concentration pathways or RCP's beginning from the year 2006. The nomenclature follows the target radiative forcing to be attained at the end of this century. The 4 RCP's are: RCP2.6, RCP4.5 and RCP6 which are three mitigated scenarios with various levels of mitigation and RCP8.5 which represents high emission scenario resulting in a radiative forcing of 8.5 W/m^2 at the year 2100.

Data from some experiments originally designed by the Cloud Feedback Model Intercomparison Project second phase or CFMIP-2 were also included and made available as a part of CMIP5 (Bony et al 2009). Among the products from this subset the most useful for this study was the CFMIP Observation Simulator Package or COSP runs. These are outputs from simulators that utilize model results to diagnose quantities directly observable from satellites. Both ISCCP and CALIPSO simulator outputs for historical and amip runs were selectively used for validating the findings from model-observation comparisons.

This dataset was obtained directly from the Program for Climate Model Diagnosis and Inter-comparison (PCMDI) Earth System Grid (ESG) data portal [**http://pcmdi9.llnl.gov/esgf-web-fe/**].

2.2. C3M

C3M (CALIPSO-CloudSat-CERES-MODIS) is an integrated data product formed by merging observations from various instruments aboard different satellite missions which are all part of NASA's A-train (Kato et al 2011). This dataset runs from July 2006 to June 2010, over a period of 4 years and provides cloud and aerosol data on a 1.9 x 2.5 grid. It was developed primarily for the purpose of process studies. In combining data from different satellite instruments, C3M also absorbs the strengths of each of them, for example MODIS which provides a wider coverage does not supply information about vertical distribution of clouds. CALIPSO on the other hand is able to furnish those details although over a narrower swath.

Different instruments also have different fields of view, what is known as footprint, so all instrumental data is subjected to an involved two- step collocation process and finally stored in the 20 km CERES grid. In the first step, 3 CALIPSO profiles and one CloudSat profiles are collocated with 1 km MODIS imager pixel using latitude-longitude information. CALIPSO and CloudSat derived cloud masks are independent and can vary from each other. Layer by layer comparison of cloud mask is carried out and identical profiles are grouped. Thereafter these 1km data are again collocated with 20km CERES footprints. Only those CERES footprints having maximum overlap with CALIPSO and CloudSat ground track for each CERES scan are included in the dataset. A 3D

Cloud Field construction algorithm is employed to reconstruct the 3-D cloud field. Mean Ice water and liquid water content are derived from radar algorithm from CloudSat 2B-CWC.

Detailed information about the data product, data quality information etc can be found : **http://ceres.larc.nasa.gov/products.php?product=CCCM**

2.3. ECMWF

ERA-Interim is a global atmospheric and surface parameter re-analysis dataset produced by the European Centre for Medium-range Weather forecasts (ECMWF) (D.P. Dee et al 2011). The ERA-Interim product goes back to January, 1979 and continues to be updated in real time every month. This reanalysis dataset is produced by assimilating observational data from various instruments at ground stations, on board of ships and buoys, attached to airborne balloons and placed in aircrafts and satellites, together with its latest forecast model output from the ECMWF IFS model (release Cy31r2) into the data assimilation system. At the core of the assimilation system is a 12 hourly 4-Dimensional variational analysis module with T255 spectral resolution (79 km) on 60 vertical hybrid levels from surface to 0.1 hPa. 6-hourly ERA interim upper atmospheric data are available on model or pressure levels, or for selected potential temperature and vorticity values. Gridded surface parameter data over both land and ocean are available at every 3-hours. We only used monthly averages of daily mean surface pressure and temperature data to supplement the satellite cloud datasets, from 2006-2010 for C3M and 1983-2009 for ISCCP.

ERA-Interim incorporates many improvements over its predecessor ERA-40, including transition from a 3-D to 4-D Var analysis, advanced forecast model as well as an increase in the number of observations assimilated, chiefly contributed by satellite sources, from 10^6 to nearly 10^7 per day. In all respects this dataset has made great strides in solving most of the science challenges encountered by ERA-40, particularly, related to difficulties in representing the hydrological cycle, improving upon the quality of the stratospheric circulation and maintaining temporal consistency of the reanalyzed fields with introduction of new observation systems.

Information about the current status and updates of ERA-Interim data can be found at **http://www.ecmwf.int/en/research/climate-reanalysis/era-interim**.

2.4. ISCCP

The International Satellite Cloud Climatology Project or ISCCP was launched in the year 1983 for the purpose of collecting satellite radiance data which upon analysis and processing yields information about global cloud distribution and its variation with time. The prime objective of ISCCP was to gather observations for understanding the role of clouds in climate and improve its representation in climate models with particular emphasis on effects of clouds on radiation.

ISCCP satellites sample data every three hours and every 30 km across the globe producing visible and infrared radiance images. Data collected from all operational weather satellites (Tiros-N, METEOSAT, GOES-WEST, GOES-EAST, GMS) are then processed at various international satellite processing centers. This data is finally received by the Global Processing Centre and thereafter processed and archived at NASA's Goddard Institute for Space Studies (GISS).

Among the many ISCCP data products, only the Climatological Summary Product (D2) was used in this study. This monthly averaged gridded cloud product (D2) is available globally on a 280 km equal area grid for the years 1983-2009. The dataset mostly includes properties of total cloudiness and various cloud types obtained by merging all satellite data into a global grid. Atmosphere and surface properties are taken from the TOVS Data set which is the TIROS Operational Vertical Sounding Product.

Announcements, updates and latest news concerning ISCCP data can be found at: **http://isccp.giss.nasa.gov/announcements.html**.

2.5. Obs4MIPs

Observations for Climate Model Intercomparison Project or Obs4MIPS is an endeavor to make observational data available for comparison with climate models (Teixeira et al 2014). Based

on the requirements of the CMIP5 output a limited number of well-established and documented datasets have been organized and made available on the CMIP5-ESGF data portal. Each of the dataset has a field that is output in at least one or more of the CMIP5 experiments. Originally launched due to joint efforts of NASA and DOE with a goal of better exploiting satellite measurements by making them easily accessible for model intercomparisons, it has now been joined by CFMIP-OBS and ESA satellite product set. Currently Obs4MIPS includes several satellite products, reanalysis data sets and in situ products. Obs4MIPs data has been processed so as to be directly comparable with CMIP5 model output fields.

The effectiveness of models in simulating cloud radiative forcing was evaluated in this study using the observed radiative forcing data from Obs4MIPS.

Further information about Obs4MIPS data product and their availability is available at : **https://www.earthsystemcog.org/projects/obs4mips/**

Chapter 3

Seasonal Change in Mid-Latitudinal Cloud Fraction and its Covariance with Climate Change

The change in season from winter to summer months represents a pattern of climate transition from a relatively cooler to a warmer phase. This progression serves as a possible mimic to the long term changes in climate as it evolves onto a warmer state due to global warming. By comparing the transformation of clouds in climate models under both these conditions, it will be examined whether the seasonal change in clouds correlate well with their climate change counterparts in the mid-latitudinal belts. Using satellite observational data, model biases in mean cloud amount and seasonal cloud changes would also be evaluated and subsequently used to constrain their analogous long term cloud projections.

3.1. Data and Models

Long-term change in cloud amount was computed for 25 GCMs participating in the CMIP5 between two decades, 2090-99 (future) and 2010-2019 (present), separated by a period of 90 years. These 25 models are listed in Table 1. Among the four commonly used future greenhouse gas concentration trajectories, the Representative Concentration Pathways 8.5 (RCP8.5) scenario runs were selected as they represent maximum warming. Monthly averaged three-dimensional cloud fraction data from each model was interpolated onto a standard longitude-latitude grid (2.5°x1.25°) in the horizontal and a set of 24 vertical pressure levels common to all the models.

The external forcing in the RCP 8.5 runs include not only the effects of increase in CO2 and other greenhouse gases, but also those of changes in aerosols, stratospheric ozone, and

transformation in land surface. Thus, the projected climate changes in RCP 8.5 may have characteristics different from the runs that include only the effects of changing CO_2. Similar analysis was thus carried out using the differences between 10 years (1990-1999) of amip control and amip4K runs for 12 GCM's (based on data availability) as well as amip control and amipFuture runs for 10 GCMs. Very similar patterns of model behavior were found among these climate change runs. The list of models for computations in this section is shown in Table 2. It was concluded that for the purposes of this study the choice of dataset was not very significant and since the number of models with amip runs were much fewer than those for RCP8.5, the latter dataset was used for analysis.

Seasonal changes in cloud amount were computed between the summer months of JJA (DJF) and winter months of DJF (JJA) for the Northern (Southern) hemisphere from 2006 – 2010. The time range of analysis was dictated by the years of observational data availability. Since most of the amip runs did not cover the entire duration of the observation dataset, monthly mean model cloud data from the RCP8.5 run was also used for seasonal difference computation. Cloud climatology of these 4 years (July, 2006 – June, 2010) was constructed for each of the 25 models used.

Monthly averaged observational cloud fraction data was obtained from the C3M dataset which runs from July, 2006 to June, 2010. Re-analysis surface temperature and surface pressure data from ECMWF-Interim dataset have been employed to supplement the observational data where required.

GCM satellite simulator output from amip-COSP runs for 5 different models (out of 10) have been used for substantiating the findings from comparison of RCP8.5 runs with satellite observations. The comparative study was restricted to the years 2006 – 2008 as most amip-COSP runs continue only till 2008.

3.2. Mean Cloud Fraction

The first objective of this study was to evaluate the performance of CMIP5 models in terms of the simulated cloud amount by comparing with satellite observations. Based on the availability of C3M data, 4-year observational cloud amount climatology was constructed using 3-Dimensional cloud fraction data. The zonally averaged vertical section of this mean cloud amount is shown in Figure 3.1(a). Similar pressure-latitude mean sections were constructed for all the 25 CMIP5 models from their RCP8.5 runs and averaged over to obtain the ensemble mean vertical cross-section as shown in Figure 3.1(b). Comparing the two figures (3-1(a) and (b)), it was found that the model mean clearly underestimated cloud fraction at all altitude levels in the lower latitudes. The vertical cloud column positioned about the equator was almost entirely absent in model ensemble average below 350 hPa. Underestimation was also seen in the mid-latitudinal and sub-polar belts but it remained restricted to mostly lower and mid-level clouds. Since the definition of cloud fraction varies between climate models and satellite data, therefore, to ensure that the bias observed was not a result of the difference in terminologies and was indeed a true feature, cloud fraction from GCM simulator output (amip-COSP simulator) for five models (CCSM4, GFDL-CM3, IPSL-CM5A-LR, MIROC5 and MRI-CGCM3) was used to construct similar pressure latitude cloud sections. In Figure 3.2 the mean vertical cloud section for these five models from the amip-COSP runs and from RCP8.5 runs are shown in the left and right columns respectively. These simulators produce a cloud amount that would actually be seen by a satellite looking down at the climate model simulated atmosphere. It was seen that the cloud amount generated by the simulators was even lower than the actual model output. To corroborate the cloud distribution in C3M dataset, total column cloud fraction from CALIPSO-GOCCP dataset was used to plot a global latitude longitude cloud distribution for the years 2006-2010. This is shown together with the total cloud distribution from C3M in Figure 3.3(a) and (b). CALIPSO-GOCCP, which is also based on data from CALIPSO spacecraft as is C3M, is however processed so as to be directly comparable to model simulator outputs. In Figure 3.3(c) and (d) the map-cross section plots for total clouds in the aforementioned CMIP5 models produced by the amip-COSP and RCP8.5 runs are also shown. This firmly established the presence of a negative bias in model generated mean cloud amount. Previous studies comparing model simulated cloud amount with satellite observations also discovered that the models had a tendency of underestimating low optically thick

clouds (Zhang et al., 2005). The next step was to examine if these model cloud fraction biases in the current climate translated in any way onto their projections of the future. In order to demonstrate this, first there is a need to formulate a relationship between a short term climate phenomenon in the present and the long term climate change. This is attempted in the next sections.

3.3. Seasonal variability of Clouds

If long term climate change of clouds is primarily determined by thermodynamics, seasonal change of clouds from winter to summer months may contain valuable information representative of climate change. To investigate this possibility, change in cloud fraction due to the shift from cold to warm season was computed over a 4-year span (2006-2010), coinciding closely with the years of observational data availability. Cloud fraction change from cold to warm season were represented by averaging over the monthly mean values in June-July-August (JJA) and December-January-February (DJF) and taking their difference. For the southern hemisphere (SH), since the warm and cold seasons are opposite to that in the north (NH), all the seasonal difference values were reversed in sign, implying JJA – DJF for NH and DJF – JJA for SH.

The observational pressure-latitude section of zonally averaged seasonal cloud fraction difference is shown in Figure 3.4(a), while, the ensemble averaged seasonal difference section of cloud fraction over all the CMIP5 models is shown in Figure 3.4(b). Overall, the cloud fraction sections from the models and observation agree reasonably well, although several finer differences do exist. One important observation that can be made here is that even though the mean cloud sections were symmetrical about the equator, the seasonal differences in both the hemispheres exhibit considerable variance. Also, clouds exhibit strong positive tendency in the tropical belt and negative tendency in the mid-latitudes and poles. This is captured by both the model-mean and the observation. The models perform better in the NH. Underestimation of cloud change is also seen at the high cloud levels although the sign of change matches with that of the observation. In the SH the models differ a lot more from the observations especially in the lower levels where observation shows strong negative tendencies yet the model values show an increase. A center of positive cloud change in sub-polar latitudes between 950 – 600 hPa pressure levels seen in the observation is almost absent in the model mean. The pattern of transition from negative to positive

tendency in the mid-latitudinal upper atmosphere is also different in the ensemble model mean section from that in the observations.

3.4. Climatological change in Clouds

The long term cloud amount change under a rapidly warming climate scenario is evaluated by analyzing cloud data from the RCP8.5 run of 25 CMIP5 models. Climatological difference in cloud fraction is computed by taking the difference between annually averaged cloud amount in the future decade (2090-99) and the present decade (2010-19) (thereafter referred to as climatological difference in this thesis). These changes were first computed for each model and then summed over to obtain an ensemble averaged climatological cloud change. Pressure-latitude distribution of the ensemble zonally averaged climatological cloud fraction change is shown in Figure 3.4(c). From this figure it is seen that in the mid-latitudes, clouds show a decreasing tendency for almost the entire atmospheric column, starting from the base to approximately 300 hPa pressure level. Further, cloud fraction change in the tropics is mostly negative near the top and positive below 450 hPa, interspersed with patches of decreasing cloud amount at few intermediate pressure levels. However, cloud changes are strongly positive close to the model top (~200hPa) as also in the sub-polar belt.

The vertical section of climatological change in cloud amount (Figure 3.4(c)) displays an impressive similarity to its seasonal cloud change counterpart (Figure 3.4(b)) in the mid-latitudinal belt, from 30°S to 60°S and 30°N to 60°N. Here, similar to the seasonal cloud fraction difference, the climatological cloud fraction also shows negative tendency in these belts for the entire atmospheric column except at high altitudes (~250hPa) where cloud fraction change becomes positive. It may be noted that despite the similarities between the climatological and seasonal cloud fraction patterns, the magnitude of these two phenomenon are significantly different. The cloud fraction changes are generally much stronger in the seasonal case as compared to the climatological one. This is a reflection of the fact that the range of surface temperature variation in the seasonal case is as large as ~ 10 - 12 K while that for climatological changes is only ~3 - 4 K. In the tropical belt, between 30°S to 30°N latitudes, the cloud change does not show any matching patterns as seen in the case of mid-latitudes. Such discrepencies could be attributed to the fact that surface

temperature in this belt does not differ much seasonally, and more importantly, the seasonal variation in the tropics is dominated by the migration of Inter-Tropical Convergence Zone (ITCZ) rather than the effect of warming. This eliminates the possibility of correlating long term cloud changes due to climate warming with seasonal changes in clouds for the tropical belt. For the subsequent sections, the focus will primarily be on the mid-latitudinal belt which is the zone of interest for seasonal cloud changes.

Climatological cloud fraction change sections were also constructed using amip, amip4K and amipFuture runs to compare with RCP8.5 sections. Amip4K and amipFuture are perturbed runs representing warming only due to SST increase. Thus they represent a climate change scenario with only CO_2 forcing that causes a change in SST values. Any other influences such as aerosol etc are eliminated by this treatment. In the first set, cloud fraction difference between 10 years (1990-1999) of amip and amip4K runs are computed. In the second set, differences between the same 10 years of amip and amipFuture are calculated. The pressure latitude vertical cloud difference section from these analyses are compared with the section from RCP8.5 data in Figure 3.5(a)-(c). It may be seen that overall patterns are well matched between all three sections in the mid-latitudinal belt although there are specific differences in the tropics.

3.5. Co-variability of Seasonal and Climatological Cloud changes

For a more quantitative analysis of the relationship between mean cloud amount, seasonal difference in cloud amount and climatological variability of clouds in the mid-latitudes, a 2-dimensional cross-section was used, enclosed on either sides by the 30° and 60° latitudes and spanning the entire atmospheric column. This constituted the total cloud column within which logarithmic pressure weighted mean of cloud fraction and its variance was computed. Essentially, two such cross-sections - one for the SH, ‘box_sh’ and the other for NH, ‘box_nh’ were formed. For the climatological variability, the values of ‘box_sh’ and ‘box_nh’ were added while for the seasonal variability, the difference between the values of ‘box_sh’ and ‘box_nh’ was calculated. Further, the surface temperature difference in the models, for both the climatological and seasonal climate change were averaged over the entire mid-latitudinal belt. These were used to normalize the cloud fraction differences and make the magnitude of the changes more comparable. An

ordered pair for each model was thus obtained, one representing the climatological cloud fraction change and the other representing the seasonal cloud fraction change. A similar treatment was also extended to the mean cloud amount in the mid-latitudes. Mass weighted mean of the cloud fraction was computed within the 2-dimensional mid-latitudinal box and the values for NH and SH were summed over. A mean cloud value was thus generated for each model which constituted another ordered pair together with the corresponding seasonal changes.

The vertical sections of cloud changes in Figure 3.4 reveal the presence of opposite signs between the upper and lower troposphere in both the seasonal and climatological cloud changes. Different sign of tendencies at different pressure levels would have a compensation effect when grouping them together as one column. Because of this, instead of averaging the data over the entire atmospheric column, correlation between the seasonal and climatological changes in the high, mid and low level clouds were studied separately. For this purpose, the pressure level based definition of cloud layers used by the International Satellite Cloud Climatology Project (ISCCP) was put to use. This classification defines low clouds as those present from the surface to 680 hPa, mid-level clouds residing between 680 and 440 hPa and high-level clouds ranging from 440 hPa to the top of the troposphere (approximately 100hPa).

The ordered pair of seasonal and climatological change values for each model in the high, mid and low levels of clouds are plotted in Figure 3.6 (a), (b) and (c) respectively, where the x- and the y- axes are the differences in climatological cloud amount and the seasonal cloud amount change, respectively. They are expressed in units of $kg/m^2/K$ based on the mass-weighing method of averaging the cloud fraction withinh each layer. These points are then linearly regressed and the correlation coefficient between x and y values obtained from the square root of the regression coefficient (r^2). The value of the correlation coefficient, r, for all the linear regression plots are indicated at the top right corner of each plot. Ensemble average over all the models, indicative of the collective model behavior, has also been shown (with a pink star) in each case. Since, the observational dataset exists for a short period of time it could only be used for computation of mean clouds and their seasonal differences. In the scatter plots between seasonal and climate cloud changes, instead of an ordered pair of x and y coordinates, only a boxed average y-value representative of cloud observations is available. This is incorporated in these and all following

relevant correlation plots as a dotted line, the horizontal extent of which has no significance and is just used for illustrative purposes.

Good correlations were seen for the low and mid level clouds with the respective correlation coefficients being ~0.84 and 0.89. The relatively smaller correlation in the case of high clouds is likely due to the fact that transition from negative to positive tendency in both the seasonal and climate changes occur at different heights for different latitudes. But in this treatment all changes above 440hPa, irrespective of sign of change, are combined together.

In addition to the presence of good correlation for mid and low level clouds, the scatter plots exhibit the following salient features: (1) All models simulated reduction of low and middle clouds in both the seasonal and climatological changes. (2) Many of the of models simulated positive climatological cloud changes, but negative seasonal changes in the high level clouds. This is likely due to the presence of a more pronounced cloud increase layer in upper troposphere for the climatological changes as in Figure 3.4. (3) The ensemble mean overestimated the seasonal reduction of middle clouds, but underestimated it in the low clouds. Given the good correlations between the seasonal and climatological cloud changes at these levels, the ensemble mean of the climatological cloud reduction is likely overestimated for middle clouds, while for low clouds it is underestimated. (4) The cloud changes differ by several folds among the models. Although the models concur in the sign of cloud changes in the low and mid level, the model spread in magnitude of reduction is larger in these layers. (5) The observed changes lie within the range of models.

As stated before from the study of vertical sections, climate models underestimate mean cloud amount. In Figure 3.7, the possibility of seasonal variation being related with the climatological mean amount of clouds in models is examined. These figures present the correlation between mean cloud amount in the x-axis and seasonal variation in the y-axis for high, mid and low level mid-latitudinal clouds. Observation is represented by a pink X-mark in these scatter plots. It is seen that even though the mean low and middle clouds are significantly underestimated, their seasonal variations are not. While there is some correlation between the mean cloud and the seasonal cloud change, it is not very strong. The interrelationship between model mean clouds with their seasonal change was further investigated by comparing the mean clouds exclusively in the months of JJA and DJF with their seasonal change. The vertical sections of the zonally

averaged mean JJA and DJF cloud fraction from observation and from models are shown in Figure 3.8. Model under estimation of low clouds is still found to be a prominent feature in these monthly climatologies. However, a study of the relationship between JJA mean clouds and seasonal differences (in Figure 3.9) and that between DJF clouds and seasonal differences (in Figure 3.10) did not reveal any siginificant relationship between them.

Because a rigid segregation into low, mid and high levels common to all the latitudes may not truly capture the transition in cloud change sign, a different method of splitting the total cloud column into different cloud regions was also employed. For each model dataset and also for the observation, every latitude is treated separately and the altitude at which transition in sign of cloud fraction tendency occurs is determined and saved as the divider. The total cloud column is then split into a lower negative tendency box capped by the divider height and a top positive tendency box with the divider height as its base. For the mean cloud amount, the divider height for seasonal difference is used to compute mass weighted cloud fraction value within the lower negative tendency and upper positive tendency boxes. In Figure 3.11(a) and (b), correlation between mean cloud amount in the pressure-latitude grid boxes with negative and positive seasonal cloud tendency and their corresponding seasonal cloud tendency values are plotted against each other. Although the correlation values do not show improvement in the cloud increase regions, the cloud reduction region shows significant relation between mean clouds and their seasonal differences. Underestimation of model clouds also appears to be confined mostly to the cloud reduction region as most of the model points as well as the model mean lies to the left of the observation point in Figure 3.11(a). In the cloud increase regions Figure 3.11(b), the ensemble mean of models lies closer to the observed value, however the models are spread over a larger range so that many of the model predicted mean cloud values are greater than or lesser than the observation. This leads to the conclusion that the two observed features : under-estimation of model clouds and overprediction of seasonal changes in clouds are well correlated in the lower tropospheric layers of cloud fraction reduction.

In Figure 3.4(c), the vertical section of the long term cloud amount projection also demonstrated the presence of a positive tendency layer at the top of the air column with a variable base height. The total column of climatological changes was similarly split into negative and positive tendency zones for each model and the mass-weighted cloud fraction amount (in $kg/m^2/K$)

computed within each region. Figure 3.11(c) and (d) illustrate the correlation between model seasonal and climatological cloud changes in the cloud reduction and cloud intensification regions respectively. While the correlation in the cloud reduction regions is very strong, it is considerably weakened in the domain of cloud enhancement. Model bias is more defined in the cloud reduction region where models overpredict negative tendency during seasonal changes which, based on the strong correlation between them, translates into increased cloud reduction predictions for the future climate. Cloud increase at higher levels is on the other hand underpredicted by most models and the ensemble model mean, however weak correlations for these regions preclude the possibility of drawing conclusions about the model patterns of future projections.

Some other important findings from this section are listed here: 1) When the reduction region was separated into mid and low level clouds, models overpredicted the seasonal reduction in mid level and underpredicted them at low-levels. Upon summing them together the net effect is dominated by the mid-level overprediction. 2) The range of model simulated cloud reduction continues to show a large spread both seasonally and climatologically and the observed change was found to lie within this range. 3) In the cloud increase regions the model spread in seasonal change is manifold smaller than the spread in seasonal cloud reductions also the range of projected change.. Also the relationship is weaker implying that the moderate correlation seen before in case of high clouds was mostly a contribution from the cloud reduction regions included in that level.

Seasonal difference vertical sections (Figure 3.4(a) and b)) for both models and observation presented an asymmetry between NH and SH. Further, it also appeared that most of the inconsistencies were located in the SH so the seasonal-climatological covariability and model biases in seasonal variability simulation were investigated separately for the two hemispheres. The covariabilty plots for NH are shown in Figure 3.12(a)-(d) and for SH in Figure 3.13(a)-(d). In the NH, mean cloud and seasonal difference in clouds correlate well with each other in both the cloud reduction and cloud increase regions with correlation values ~ 0.83 and 0.71 respectively (Figure 3.12(a)and(b)). The correlation for Cloud increase region was re-calculated using Spearman rank correlation method which is a particularly useful method for correlating data sets with large outliers. Bias in mean cloud amount is present in both the regions however, the seasonal difference biases seem to be confined to the domain of cloud enhancement. In cloud increase regions thus, models with low mean cloud amount have lower seasonal changes.

Correlation between seasonal and climatological cloud changes are strong in the cloud reduction regimes, but weaken considerably in the cloud increase regions. In the cloud reduction regime, seasonal change biases with respect to mean are very small, but models are spread in all directions about the model mean and the observational point. Given the fairly strong relationship between the seasonal and climatological differences in the NH cloud reduction regions, it may be concluded here that biases in mean model climatological predictions in this regime are also not significantly large. In the domain of cloud enhancement on the other hand, the correlation between climate and seasonal cloud change is not that compelling although the biases in seasonal difference are quite noticeable. All models except one (GFDL-CM3) predict a smaller increase in clouds seasonally compared to the observation. Whether this seasonal bias translates into long term climate projections by the model cannot be deduced based on the weak correlation between them.

In the SH, correlations between mean clouds and their seasonal difference is quite weak. Due to the presence of several outliers in the case of cloud increase regions, the correlation coefficients were recomputed using Spearman's method. However, the relationship still did not show any significant improvement. Analogous to the case of NH, seasonal and projected climate correlations are higher in the cloud reduction zones as compared to the cloud increase zones. Biases in seasonal differences are large in the cloud reduction region in SH and likely the primary contributor to the biases seen in total column values. The overprediction of cloud decrease during seasonal changes thus occurs mostly in the SH mid latitudes. Based on the presence of a robust correlation between seasonal and climatological changes it may be expected that these biases carry over to the long term climate changes in the mid-latitudinal SH.

Separation of the mid-latitudinal belt into NH and SH led to the following conclusions : 1) Correlations are seen between the mean and the seasonal cloud changes in both NH and SH but the former contributes more to the total belt correlations. 2) No improvement was noticed in the relationship between seasonal and climatological increase in upper level clouds. 3) In the cloud reduction regions, both NH and SH show strong relationship between seasonal and climatological changes. Seasonal change biases mostly stem from SH where the spread in model values of seasonal change is four times as large and the climatological change is twice as large as in NH.

3.6. Summary

Similarities in the zonally averaged pressure-latitude sections of cloud fraction seasonal and climatological differences in the mid-latitudinal belt were detected. Using CMIP5 model runs from 25 climate models, a detailed investigation of the correlations between these changes at the low-, mid- and high- cloud levels were carried out. The important results emerging from this study are summarized below :

1. Models underestimate mean cloud amount, particularly at the low and mid cloud levels, in the mid-latitudinal belt. The underestimation in mean clouds is correlated to their seasonal difference biases only in the cloud reduction regions. In these regions, the models exhibit an overestimation of cloud reduction at mid-levels and under-prediction at low cloud levels.

2. Good correlation exists between seasonal and climatological cloud reduction in the low and mid-level clouds. In the high-level, where clouds show increase, the relationship is not very strong.

3. In the cloud reduction regions, majority of the models as well as the mean overestimate decrease in clouds. This overestimation of the seasonal cloud decrease translates into larger cloud reductions in the projected climate change. In regions of cloud increase, at upper tropospheric levels, models underpredict cloud increase. However the absence of strong correlations in these layers preclude the possibility of constraining model spread in projections of cloud increase.

4. It is in the SH mid-latitudinal belt where models exhibit larger seasonal change biases and larger spread in magnitude of reduction. In the NH belt, the model mean behavior concurs with observation and translates into an estimate of projected change that lies midway in the range of model simulated values.

Table 1: List of CMIP5 models and their modeling centers used in Chapter 3, 4 and 5.

MODEL	**INSTITUTION**
BCC-CSM1.1	Beijing Climate Center, China Meteorological Administration, China
BNU-ESM	College of Global Change and Earth System Science, Beijing Normal University, China
CCSM4	National Center for Atmospheric Research, United States
CESM1-BGC	National Science Foundation, Department of Energy, National Center for Atmospheric Research, United States
CESM1-CAM5	
CMCC-CESM	Centro Euro-Mediterraneo per I Cambiamenti Climatici, Italy
CMCC-CM	
CSIRO-Mk3.6.0	Commonwealth Scientific and Industrial Research Organisation in collaboration with the Queensland Climate Change Centre of Excellence, Australia
FGOALS-g2	LASG, Institute of Atmospheric Physics, Chinese Academy of Sciences; and CESS, Tsinghua University, China
GFDL-CM3	NOAA Geophysical Fluid Dynamics Laboratory, United States
GFDL-ESM2G	
GFDL-ESM2M	
GISS_E2-H	NASA Goddard Institute for Space Studies, United States
GISS-E2-R	
GISS-E2-R-CC	
INM-CM4	Institute for Numerical Mathematics, Russia
IPSL-CM5A-LR	Institut Pierre-Simon Laplace, France
IPSL-CM5A-MR	
IPSL-CM5B-LR	

MIROC5	Atmosphere and Ocean Research Institute (The University of Tokyo), National Institute for Environmental Studies, and Japan Agency for Marine-Earth Science and Technology, Japan
MIROC-ESM	Japan Agency for Marine-Earth Science and Technology, Atmosphere and Ocean Research Institute (The University of Tokyo), and National Institute for Environmental Studies, Japan
MPI-ESM-LR	Max Planck Institute for Meteorology, Germany
MPI-ESM-MR	
MRI-CGCM3	Meteorological Research Institute, Japan
NorESM1-M	Norwegian Climate Centre, Norway

Table 2: List of CMIP5 models whose amip, amip4K and amipfuture runs were analyzed.

MODEL	**INSTITUTION**
BCC-CSM1.1	Beijing Climate Center, China Meteorological Administration, China
CanAM4	The Fourth Generation Atmospheric General Circulation Model, Canadian Centre for Climate Modelling and Analysis
CCSM4	National Center for Atmospheric Research, United States
CESM1-CAM5	National Science Foundation, Department of Energy, National Center for Atmospheric Research, United States
CNRM-CM5	Centre National de Recherches Météorologiques (National Centre for Meteorological Research, France
FGOALS-g2	LASG, Institute of Atmospheric Physics, Chinese Academy of Sciences; and CESS, Tsinghua University, China
HadGEM2-A	Hadley Global Environmental Model2-Atmosphere, European Network for Earth System Modeling
IPSL-CM5A-LR	Institut Pierre-Simon Laplace, France
IPSL-CM5B-LR	
MIROC5	Atmosphere and Ocean Research Institute (The University of Tokyo), National Institute for Environmental Studies, and Japan Agency for Marine-Earth Science and Technology, Japan
MPI-ESM-LR	Max Planck Institute for Meteorology, Germany
MPI-ESM-MR	
MRI-CGCM3	Meteorological Research Institute, Japan

Figures

(a)

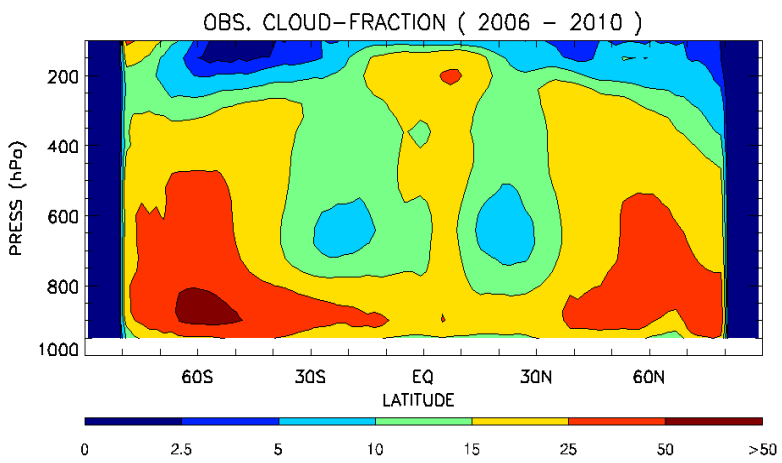

(b)

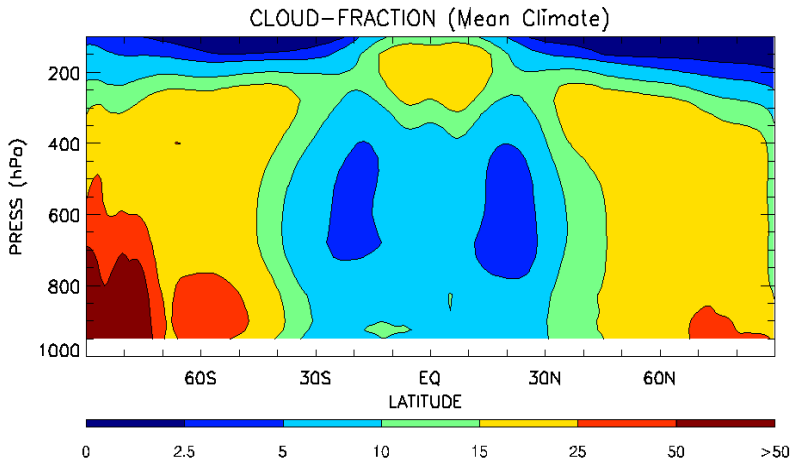

Figure 3.1: Zonally averaged pressure-latitude section of mean cloud fraction (expressed in %) from July, 2006 – June, 2010 using (a) C3M observation data (b) ensemble mean over RCP8.5 runs of 25 CMIP5 models.

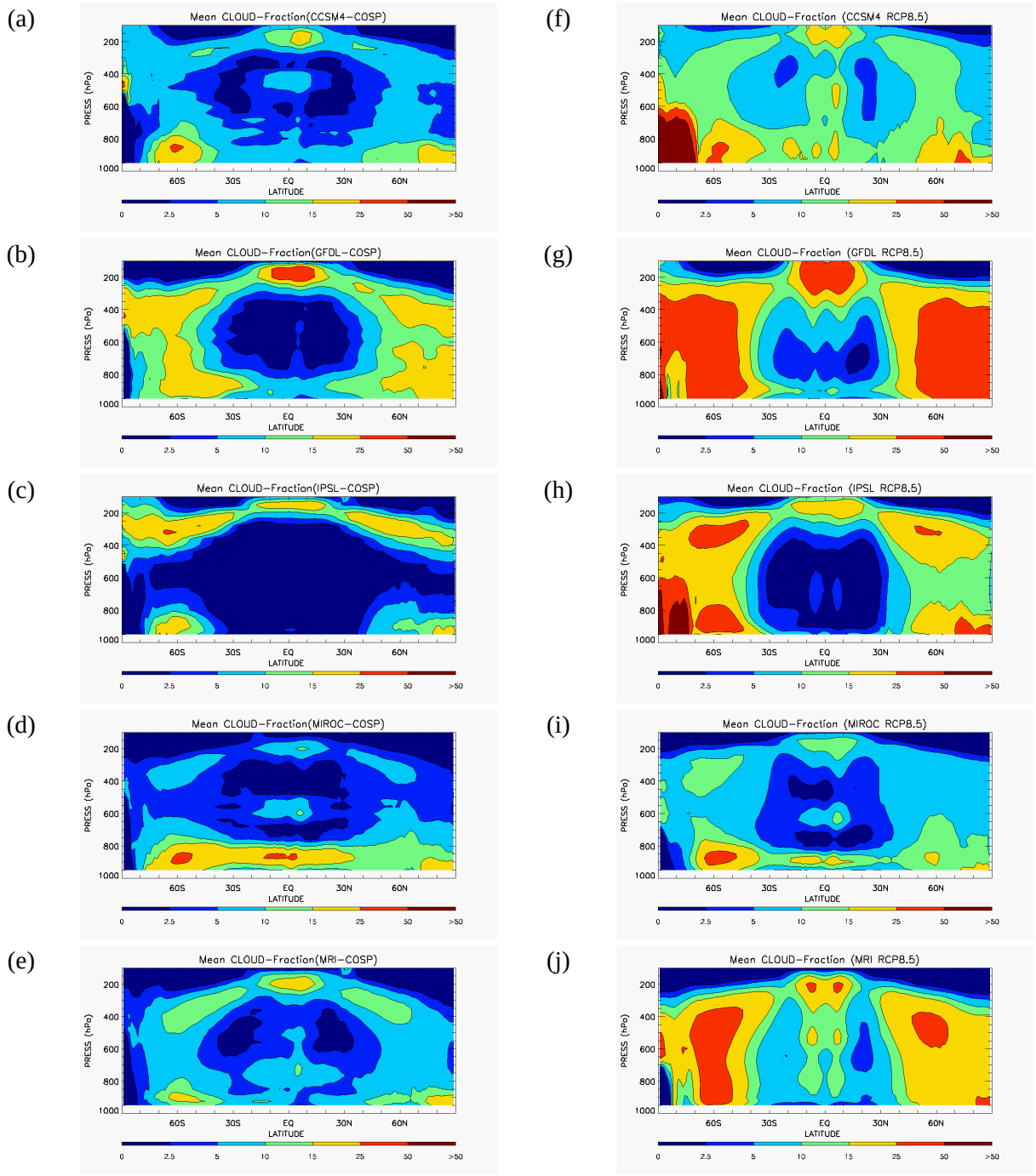

Figure 3.2 : Zonally averaged pressure-latitude section of mean cloud fraction (expressed in %) in the following five models : CCSM4, GFDL-CM3, IPSL-CM5A-LR, MIROC5, MRI-CGCM3 from (a)-(e) amip-COSP product (2006-years available) and (f)-(j) RCP8.5 product (2006 – 2009)

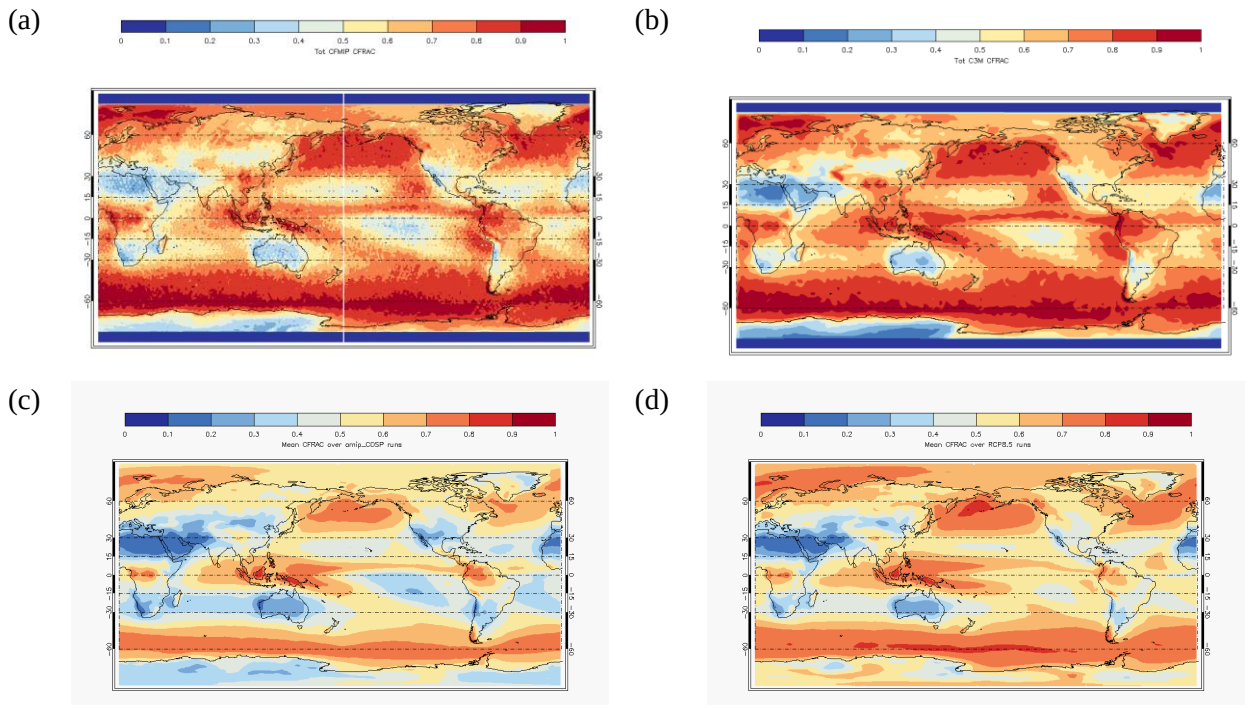

Figure 3.3 : Map of average total column cloud fraction distribution (2006-2009) from (a) CALIPSO-GOCCP observations, (b) C3M observations, (c) Mean over amip-COSP runs (2006-2008) of 5 CMIP5 models (CCSM4, GFDL-CM3, IPSL-CM5A-LR, MIROC5, MRI-CGCM3) and (d) Mean over RCP8.5 runs of the same set of models

(a)

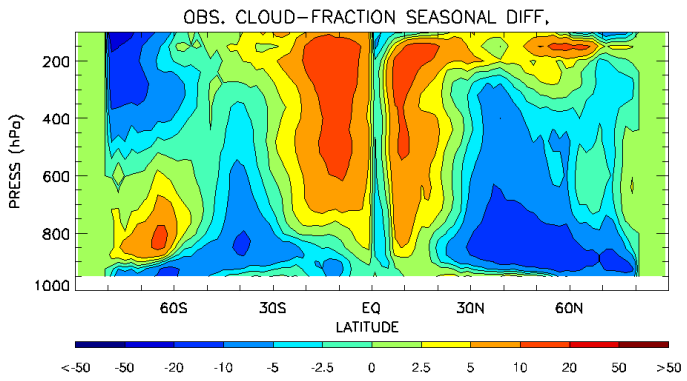

(b)

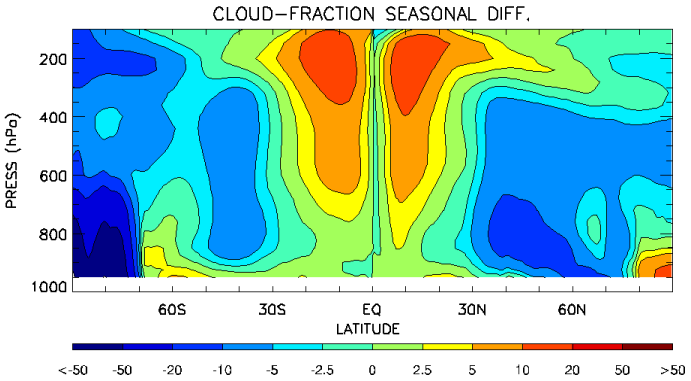

(c)

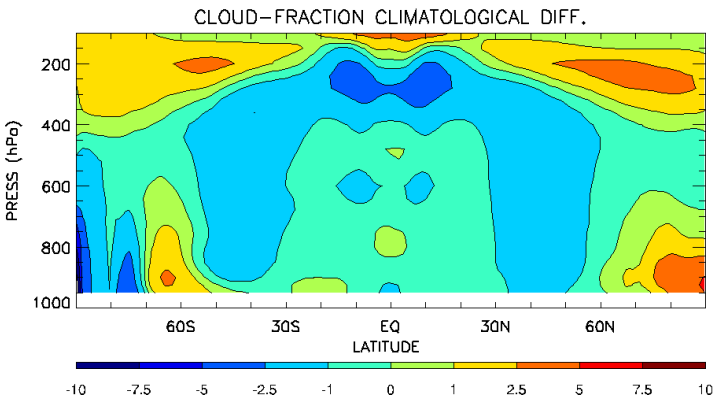

Figure 3.4 : Zonally averaged pressure-latitude section of seasonal difference (JJA - DJF) between July, 2006 - June, 2010 in cloud fraction (expressed in %) using (a) C3M observations and (b) ensemble model mean over RCP8.5 runs of 25 CMIP5 models. Seasonal differences in SH have been reversed in sign. (c) Zonally averaged pressure-latitude section of climatological difference in cloud fraction from ensemble model mean of 25 CMIP5 models between 2010-19 and 2090-99.

(a)

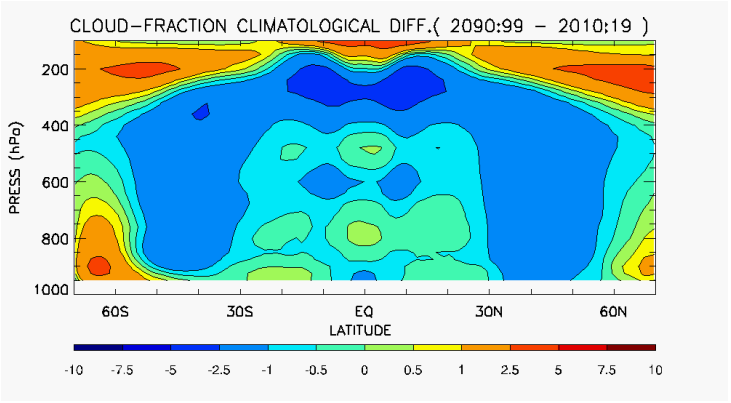

(b)

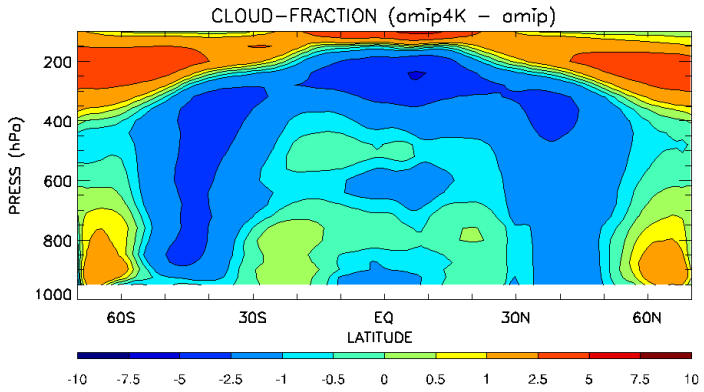

(c)

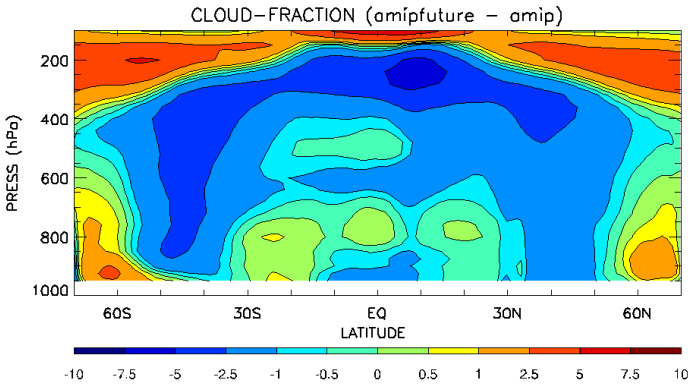

Figure 3.5 : Zonally averaged pressure-latitude section of (a) ensemble mean climatological difference in cloud fraction (expressed in %) between 2010-19 and 2090-99 using RCP8.5 runs of 25 CMIP5 models (b) ensemble mean cloud fraction (expressed in %) difference between amip (control) and amip4K (perturbed) runs over 12 models and (c) between amip(control) and amipFuture (perturbed) runs over 11 models between 1990-1999.

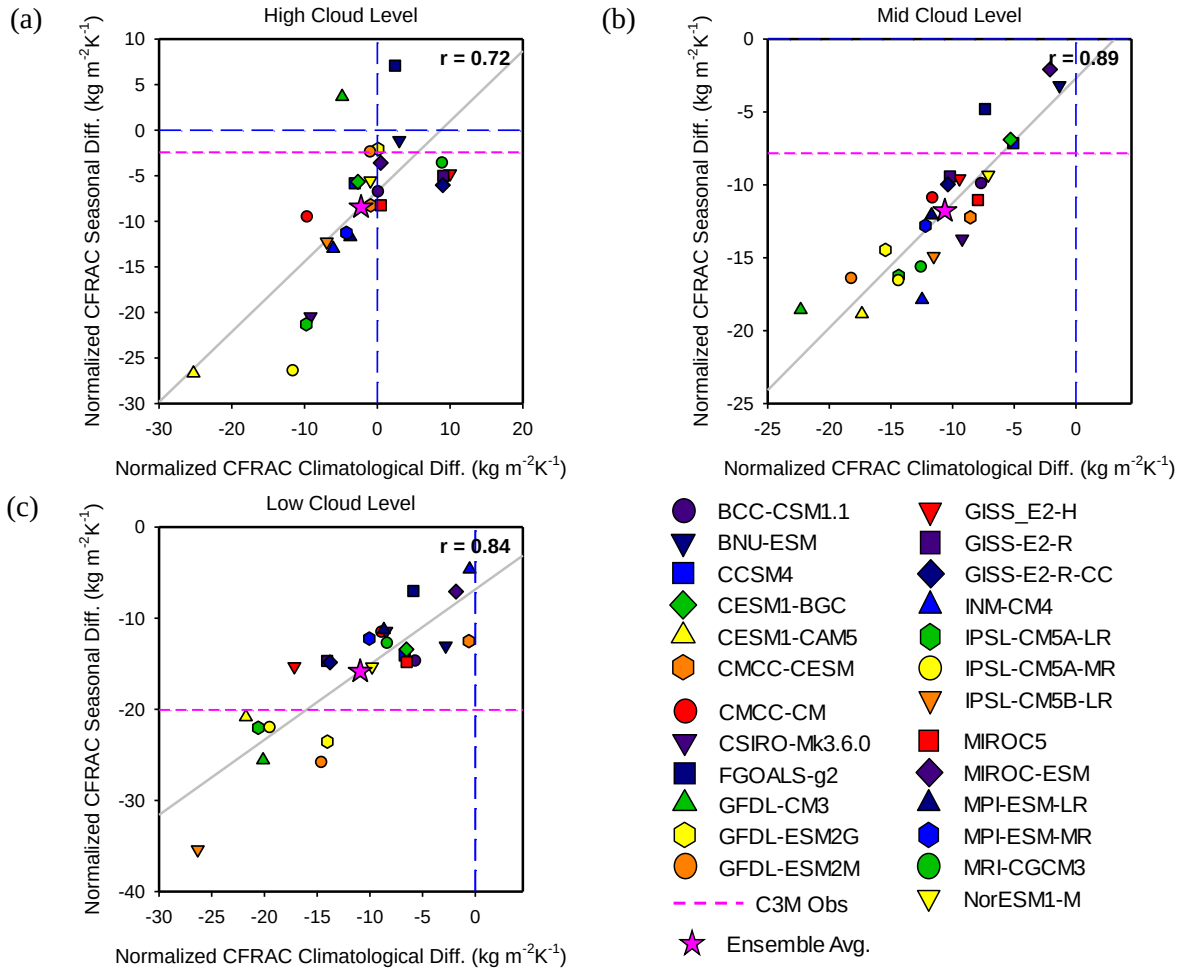

Figure 3.6 : Scatter plots showing the relationship between Temperature normalized and Mass weighted Seasonal change (y-axis) and Climatological difference (x-axis) in mid-latitudinal cloud fraction (in kg/m^2/K) for 25 CMIP5 models (listed with their symbols in the key) in the (a) High-level clouds (440hPa and above), (b) Mid-level clouds (680 hPa -440 hPa) and (c) Low-level clouds (below 680 hPa). Grey solid line is the linear regression fit. Observed values of Seasonal change in cloud fraction are represented by pink horizontal lines. Correlation coefficient values are indicated at the top right corner of each figure. Zero x- and y-axes are included as blue dashed lines.

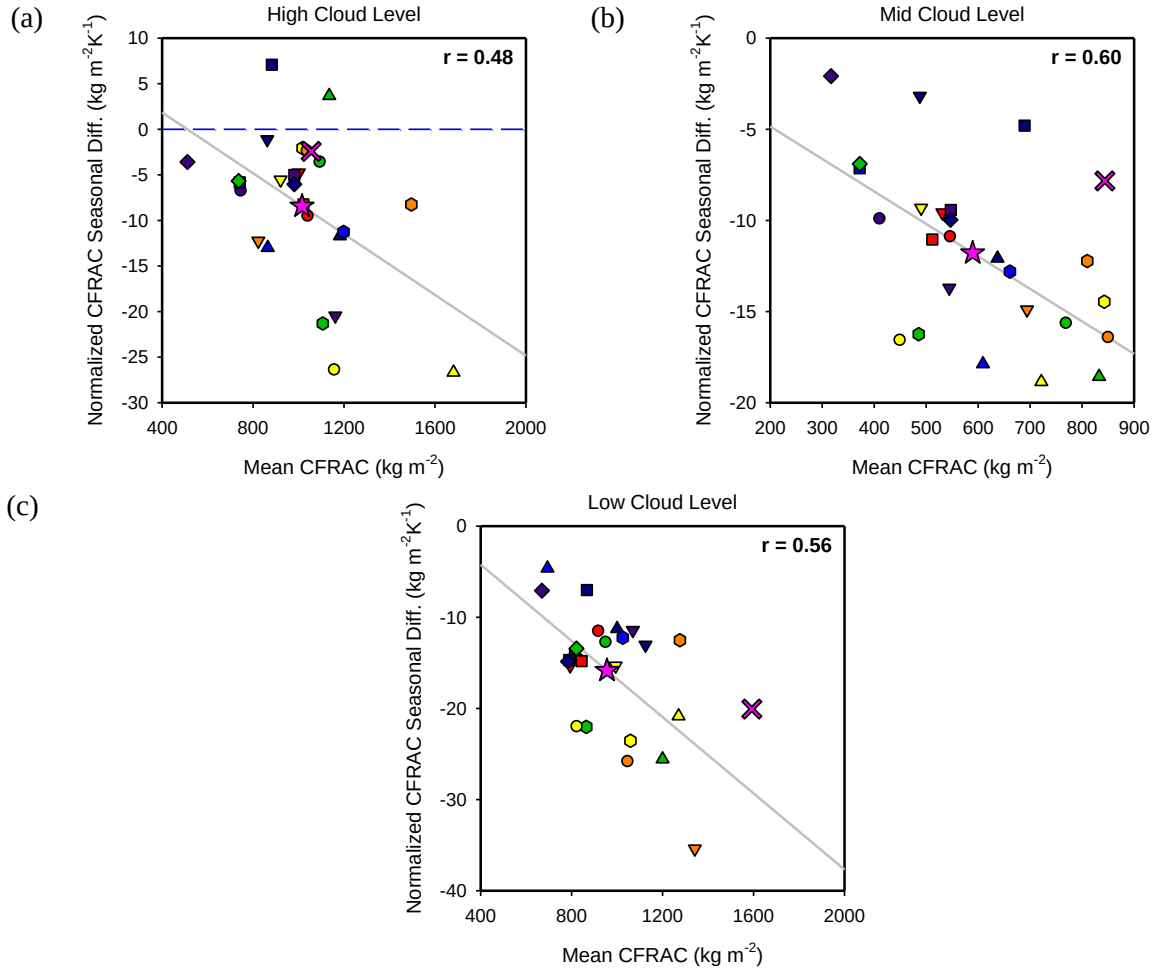

Figure 3.7 : Scatter plots showing the relationship between mid-latitudinal Mass weighted Temperature normalized Seasonal change in kg/m^2/K (y-axis) and Mass weighted Mean value (x-axis) of cloud fraction in kg/m^2 in the (a) High-level clouds (440hPa and above), (b) Mid-level clouds (680 hPa -440 hPa) and (c) Low-level clouds (below 680 hPa) for 25 CMIP5 models (key in Figure 3.6). Grey solid line is the linear regression fit. Observed values of Mean and Seasonal change in cloud fraction are represented by a pink cross. Correlation coefficient values are indicated at the top right corner of each figure. Zero x- and y-axes are included as blue dashed lines.

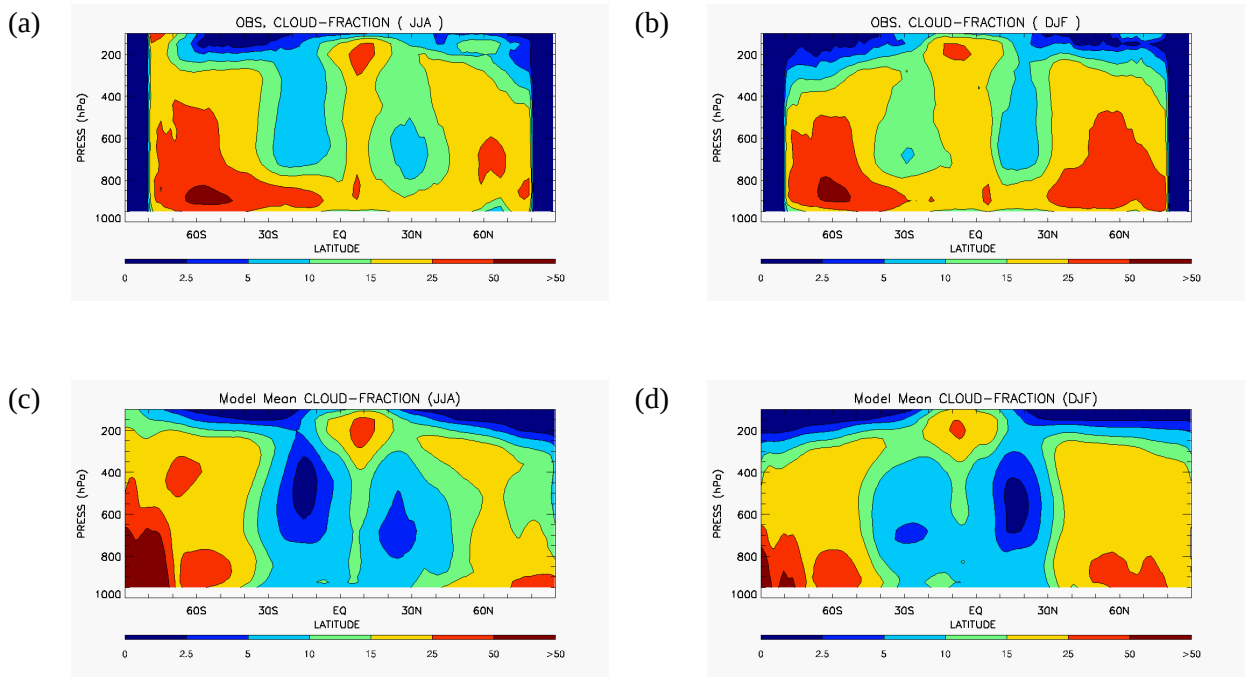

Figure 3.8 : Zonally averaged pressure-latitude section of mean cloud fraction (expressed in %) for (a) June-July-August and (b) December-January-February months using C3M observation data and (c) JJA and (d) DJF using ensemble mean over RCP8.5 runs of 25 CMIP5 models between 2006-2010

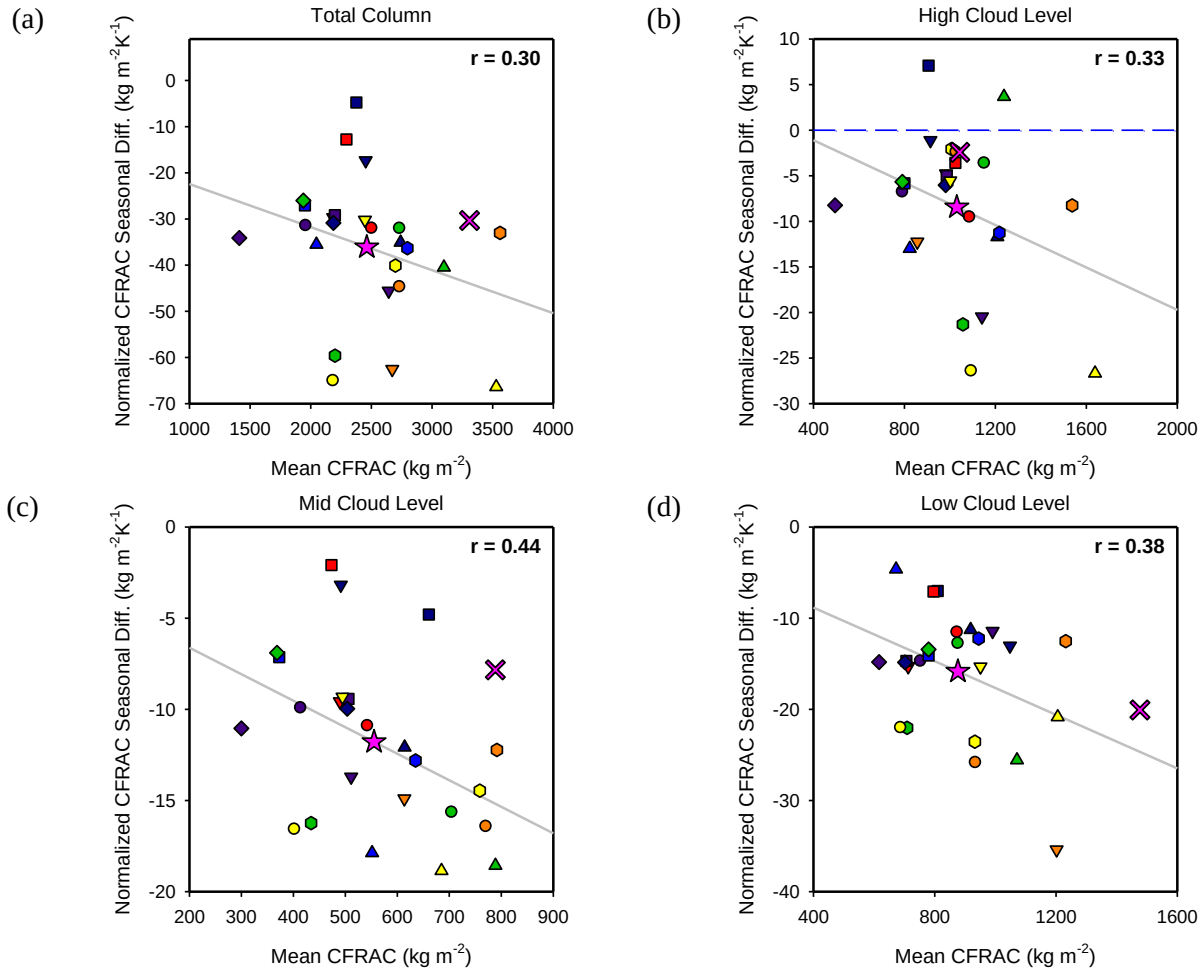

Figure 3.9 : Scatter plots showing the relationship between mid-latitudinal Temperature normalized Mass weighted Seasonal change (y-axis) in kg/m^2/K and Mass weighted Mean values (x-axis) for JJA months in kg/m^2 of cloud fraction for 25 CMIP5 models (key in Figure 3.6) for (a) Total Column, (b) High Level Clouds, (c) Mid-Level Clouds and (d) Low Level Clouds. Observed values indicated by pink cross. Grey solid lines represent the linear regression fit. Dashed blue lines indicate the zero x- and y-axes while Correlation coefficients are noted at top right corner in each plot.

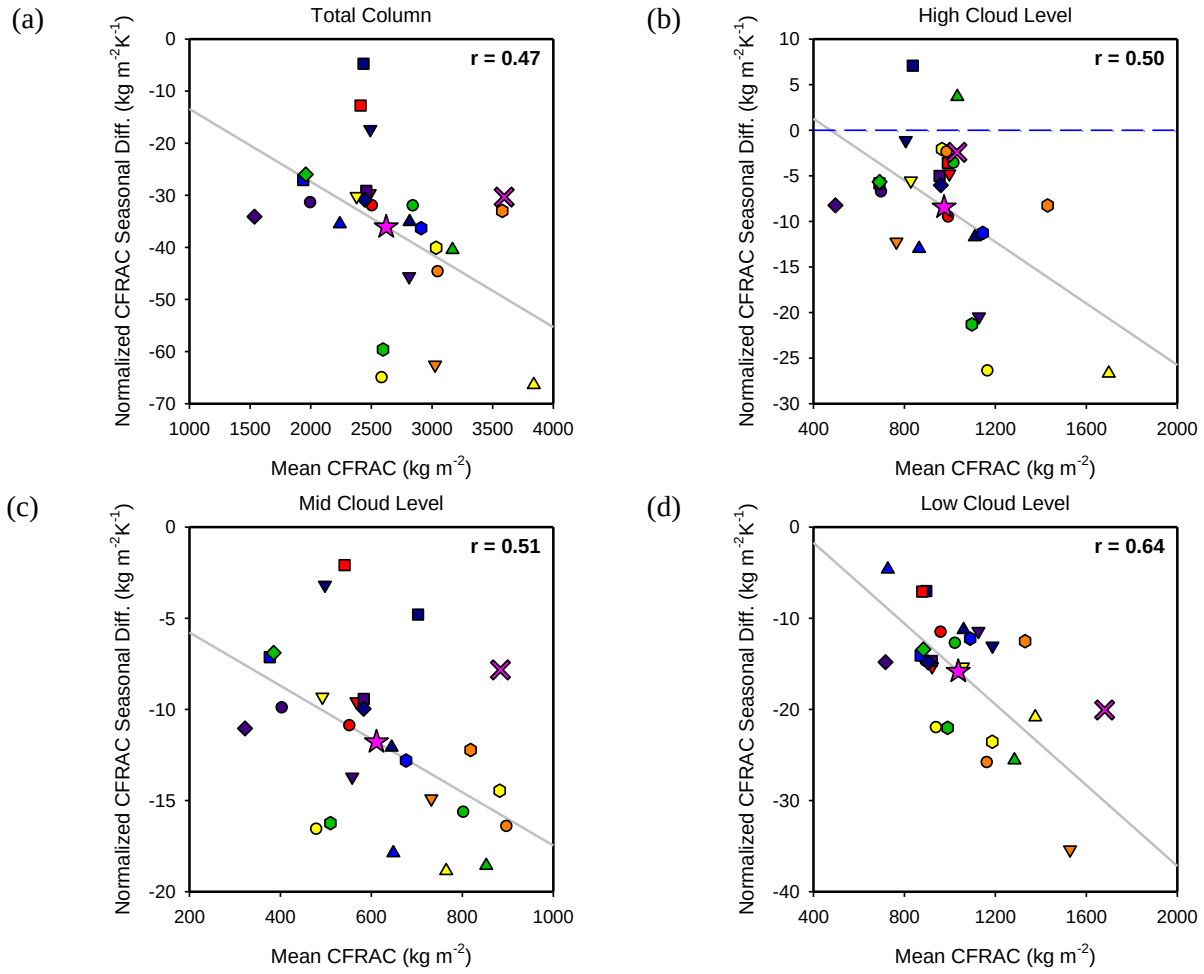

Figure 3.10 : Scatter plots showing the relationship between mid-latitudinal Temperature normalized Mass weighted Seasonal change (y-axis) in $kg/m^2/K$ and Mass weighted Mean values (x-axis) for DJF months in kg/m^2 of cloud fraction for 25 CMIP5 models (key in Figure 3.6) for (a) Total Column, (b) High Level Clouds, (c) Mid-Level Clouds and (d) Low Level Clouds. Observed values indicated by pink cross. Grey solid lines represent the linear regression fit. Dashed blue lines indicate the zero x- and y-axes while Correlation coefficients are noted at top right corner in each plot.

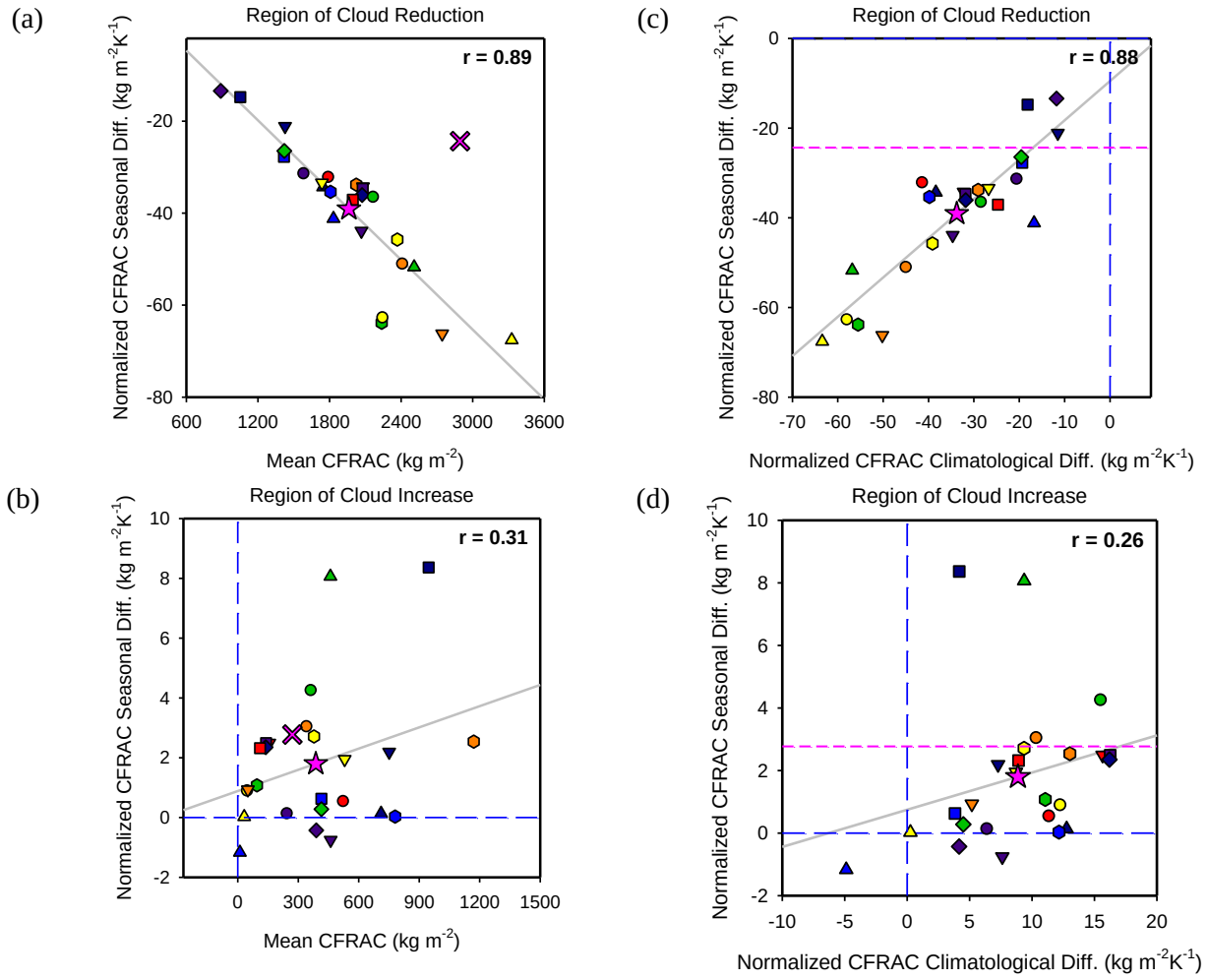

Figure 3.11 : Scatter plots showing the relationship between mid-latitudinal Mass weighted (a) and (b) Temperature normalized Seasonal change (y-axis) in kg/m^2/K and Mean values (x-axis) in kg/m^2 of cloud fraction for 25 CMIP5 models (key in Figure 3.6) in the layers of Seasonal Cloud reduction and Cloud Increase respectively and (c) and (d) between Mass weighted Temperature normalized Seasonal change (y-axis) and Climatological difference (x-axis) in cloud fraction (kg/m^2/K) in the layers of corresponding Cloud reduction and Cloud Increase respectively. Observed values are indicated by pink cross in (a) and (b) and pink dashed line in (c) and (d). Grey solid lines represent the linear regression fit. Dashed blue lines indicate the zero x- and y-axes while Correlation coefficients are noted at top right corner in each plot.

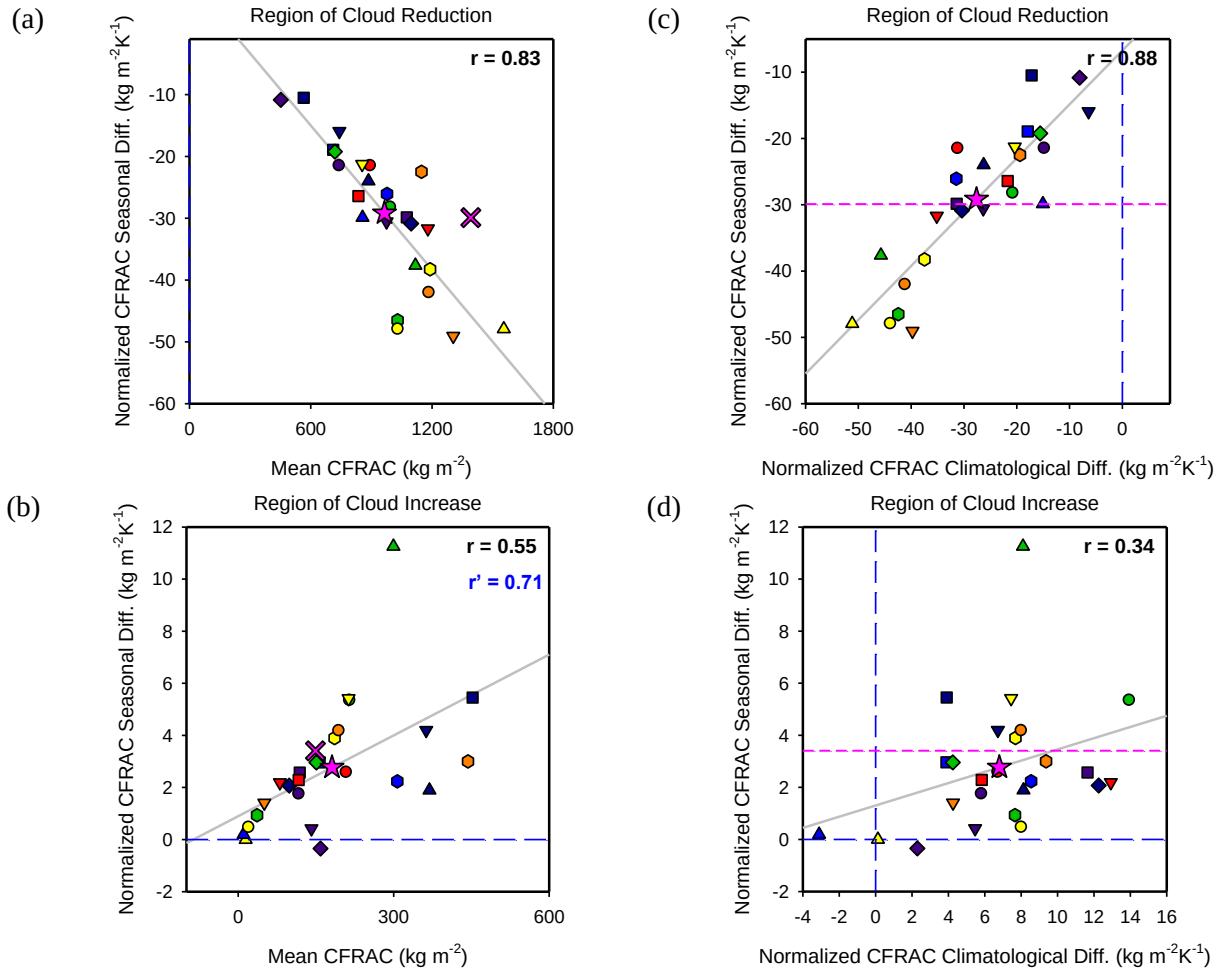

Figure 3.12 : Scatter plots showing the relationship between NH mid-latitudinal Mass weighted (a) and (b) Temperature normalized Seasonal change (y-axis) in kg/m^2/K and Mean values (x-axis) in kg/m^2 of cloud fraction for 25 CMIP5 models (key in Figure 3.6) in the layers of Seasonal Cloud reduction and Cloud Increase respectively and (c) and (d) between Mass weighted Temperature normalized Seasonal change (y-axis) and Climatological difference (x-axis) in cloud fraction (kg/m^2/K) in the layers of corresponding Cloud reduction and Cloud Increase respectively. Observed values are indicated by pink cross in (a) and (b) and pink dashed line in (c) and (d). Grey solid lines represent the linear regression fit. Dashed blue lines indicate the zero x- and y-axes while Correlation coefficients are noted at top right corner in each plot. Spearman's rank correlation coefficient also indicated for (b) in blue.

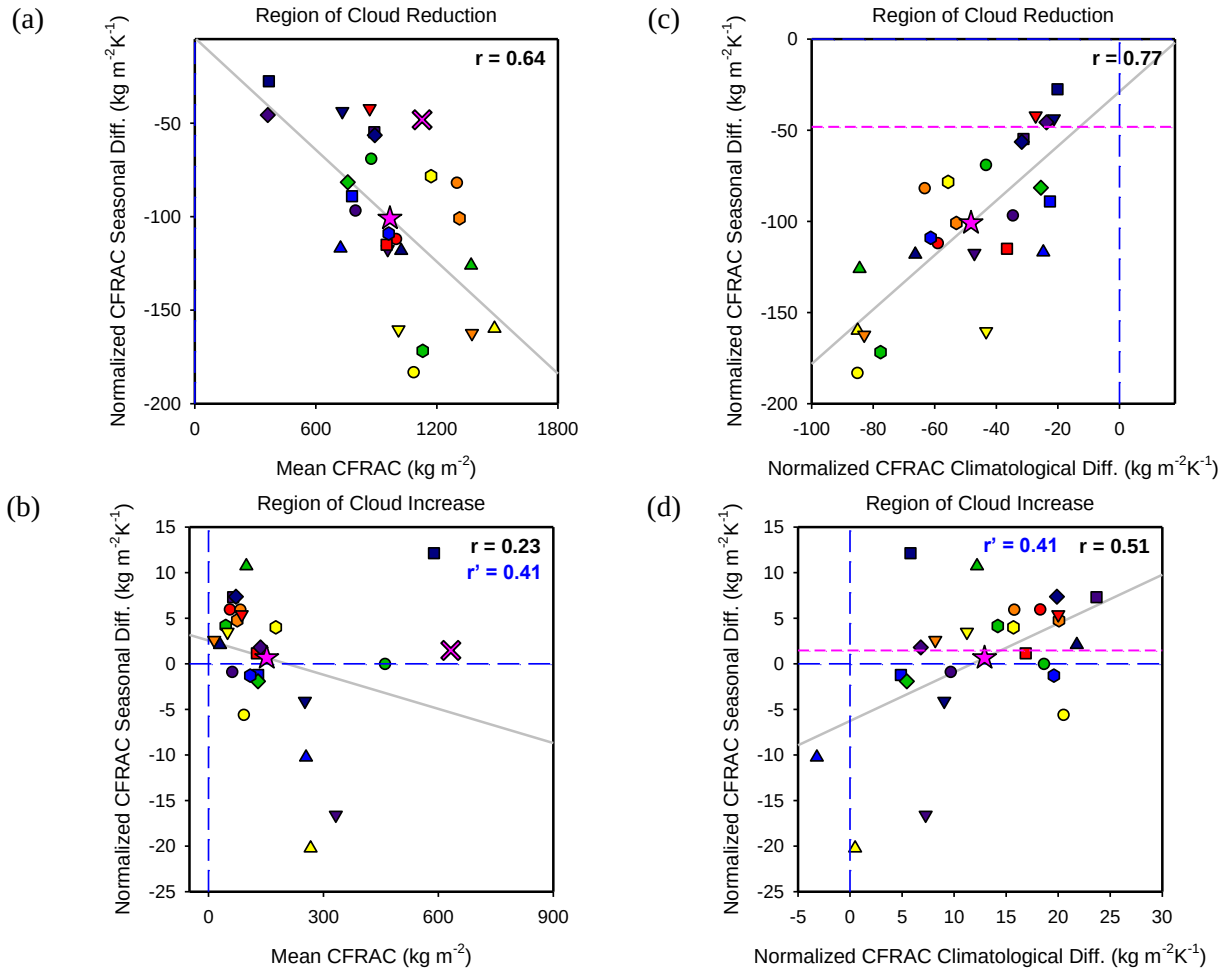

Figure 3.13 : Scatter plots showing the relationship between SH mid-latitudinal Mass weighted (a) and (b) Temperature normalized Seasonal change (y-axis) in kg/m^2/K and Mean values (x-axis) in kg/m^2 of cloud fraction for 25 CMIP5 models (key in Figure 3.6) in the layers of Seasonal Cloud reduction and Cloud Increase respectively and (c) and (d) between Mass weightedTemperature normalized Seasonal change (y-axis) and Climatological difference (x-axis) in cloud fraction (kg/m^2/K) in the layers of corresponding Cloud reduction and Cloud Increase respectively. Observed values are indicated by pink cross in (a) and (b) and pink dashed line in (c) and (d). Grey solid lines represent the linear regression fit. Dashed blue lines indicate the zero x- and y-axes while Correlation coefficients are noted at top right corner in each plot. Spearman's rank correlation coefficient also indicated for (b) and (d) in blue.

Chapter 4

Co-variability of Seasonal and Climatological Change in Mid-Latitudinal Cloud Hydrometeors

In the previous chapter it was established that seasonal variability in cloud fraction exhibits a strong correlation with long-term cloud fraction changes in the mid-latitudinal belt. However, rather than the amount of cloud or cloud fraction, it is the cloud hydrometeor content (i.e. cloud ice and cloud liquid water) that has a greater bearing on the radiative properties of clouds. Based on its relevance to climate change research, constraining cloud radiative forcing is one of the overarching goals of this dissertation. In this chapter, the next step towards this goal is taken, first, by determining model biases in simulating mean and seasonal changes in cloud hydrometeors as compared to observations. This is followed by a demonstration of the co-variability of mean, seasonal and climatological changes in cloud hydrometeors.

4.1. Data and Models

Long-term changes in cloud ice, cloud liquid and total cloud hydrometeor content were computed for the same set of 25 CMIP5 GCMs listed in Table 1. Monthly averaged three-dimensional cloud hydrometeor data from each model was interpolated onto a common longitude-latitude-pressure level grid. The differences were then computed between the annual averages of two decades, 2090-99 (future) and 2010-2019 (present) from the RCP8.5 scenario runs. Cloud hydrometeor climatological variation were also computed using the difference between 10 years (1990-1999) of amip control and amip4K runs for 12 GCM's and amip control and amipFuture runs for 10 GCMs to support the findings from RCP8.5 datasets.

Seasonal changes in model cloud hydrometeor (ice, liquid, liquid+ice) content were calculated for all the models between the summer months of JJA (DJF) and winter months of DJF (JJA) for the Northern (Southern) hemisphere from 2006 – 2010. An ice, liquid and total hydrometeor climatology for these four years was also constructed to generate model mean values.

Monthly averaged observational cloud hydrometeor data were obtained from the C3M dataset from July, 2006 to June, 2010. Re-analysis surface temperature and surface pressure data from ECMWF-Interim dataset were employed to supplement this observational data. The hydrometeor product from C3M models had to be processed further due to a difference in the unit used between them and the hydrometeor product from CMIP5 models. In the GCM output, cloud ice content (for example) is expressed as mass fraction of cloud ice in air which is calculated as the mass of cloud ice in the grid cell divided by the mass of air and the mass of water in all phases within the same cell. The observed cloud ice content however is expressed in density units of kg/m3. To enable comparisons between them, the observed values of cloud hydrometeors were converted into mass fraction units as used in the models. For each grid cell, the ice and water density values were divided by the sum of air and ice+water density in that grid.

For cloud hydrometeor products, CMIP5 GCM satellite simulator output was not available. So the satellite product was directly compared with the GCM output. However, similar comparison of cloud hydrometeor profiles from LMDZ5 GCM satellite simulator output and satellite data product (CALIPSO-GOCCP) have been conducted in the past (Cesana and Chepfer, 2013) which will be referenced in this study..

4.2. Mean and Seasonal difference profiles of Cloud Hydrometeors

Using the four-year cloud hydrometeor climatology from C3M data, a zonally averaged pressure-latitude section of mean cloud ice, cloud liquid and total cloud hydrometeor (sum of cloud ice and liquid) is computed as shown in Figure 4.1(a)-(c). CALIPSO-GOCCP satellite product also provides information about cloud ice and water expressed in terms of ice cloud fraction and water cloud fraction respectively. Zonally averaged vertical section of these variables have also been

plotted in Figure 4.2(a) and (b) to corroborate the C3M profiles. In the same manner, vertical sections of mean cloud hydrometeors were generated for each CMIP5 model and then summed over to obtain the ensemble averaged pressure-latitude section of mean cloud hydrometeor, shown in the Figure 4.3(a)-(c).

A comparison of the model ensemble mean and observation profile reveals some differences for the cloud ice content. In the case of cloud liquid water however there are very large discrepencies that carry over to total cloud hydrometeor. Due to the non-availability of COSP outputs for cloud hydrometeors, it was not possible to verify if the gross overestimation of cloud water by models as compared to observation is a true model deficiency or an artefact of satellite-model data incompatibility. However, Cesana and Chepfer (Cesana and Chepfer, 2013) compared ice and water cloud fractions between satellite simulator outputs and CALIPSO-GOCCP data and revealed that model biases in cloud water are a real feature (Figure 4.4, middle column), although the differences may not be as large as seen when directly comparing with GCM output. The overprediction of cloud water in the low cloud levels in the mid-latitudes and subpolar belts is seen in both the GCM and the GCM simulator outputs.

A comparison of the cloud ice content between model mean and observation exhibits overestimation by models in the lower atmosphere, poleward of 45 degree latitude in both NH and SH. Overestimation is also seen at higher altitudes in tropical belts. These features are also seen in the ice cloud fraction comparisons of Cesana and Chepfer (Cesana and Chepfer, 2013). Overall the CMIP5 models perform better in simulating mean cloud ice than mean cloud water content.

Next, the seasonal change in cloud hydrometeors is computed between four seasonal cycles of JJA and DJF months using the C3M data with JJA-DJF for NH and DJF-JJA for SH. The pressure-latitude zonally mean profiles of observed seasonal variability in cloud ice, cloud liquid and cloud total hydrometeor are shown in Figure 4.5 (a), (b) and (c) respectively. Seasonal differences in cloud hydrometeors are also computed for all the 25 CMIP5 models listed in Table 1. Ensemble mean sections of seasonal variation in cloud hydrometeors are shown in Figure 4.5 (d), (e) and (f) respectively. Regardless of the biases between model and observational profiles, some common features dominate the seasonal difference patterns in both the data sets. In the mid-latitudinal belt, for example, which is defined in this study to range between 30°S - 60°S and 30°N

- 60°N, seasonal cloud hydrometeor (both ice and water and their sum) difference shows a strong negative tendency over a large portion of the vertical column. The negative tendency column is larger for cloud ice and both models and observation very nearly concur on both its extent and magnitude. For cloud water however, observational tendency appears much subdued than model mean. Over-estimation of cloud water by the models is reflected once again in their overestimation of cloud water seasonal variation. The negative tendency completely reverses in sign at higher atmospheric levels. The height at which the tendency flips sign varies between cloud ice and cloud water on one hand and between observed changes and model simulated changes on the other. In the case of cloud water the transition is achieved at a lower altitude level than ice which is understandable given that ice clouds abound at higher levels and water clouds at lower levels of the atmosphere. In the polar belt, cloud water shows a tendency to increase with warmer climate at low cloud levels. This is seen in both model mean and observation. Presence of a narrow belt of positive tendency near the surface is seen in the model mean cloud water profile poleward of 20 degree latitude in both NH and SH which is totally absent in the observed cloud water seasonal difference.

4.3. Climatological changes in Cloud Hydrometeors

Chapter 3 demonstrated the presence of a robust correlation between cloud fraction changes during the seasonal transition from winter to summer and long term climate shift towards a warmer climate in the mid-latitudinal belt. Based on this relation, model biases in seasonal variation of cloud could be used to indicate possible biases in model projections of clouds in the future climate. In this section and the next, the possibility of relating seasonal and climatological changes in cloud hydrometeors is investigated with the aim of exploiting their relationship to constrain future projections.

Climatological difference in cloud ice, water and total hydrometeors have been computed between the future (2090-99) and the present (2010-19) decade for each of the models and averaged over to obtain the ensemble mean. The pressure-latitude distribution of the ensemble zonally averaged climatological change in cloud ice, cloud liquid and their sum is shown in Figure 4.6(a), (b) and (c) respectively. The climatological change in cloud ice shows distinct similarities

with its seasonal change analogue in the mid-latitudes. Similar to the seasonal change, a negative tendency region covers most of the mid-latitude atmospheric column with positive tendency near the top. The pattern of cloud water change also exhibits similarities between the seasonal and climate change sections with a narrow positive tendency layer at the bottom, a shorter negative tendency region in the mid-levels capped by a positive tendency top layer. The viability of the pattern of changes obtained using model data from RCP8.5 runs is verified by constructing similar vertical sections of long term climate change using amip, amip4K and amipFuture runs. The relevant plots are shown in Figure 4.7. Since the similarities are mostly restricted to the mid-latitudes, futher analysis is carried out only in those belts. As in the case of cloud fraction, seasonal difference in the tropics does not appear to present any strong relationship with climatological change in cloud hydrometeors.

4.4. Co-variability in Cloud Hydrometeors

While a comparison of the ensemble averaged cloud hydrometeor sections provide qualitative evidence of interrelationship between climatological and seasonal cloud variable changes, further quantitative assessment is required to substantiate these findings. The following analysis was thus carried out in order to emphasize the observed correlation between seasonal and climatological hydrometeor changes in climate models and also to determine any existing relationship between the aforementioned seasonal change and the mean values of cloud hydrometeors. For each model, two cross-sections were used, encompassing the 30° to 60° latitudes and spanning the entire atmospheric column from surface to 100hPa pressure level, representing the NH and SH bands. Within each of these sections, a mass weighted vertical average of the mean and the change in cloud hydrometeor value, both seasonal and climatological, was computed at every latitude and then averaged over. For the mean and climatological difference in hydrometeors the values in box_nh and box_sh were summed over while for the seasonal variability box_sh values were subtracted from box_nh. All difference values were normalised using the mean surface temperature difference pertaining to that latitudinal belt. A set of cloud hydrometeor (ice, liquid and their sum) mean values (in kg/m^2) and their normalized seasonal and climatological changes (in $kg/m^2/K$) in the mid-latitudinal atmospheric column were thus

generated for each model. Pairs of a) mean and seasonal difference and b) seasonal and climatological difference were then used to obtain a scatter plot displaying model spread in the two parameters and the degree of their covariability. The observational values of mean cloud hydrometeor amount and its seasonal change were also computed and have been indicated in the relevant plots using a pink X-mark. For some of the scatter plots that exhibited presence of large outliers, the correlation coefficients were re-computed using Spearman rank Correlation method.

Improved values of correlation coefficients were obtained upon dividing the total atmospheric column into different cloud levels and examining the cloud behaviour within them individually. Cloud classification into high, mid and low level clouds on the basis of pressure levels was carried out as in the case of cloud fraction by using the ISCCP cloud classification scheme. A detailed discussion of the observed interrelationship between total column and low-, mid-, high- level cloud ice, cloud liquid and cloud hydrometeor changes follows in the next sub-sections.

4.4.1. Cloud ICE

Figure 4.8(a) exhibits the scatter plot between model values of mean cloud ice and its seasonal difference in the whole atmospheric column. Based on the square root value of regression coefficient r^2 from the linear fit, the two variables appear to be very well correlated, implying that models with higher mean cloud ice show larger seasonal decrease. Further, the ensemble mean value of model simulated ice cloud amount also compares well with the observed value. However, individually the models appear to generate a range of values for cloud ice. For example, all versions of the IPSL (IPSL-CM5A-LR; IPSL-CM5A-MR; IPSL-CM5B-LR) and GISS models (GISS-E2-H; GISS-E2-R; GISS-E2-R-CC) produce very large cloud ice while models like FGOALS-g2, inmcm4 and CESM1-CAM5 represent the lower end of the spectrum producing low cloud ice amount. Thus, even though the ensemble mean follows the observational value closely there still exists significant spread among CMIP5 model mean cloud ice simulation.

Cloud Ice mean climate and seasonal difference correlations are weak in the high and moderate in the mid level clouds (Figure 4.8(b) and (c)) possibly because of the offsetting signs of

ice variation in the middle and upper troposphere as shown in Figure 4.5(d). In these levels, removing large contributions from outlier points further weakens the relationship. The correlation is very strong in case of low clouds (Figure 4.8(d)), and it is the ice change in low clouds that is responsible for the high correlations in total column ice change in Figure 4.8(a) Ensemble model mean cloud ice agrees well with observation in the mid-level but appears to be slightly overpredicted for the high- and low- clouds.

However, the models continue to show a large spread all around the mean value for mid-level clouds while for the low clouds majority of the models overpredict cloud ice content. The spread in mean climate values is somewhat smaller for the high level clouds except for the previously mentioned set of six IPSL and GISS models. While IPSL model cloud ice are consistently high at all levels, GISS overpredicts mostly at high and low levels. It may be inferred at this point that these models are responsible for the ensemble mean and observation discrepencies in Figure 4.8(a) and (d).

The relationship between seasonal and climatological cloud ice changes is examined next in the correlation plots of Figure 4.9(a)-(d). Both the total column and the high cloud ice seasonal changes do not seem to be strongly correlated to their climatological counterpart, yet, the mid and low level clouds exhibit very high correlation values. An intermodel discrepency in the sign of change is seen for both seasonal and climatological difference in the total and high cloud ice. For seasonal change in total column cloud ice (Figure 4.9a)), both the ensemble mean and observed values (indicated by the pink dashed line) predict cloud reduction of comparable magnitude as do a vast majority of the models. For the climatological change on the contrary, both total column cloud ice increase and decrease appear to be prevalent among the models. This spread is largely caused by the discrepencies in high clouds (Figure 4.9(d)). For ice in high clouds (Figure 4.9(b)), climatological change exhibits unanimous increase but seasonal change values straddle between positive and negative change. Observation and ensemble mean also differ in the sign of high cloud ice change.

Seasonal change in mid level cloud ice (Figure 4.9(c)) in the models seem to show a very small difference compared to observation. In the case of low clouds (Figure 4.9(d)), cloud ice decreases both seasonally and climatologically while the seasonal reduction is somewhat

overpredicted by a majority of the models as compared to the observed value. This compensates for overprediction of mean cloud ice increase by models seen in Figure 4.8(b) for high clouds.

In the description of vertical sections of cloud ice change in Figure 4.5 and Figure 4.6, it had been discussed that the sign of seasonal and climatological differences abruptly change in the upper reaches of the atmosphere. The height at which this transformation takes place however varies from latitude to latitude, seasonal change to climatological change, and p from one model to the other as well. Therefore, a rigid compartmentalization into low, mid and high clouds may not bring out the significant features of the cloud ice difference profile as is reflected in the low correlation values obtained above.

The alternating pattern of cloud ice changes in the mid-latitudinal belt warrants a separate treatment for the ice reduction and ice increase regimes. At each latitude the pressure level at which the change in cloud ice flips sign is recorded. This level marks the upper boundary of the cloud reduction region and the base for the cloud increase region. Mass weighted cloud ice reduction below the critical height and cloud ice increase above it are then computed for the entire belt for each model. Symmetry in the pattern of both climatological and seasonal difference allows the merging of NH and SH values. The correlation of model seasonal and climatological cloud ice reduction in the lower mid-latitudinal column is shown in Figure 4.10(a). The covariability of pattern seen in the vertical section plots are strongly affirmed by the high correlation coefficient obtained here. Models with larger reduction of cloud ice in the seasonal variation also have larger reduction in the climatological change. While the ensemble mean of ice reduction is close to the observations, there is a large spread among the models.

Upon integration of the ice increase in the upper troposphere, very high correlation values were also found between the seasonal variation and climatological variation as presented in Figure 4.10(b). A recomputation of the correlation in the scatter plot using Spearman's method re-affirmed the presence of relationship despite the model clusters in different parts of the plot. Therefore, the interrelationship between seasonal and climatological changes in cloud ice, which comprise of decrease in ice content through most of the vertical atmospheric column and increase at the very high levels, is strongly established using this treatment.

In the cloud decrease region, the ensemble mean of the models agrees well with the observed changes although most models exhibit a cloud decrease value less than the observation. What brings the ensemble mean up close to the observation is the high cloud ice change seen in all three versions of the IPSL and GISS models. Based on the relation with climatological change, models with very large (IPSL and GISS) and very small (most other models) ice change between seasons also project larger and smaller climate changes in ice respectively. The observational value here gives an estimate of the range of cloud reduction that may be expected in the future which is larger than what most models predict. In the regime of cloud increase, model mean slightly overestimates the magnitude of increase. In this region, the GFDL and GISS models predict much larger cloud ice increase thus contributing to the ensemble mean and observation mismatch. Magnitude of IPSL cloud ice increase does not appear to be as high as ice reduction.

Next, the presence of correlation between the seasonal ice change and mean ice values among the models is investigated. In the reduction region, (Figure 4.10(c)), the mean cloud ice amount was also found to co-vary with seasonal change thus translating the mean cloud ice biases to seasonal and consequently climatological change projections. In the cloud increase region, Figure 4.10 (d),the correlation was comparatively less, possibly due to the contribution from a particular cluster of models. Computation of the Spearman correlation coefficient indicated that the correlations were still high in this case. The IPSL models for example, do not simulate an excess of seasonal increase, yet the mean cloud ice in the increase regions is quite high. The GISS and GFDL models on the other hand exhibit very large seasonal difference which are not proportionate to the model mean ice excesses.

In summary, high correlation is found between the seasonal variations and mean values of cloud ice in the models. This seasonal variation is primarily driven by cloud ice in the low clouds. There is also a very good correlation of the seasonal and climatological low-cloud ice variations. The ensemble mean of the models captures the observed value of mean cloud ice and seasonal variation, but the models display a wide array of differences. Models with the largest low-cloud ice show the largest seasonal variation and largest reduction of cloud ice in the climatological variation.

4.4.2. Cloud Liquid

A quantitative analysis of the relationship between mean cloud liquid and its seasonal and climatological variation for the total atmospheric column as well as for low-, mid- and high- cloud levels was performed next. Figure 4.11(a)-(d) present the correlation scatter plots between mean cloud liquid and its seasonal variation for various regions. For the total column cloud liquid, the mean and seasonal changes do not display any interrelationship. As expected from the vertical section comparisons, the ensemble model mean cloud liquid is overpredicted compared to the observations. This is true not only of the total column cloud liquid but also for all the other cloud levels. Absence of correlation is also seen at the low cloud levels while at the mid level correlations are only slighlty better. However, this was also ruled out following the low correlation coefficient obtained using Spearman method. The strong correlation at high cloud levels does not hold much significance due to the scant presence of liquid clouds at those levels. It is also seen that the seasonal variation of total cloud water is dominated by that of low clouds, for which no relationship is found between the seasonal variation and mean value.

Even though the mean and the seasonal change in cloud liquid do not show any relationship, their seasonal and climatological changes are still strongly correlated as displayed in Figure 4.12(a)-(d). High correlation coefficients from linear fits are strong evidence of the seasonal and climatological covariability for the total column as well as low-, mid- and high-cloud levels. Despite the presence of outliers, correlation values computed using both Pearson and Spearman correlation methods still agreed well with each other. The straddling of cloud liquid change values between positive and negative sign is a significant feature in the total column correlation plot. It is very likely a contribution from the lower and mid-cloud levels where models show dissent in the nature of seasonal cloud liquid changes. In these levels, cloud liquid increase and decrease both appear to be equally likely among the ensemble of models. Both the model mean and the observed values however predict a small cloud liquid increase due to change in seasons, observed change being further smaller in magnitude.

The total column cloud liquid change patterns are primarily dominated by the patterns in low and mid cloud liquid changes as liquid clouds are more abundant there. In all three regions as shown by the Figure 4.12(a),(c) and (d), majority of the models predicting increase due to seasonal

change also predict long term climatological increase and vice versa. The magnitude of increase in the models is typically larger than the observed increase which may be a consequence of the high mean cloud liquid estimation in models. The model CMCC-CESM is a prominent outlier in these plots predicting larger increases in both cases. Its behavior at mid and high levels are however comparable to that of other models.

At the high cloud levels (Figure 4.12(b) and (c)), cloud liquid content increases both seasonally and in the long term. At these levels, most of the models predict a change in magnitude slightly less than the observation and exhibit a small spread about the model mean value. A few outlier models are present in both cases but they are not common to the two regions. These outliers increase the model mean values and contribute to their difference from observations. The key findings from this section include the strong relation between seasonal and climatological changes in cloud liquid, dissent among models in the sign of change although the model mean and observation concur and finally model values of seasonal change exhibit a spread about the observation with larger positive or negative magnitudes.

The difference in sign of cloud liquid change among models necessitates a closer look at the vertical profiles of change to determine if there are intermittently sign changing patterns as seen in the case of cloud ice. Examining the nature of variations in midlatitudinal belt in Figure 4.5, one may see that the atmospheric column can again be split into positive and negative tendency regimes for both seasonal and climatological changes. These patterns are more prominent in the case of ensemble model mean values than the observation but the overall nature of variation is the same. A decreasing cloud liquid region is topped by a layer of increase that extends to the very top of the atmospheric column. In the case of the models, a narrow belt of positive tendency is seen at the bottom of the column which is very faint in the observations. This would be treated separately in a later section. For the cloud liquid seasonal and climatological changes, the atmospheric column is split into two parts, a reduction region at the bottom and an increase region at the top. The boundary height that divides the two regions is determined separately for each model, at each latitude and independently for seasonal and climatological changes. Mass weighted cloud liquid change within each region is then computed for the models and observation.

Figure 4.13 (a) and (b) display the correlation between seasonal and climatological cloud liquid changes in these two regions while Figure 4.13 (c) and (d) exhibit the correlation between mean cloud liquid content in the specific regions with their analogous seasonal difference.

Cloud liquid seasonal and climatological changes in models show strong correlation in both the liquid reduction and increase regions. Spearman's rank correlation coefficients show slightly lesser values than the Pearson correlation coeffcients, however all the relationships are still significant at the 1% level. Correlation appears to be better for the increase regimes as opposed to reduction regimes as seen for cloud ice changes. Large seasonal cloud liquid changes in the model CMCC-CESM which also forecasts large climatological cloud liquid increase likely contributes to the high correlation value. In the cloud liquid reduction regions, the models bcc, CCSM4, CESM1-BGC, CSIRO-Mk and NorESM emerge as outliers displaying large cloud reductions seasonally. These five models also exhibit a large mean cloud liquid bias in Figure 4.13(c) which translates into large seasonal difference biases. Based on these relationships it may be deduced that the seasonal changes in cloud liquid covaries with their long term climatological changes such that the biases in cloud liquid seasonal change predictions carry over to the future projections of cloud liquid. Model overprediction of both seasonal cloud liquid increase and decrease as compared to observations is evident from the Figures. Thus, models are over sensitive to warming in terms of change in cloud liquid amount. Since this is a direct comparison of the models and observational values, the differences may be more exaggerated than they truely are. However, basic signatures of model overprediction of cloud liquid at the mid-latitudes based on analysis of satellite simulator output have also been seen in the past (Cesana and Chepfer, 2013). Correlation between mean and seasonal change in cloud liquid are also quite robust based on Figure 4.13(c)and (d).

The presence of a narrow belt of cloud liquid increase near the base of the atmosphere was detected in the seasonal cloud water change sections. A modified zonewise segregation of the atmospheric column into two regions was done to incorporate this layer. Correlation within this modified layer, which comprises the cloud decrease regions as well as the cloud increase in the surface layer is shown in Figure 4.14(b) compared with the correlation plot for only cloud liquid reduction region as before in Figure 4.14(a). The result is a two-fold improvement in both strength of correlation as well as proximity of model mean to observed values. This indicates that models have a tendency of being oversensitive to warming in terms of cloud water reduction accompanied

by a conspicuous cloud water increase at the very low levels. The combination of the two, involving some degree of compensation, is however close to the changes in observation under similar warming conditions.

In summary, the seasonal and climatological cloud water changes are dominated by those from low and mid level clouds. There is no systematic relationship between the seasonal variations of liquid water and the mean values among the models, but there is a strong positive relationship between the climatological variations and seasonal variations. The ensemble means overpredict the magnitudes of cloud increases in the middle troposphere and reductions in the low troposphere, with the net effect of overprediction of the cloud water increase. Models differ from each other in the sign of total cloud water change both seasonally and climatologically.

4.4.3. Total Cloud Hydrometeors

Seasonal and climatological changes in mid-latitudinal total cloud hydrometeors were also analyzed to check for the presence of correlations. Total cloud hydrometeor, computed as the sum of cloud ice and cloud liquid content, provides a more realistic estimation, particularly at low- and high-cloud levels, where either water or ice clouds are scarce. As expected, cloud hydrometeor correlations at low-level are dominated by cloud water contribution while cloud ice dominates at higher levels. The correlation between mean cloud hydrometeor and its seasonal variability for the total column and the high, mid and low level clouds are shown in Figure 4.15(a)-(d), while the corresponding plots showing seasonal and climatological co-variability are presented in Figure 4.16(a)-(d). The large bias between observation and ensemble model average value of mean hydrometeor seen in all the cases, originates from cloud water biases discussed before.

Mean hydrometeor values do not appear to correlate well with their seasonal changes except at the mid-cloud levels. This is because the major contribution to the total column value comes from the low level clouds which in turn exhibit a poor correlation for liquid water as discussed before. Nevertheless, high correlation is still seen in the case of the seasonal and climate change across the whole column and at low and mid-cloud levels, which is consistent with the findings in the previous two sections about this relationship and the dominance of lower

tropospheric clouds. Slightly reduced correlation coefficients obtained using Spearman's method are still significant at 1% level.

Model biases in seasonal change are mostly restricted to the upper atmosphere, i.e, mid- and high-levels which possibley owes its origin to the reversal of the sign of change as was seen in the case of cloud ice and water individually. The seasonal change ensemble average in case of low clouds is much closer to the observed value, however, the model points are widely scattered around the average. Therefore, it is difficult to envision any kind of collective behavior of the models with respect to observations.

A note may be made at this point about the performance of the model CMCC-CESM whose low cloud water and consequently low cloud hydrometeor values appear to be far removed from all the other models. A closer inspection of both seasonal and climatological cloud water difference sections for this model reveals the presence of strong positive tendencies at the lower altitudes of mid-latitudinal belt in both northern and southern hemispheres. This contributes to comparatively larger positive values for CMCC-CESM in both x- and y-axes. However, since this feature is seen to be present in both its climatological and seasonal difference alike, this point is not discarded as an outlier.

The ensemble average over the models for high-level clouds indicate that most of the models predict a positive seasonal change in hydrometeors, while the observation shows a negative value far removed from all of them. To resolve these issues, cloud hydrometeor vertical section was also split into separate negative and positive tendency regions. This established a higher degree of correlation both between the mean climate and seasonal variability as also seasonal and climatological changes in regions of cloud hydrometeor reduction (Figure 4.17(a) and (c)). In the regions of positive tendency (Figure 4.17(b) and (d)), typically higher than about 400hPa, the relationships are not very strong. Also, biases in these sections are larger than those in cloud reduction regions.

Based on the high values of correlation, cloud hydrometeor reduction regions are more interesting in terms of examining the biases they exhibit and analyzing how these biases would express themselves in the long term. In Figure 4.17(a), the model mean only slightly overshoots the observation, but, the models in general predict much larger as also much smaller values of

change. Among the models that predict larger change, few were outliers in case of cloud ice (IPSL and GISS) and few others (CCSM4, CESM-BGC etc) in case of cloud water. While, the cloud ice outliers predicted both increased reduction and increased growth, the cloud water outliers that predicted increased reduction did not stand out in terms of the amount of water increase. Here, for cloud hydrometeors, models with large reduction do not have consequent large decrease along the lines of cloud liquid.

4.5. Co-variability of area and intensity of hydrometeor change

An investigation into the nature of cloud ice and liquid change that correlates with its climatological analogue was also conducted. The aim was to determine if it was the change in area of cloud ice/liquid or the change in cloud ice/liquid density that contributed more to the observed correlations. Within each of the cloud reduction and increase regions, the total number of pressure-latitude gridboxes and the sum of the total value of change in cloud hydrometeor was computed. The number of grids gave an estimation of the area of cloud ice/liquid reduction or increase while the ratio of total amount of change to number of grid box would give a measure of the density of hydrometeor change. These plots are shown in Figure 4.18, Figure 4.19 and Figure 4.20 for cloud ice, liquid and total hydrometeors.

In the case of cloud ice, both the area of cloud ice decrease as well as the average reduction amount correlate well. The average cloud ice growth however correlates better than the area of growth. For cloud liquid and cloud hydrometeors, the areas of reduction and increase correlate better than the intensity of growth or reduction per grid box. Therefore, the intermodel differences and the correlations between seasonal and climatological changes are primarily caused by the area rather than the intensity in the zonally averaged distributions.

4.6. Summary

Zonally averaged pressure-latitude sections of seasonal and climatological differences in both cloud ice and liquid revealed significant similarities in pattern in the mid-latitudinal belt. They

were characterized by the presence of negative tendencies at the lower atmosphere with positive tendency regions above it. A detailed investigation of correlations between the mean, seasonal difference and climatological changes in cloud hydrometeors was carried out using CMIP5 model runs for 25 models. The important results from this study are summarized below :

1. Mean cloud ice, their seasonal difference and their long term climatological changes are all well-correlated for the low and mid clouds. Observed mean and seasonal change values match well with the ensemble model mean even though models themselves exhibit a larger spread of values about the mean. Division of the total atmospheric column into cloud ice increase and reduction zones further improved these relationships. Models simulating larger mean cloud ice amounts predict larger seasonal as well as climatological decrease in ice in the lower troposphere regions. In the layers above, seasonal and climatological increases in cloud ice are also well correlated with models slightly overestimating the seasonal increases compared to observations.

2. Mean cloud liquid and their seasonal change do not show any relationship as in the case of cloud ice. However, their seasonal and climatological changes are well-correlated particulaly at the low and mid cloud levels. Models simulate both negative and positive changes in cloud water seasonally with the ensemble mean concurring with the observed seasonal increase in cloud water. Models are over-sensitive to warming in terms of their cloud water change, which is more negative in the reduction regions and more positive in the increase regions as compared to observation.

3. Seasonal and Climatological variations in cloud hydrometeors are well correlated particularly in the hydrometeor reduction regions in lower troposphere. The correlations are found to be more due to the area of change rather than the intensity of change in cloud hydrometeors

Figures

(a)

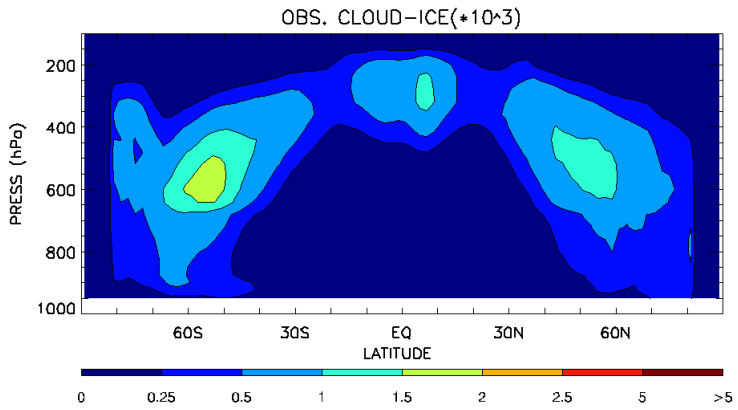

(b)

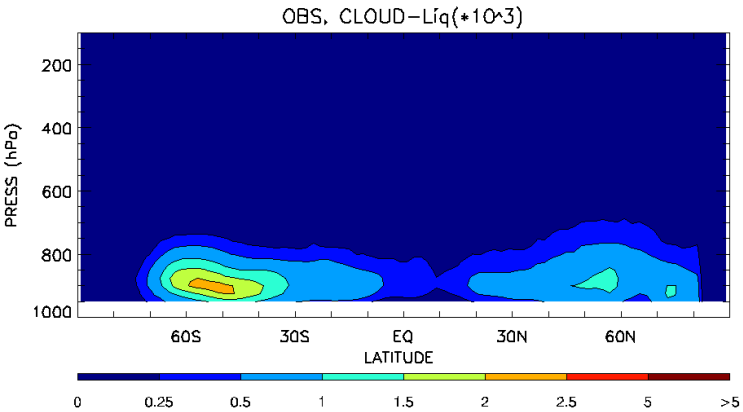

(c)

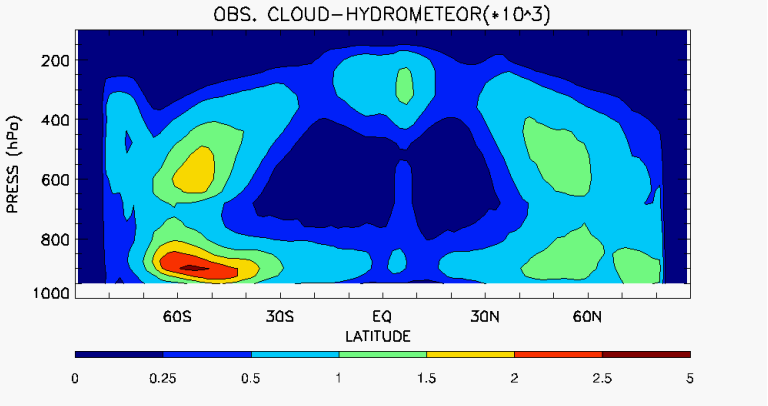

Figure 4.1 : Zonally averaged vertical pressure-latitude section of (a) mean cloud ice, (b) mean cloud liquid and (c) mean cloud hydrometeor (mass fraction percentage in air multiplied by 10^3) from July,2006 to June,2009 using C3M observation dataset.

(a)

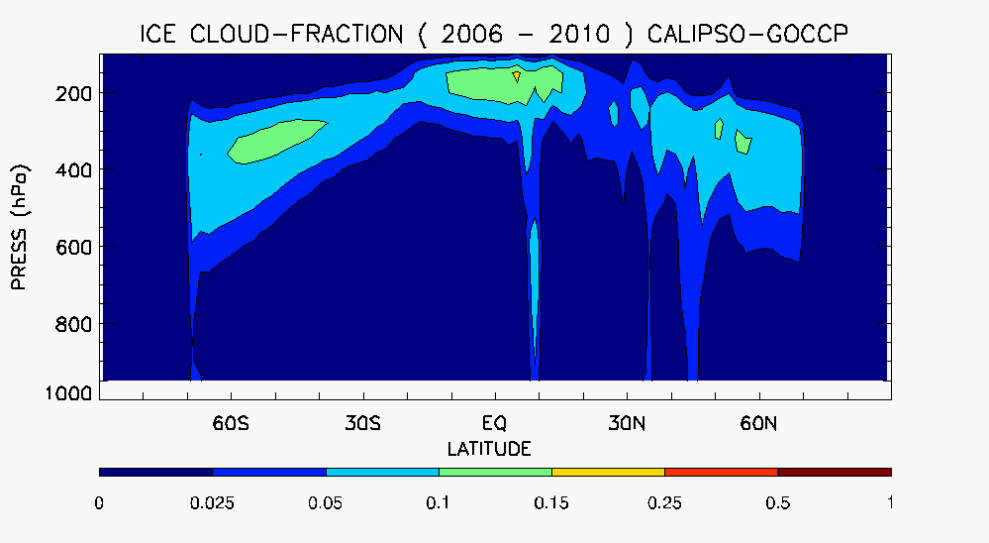

(b)

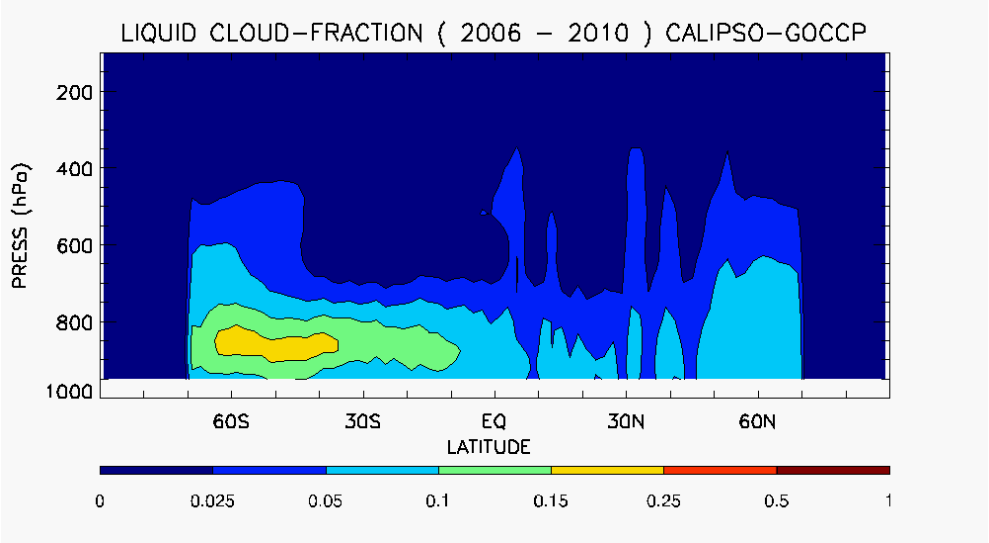

Figure 4.2 : Zonally averaged vertical pressure-latitude section of (a) mean ice cloud fraction and (b) mean liquid cloud fraction from 2006-2010 using CALIPSO-GOCCP dataset.

(a)

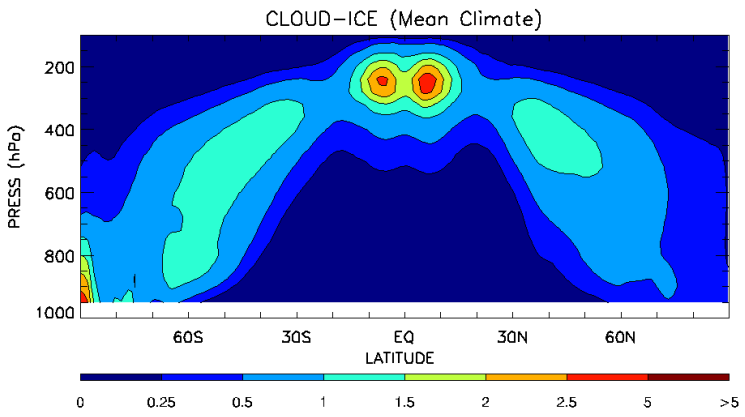

(b)

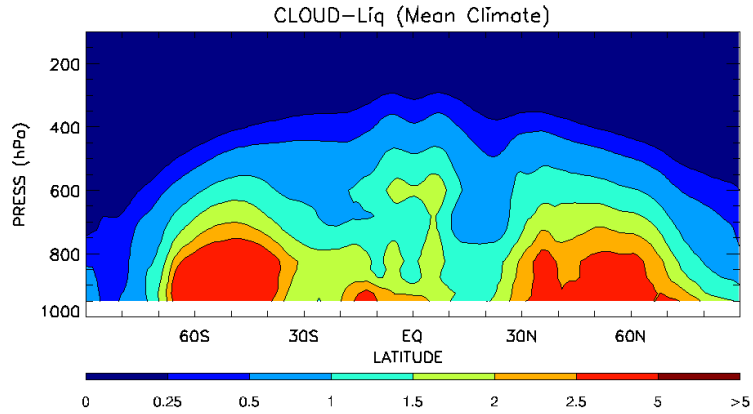

(c)

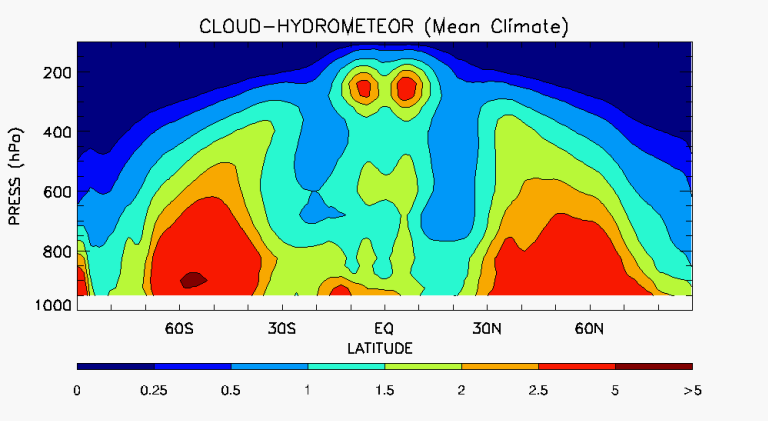

Figure 4.3 : Zonally averaged vertical pressure-latitude section of (a) mean cloud ICE, (b) mean cloud LIQ and (c) mean cloud Hydrometeor (mass fraction percentage in air multiplied by 10^3) from July,2006 to June,2009 using ensemble mean over RCP8.5 runs of 25 CMIP5 models.

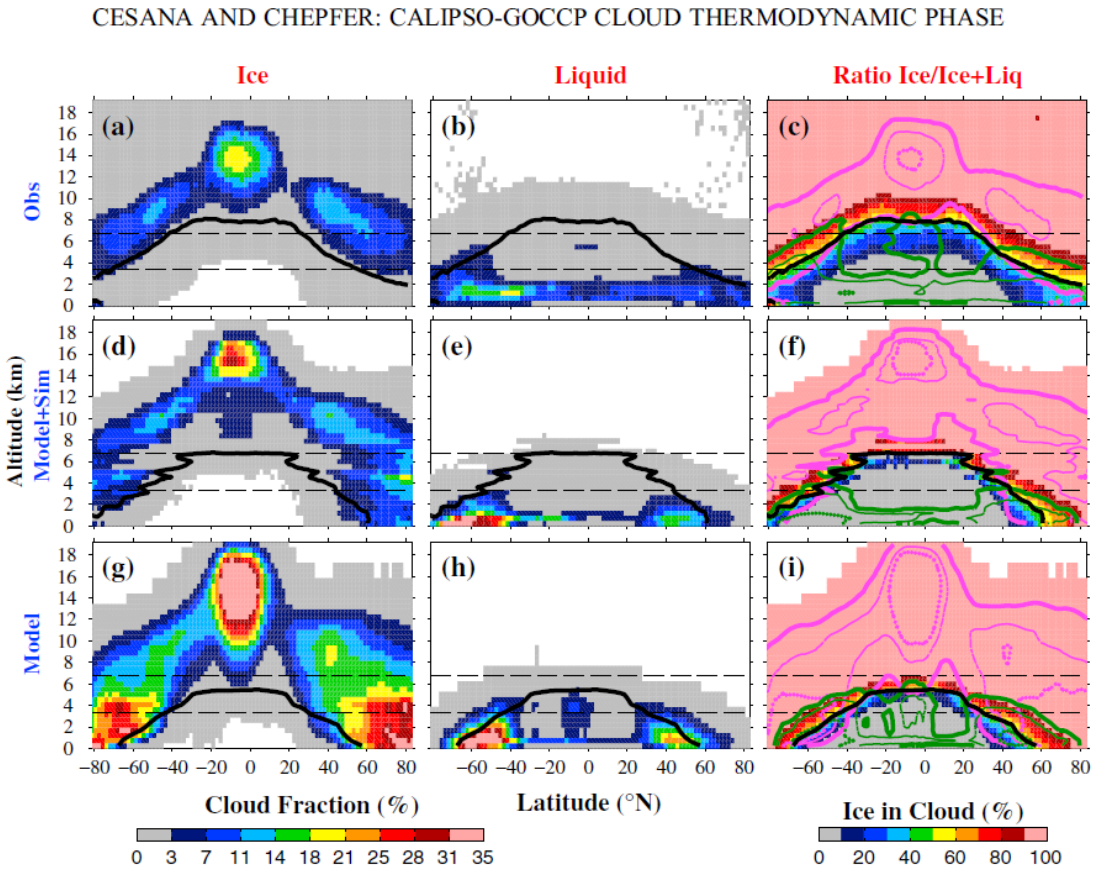

Figure 4.4 : Adapted from Figure 7 from a study by Cesana and Chepfer. The first two columns show the vertical distribution of cloud ice and cloud liquid phase clouds for the months of Jan, Feb and March, in CALIPSO-GOCCP observations(first row), in COSP-Lidar simulator from GCM (second row) and directly from LMDZ GCM (third row)(Cesana and Chepfer, 2013).

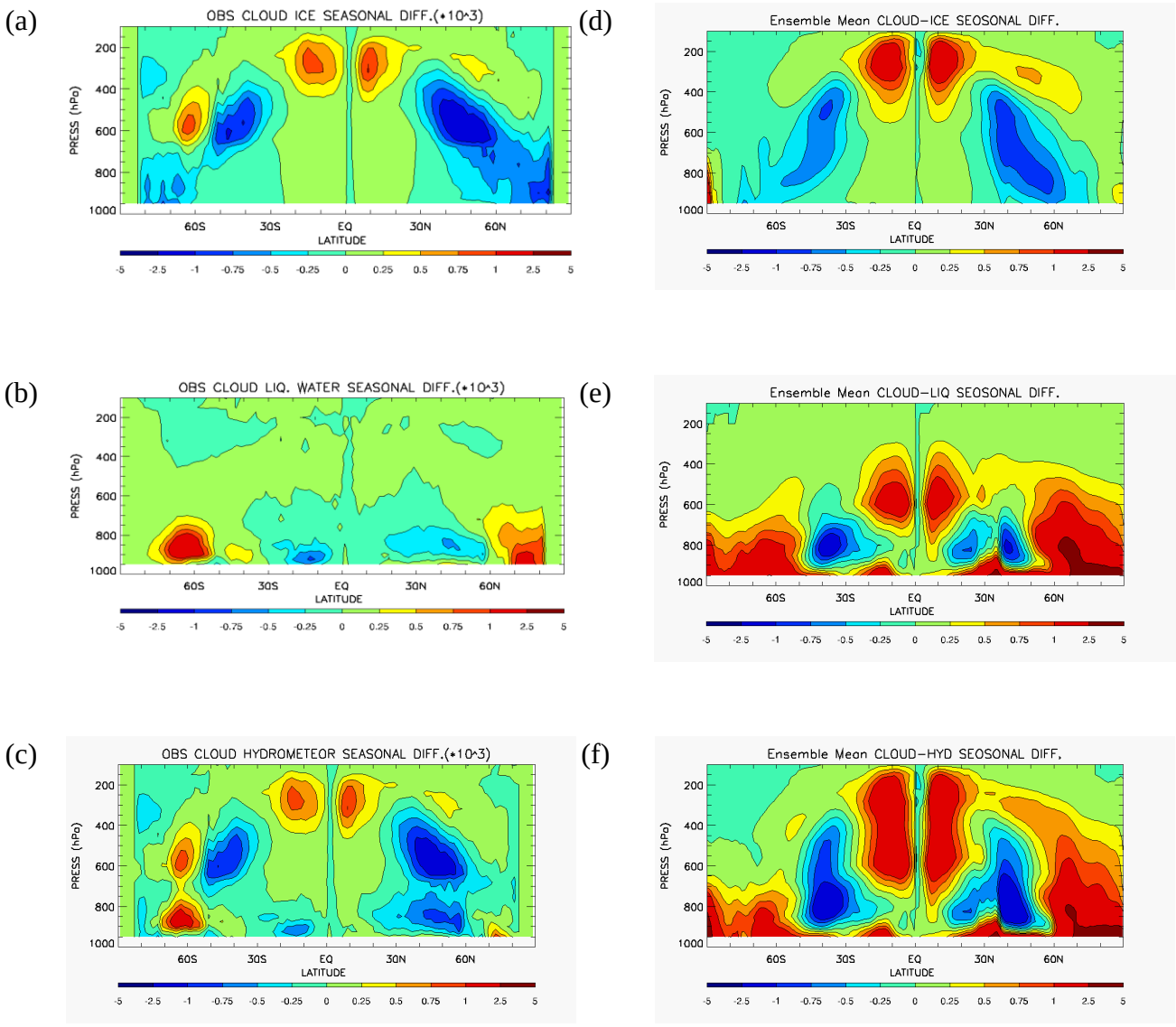

Figure 4.5 : Zonally averaged pressure-latitude section of seasonal difference (JJA - DJF) between July, 2006 - June, 2010 in observed (a) Cloud ICE, (b) Cloud LIQ, and (c) Cloud HYD (mass fraction multiplied by 10^5) and model mean values over RCP8.5 runs of 25 CMIP5 models in (d) Cloud ICE, (e) Cloud LIQ, and (f) Cloud HYD. Seasonal differences in SH have been reversed in sign.

(a)

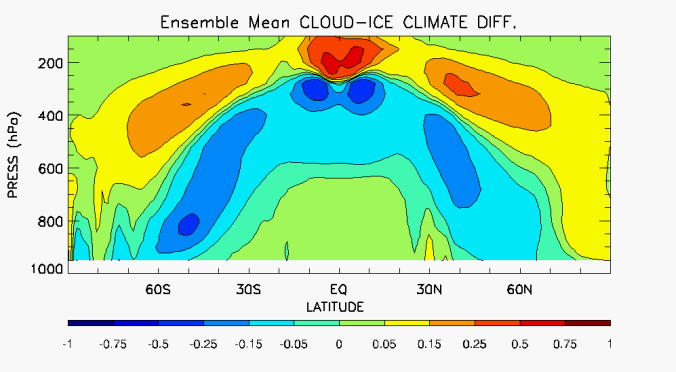

(b)

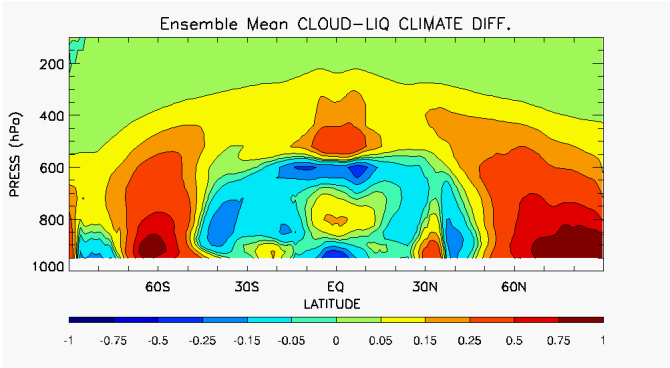

(c)

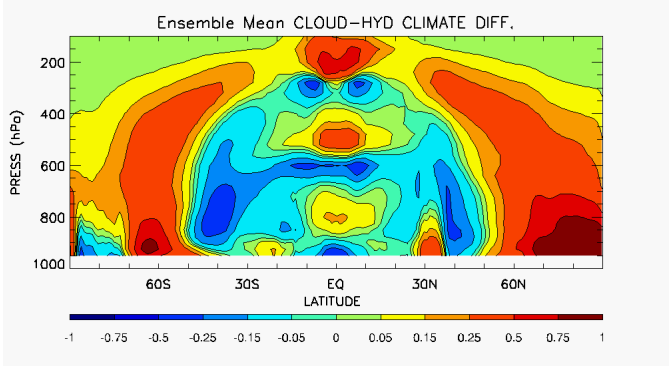

Figure 4.6 : Ensemble mean zonally averaged pressure-latitude section of climatological difference (between 2010-19 and 2090-99) in (a) Cloud ICE, (b) Cloud LIQ and (c) Cloud HYD (mass fraction multiplied by 10^5) over RCP8.5 runs of 25 CMIP5 models.

(a)

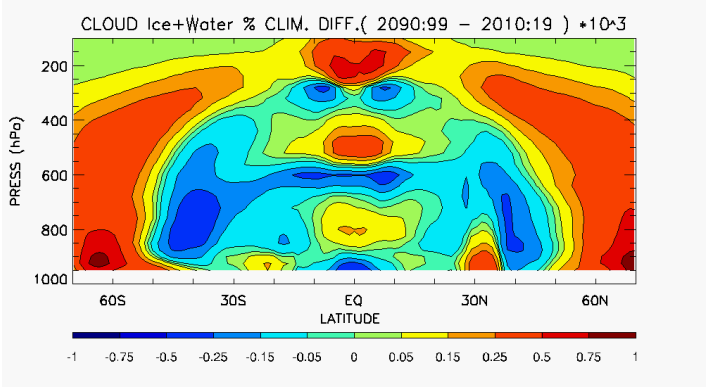

(b)

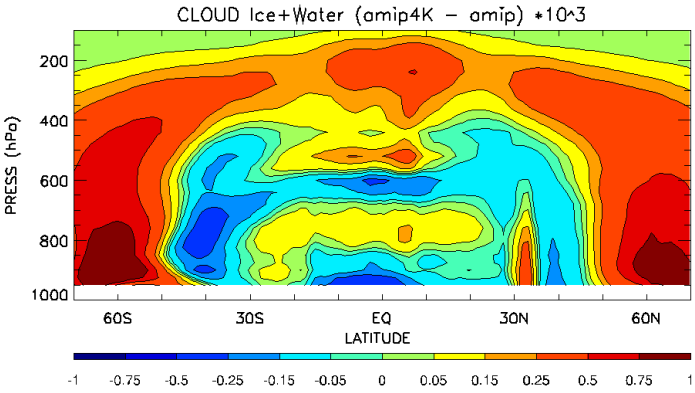

(c)

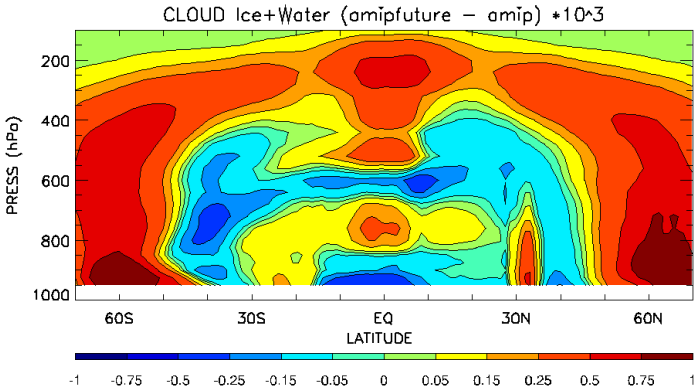

Figure 4.7 : Zonally averaged pressure-latitude section of Normalized (a) ensemble mean climatological difference in total cloud Hydrometeors (mass fraction multiplied by 10^5) between 2010-19 and 2090-99 using RCP8.5 runs of 25 CMIP5 models (b) ensemble mean cloud Hydrometeor difference between amip (control) and amip4K (perturbed) runs over 12 models and (c) between amip(control) and amipFuture (perturbed) runs over 11 models between 1990-1999.

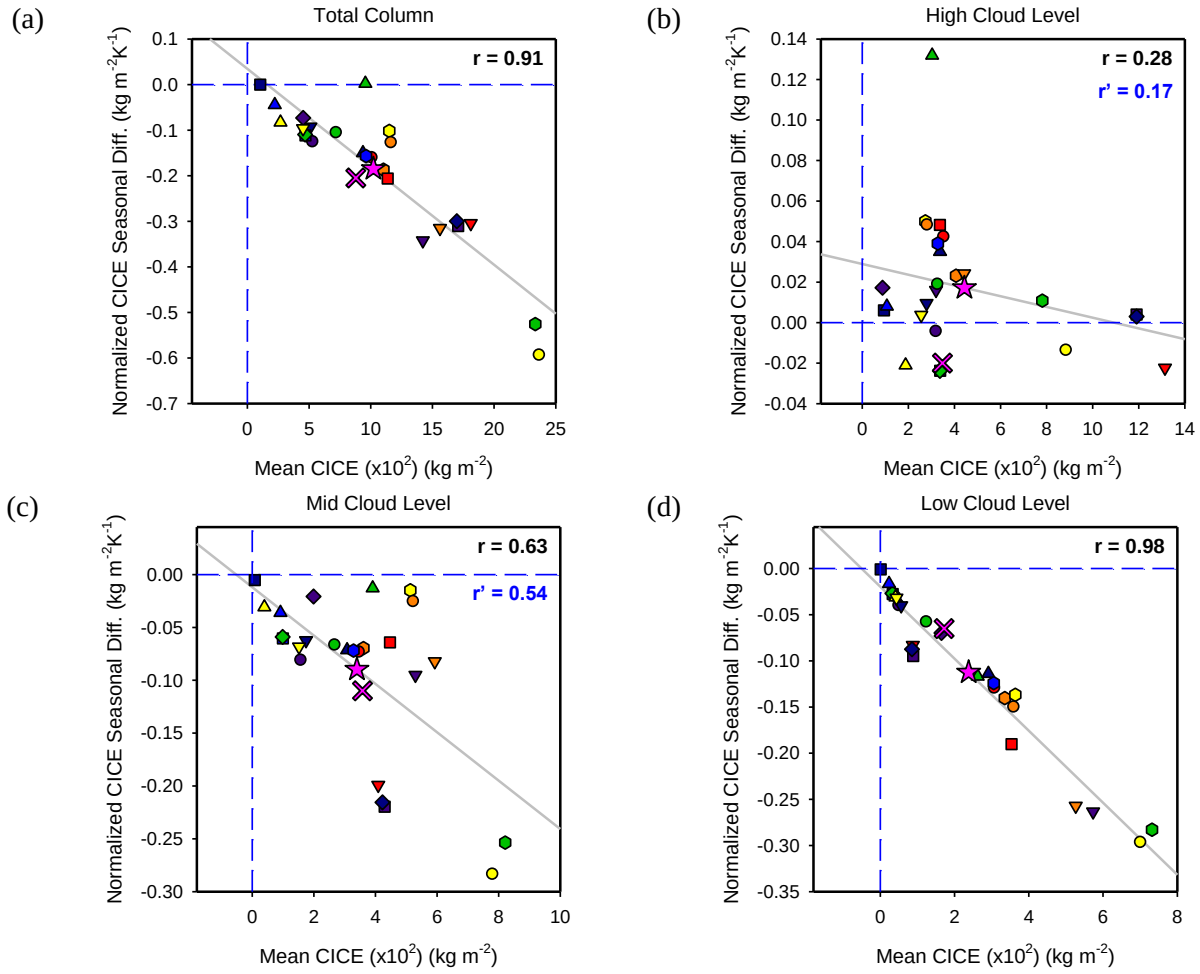

Figure 4.8 : Scatter plots showing the relationship between Temperature normalized Mass-weighted Seasonal change (y-axis) in kg/m^2/K and Mass-weighted Mean values (x-axis) in kg/m^2 of mid-latitudinal cloud ICE mass fraction (*10^2) for 25 CMIP5 models (key in Figure 3.6) in the (a) Total cloud column, (b) High-level clouds (440hPa and above), (c) Mid-level clouds (680 hPa -440 hPa) and (d) Low-level clouds (below 680 hPa). Grey solid line is the linear regression fit. Observed values of Mean and Seasonal change in cloud ICE are represented by pink crosses. Correlation coefficient values (Black: Pearson; Blue: Spearman) are indicated at the top right corner of each figure. Zero x- and y-axes included as blue dashed lines.

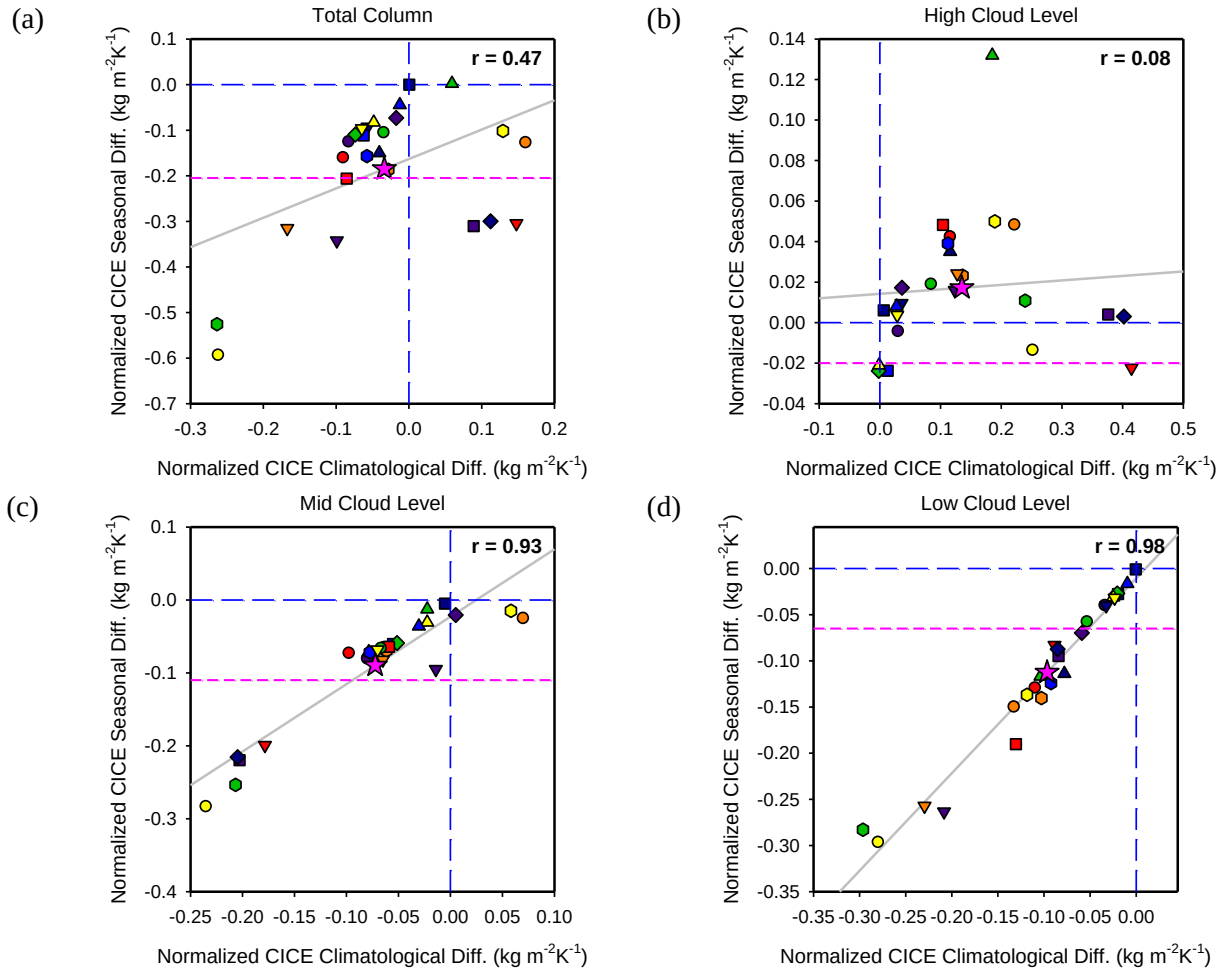

Figure 4.9 : Scatter plots showing the relationship between Mid-latitudinal Temperature normalized Mass-weighted Seasonal change (y-axis) and Climatological difference (x-axis) in kg/m^2/K in cloud ICE mass fraction (multiplied by 100) for 25 CMIP5 models (key in Figure 3.6) in the (a) Total cloud column, (b) High-level clouds (440hPa and above), (c) Mid-level clouds (680 hPa -440 hPa) and (d) Low-level clouds (below 680 hPa). Grey solid line is the linear regression fit. Observed values of Seasonal change in cloud ICE are represented by pink horizontal lines. Correlation coefficient values are indicated at the top right corner of each figure. Zero x- and y-axes are included as blue dashed lines

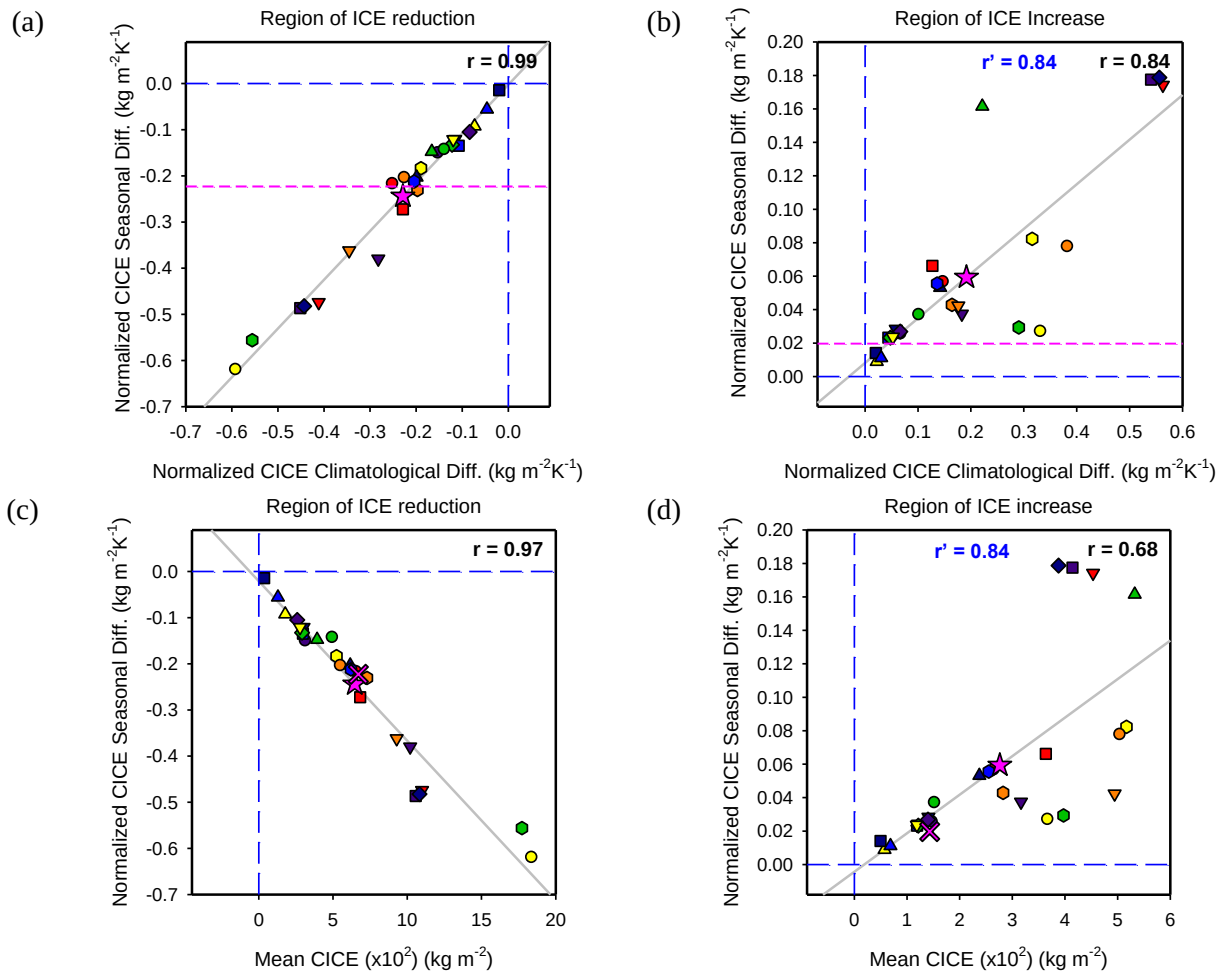

Figure 4.10 : Scatter plots showing the relationship between Temperature normalized Mass-weighted Seasonal change (y-axis) and Climatological difference (x-axis) in kg/m^2/K in mid-latitudinal cloud ICE mass fraction (multiplied by 100) for 25 CMIP5 models (key in Figure 3.6) in the corresponding layers of (a) Cloud ICE reduction and (b) Cloud ICE Increase respectively, and, between Mass-weighted Mean Cloud ICE mass fraction (x-axis) in kg/m^2 and Seasonal change (y-axis) in the layers of (c) Seasonal Cloud ICE reduction and (b) Seasonal Cloud ICE Increase. Grey solid lines represent the linear regression fit. Dashed blue lines indicate the zero x- and y-axes while Correlation coefficients (Black: Pearson; Blue: Spearman) are noted at top right corner in each plot. Observed CICE indicated by pink dashed line in (a),(b) and pink cross in (c),(d).

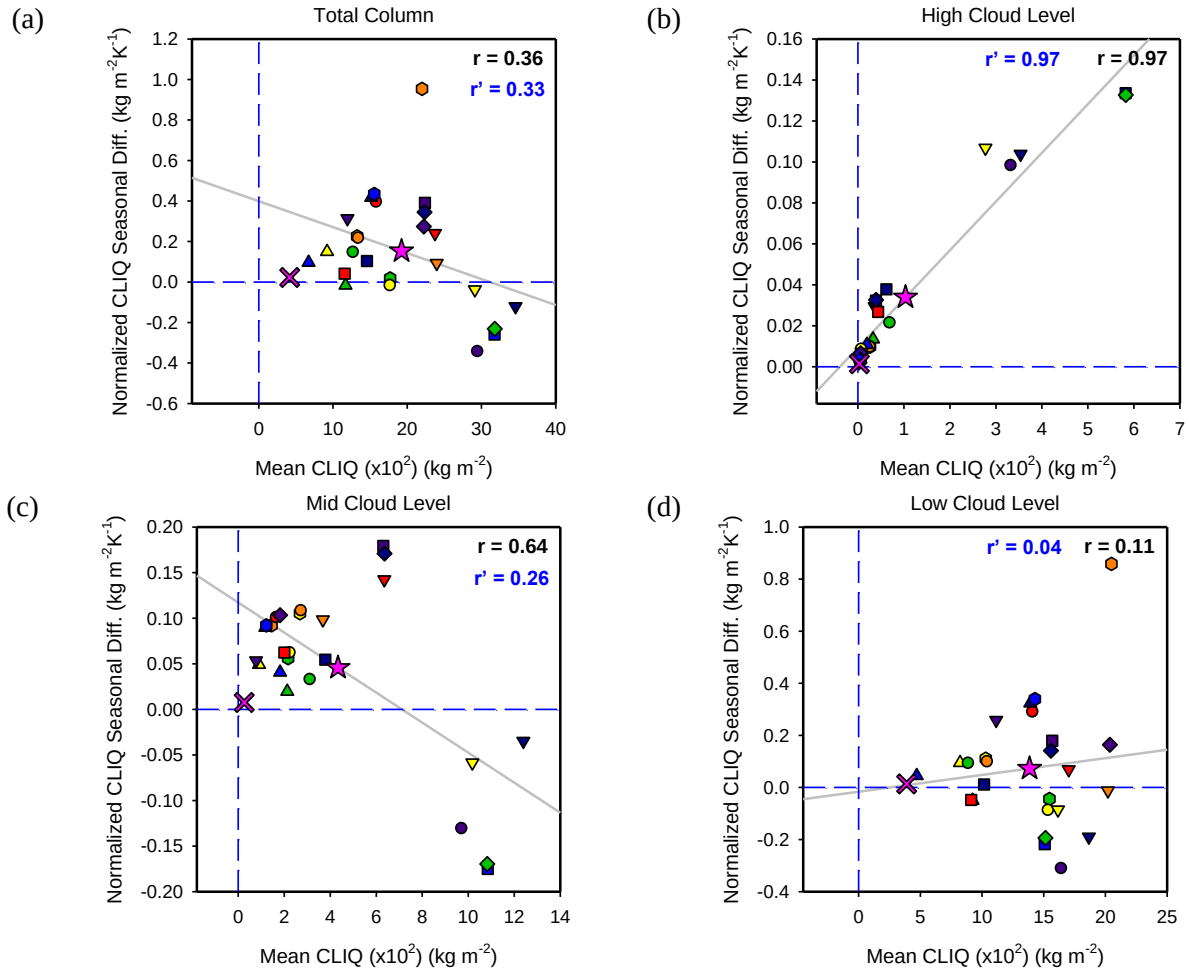

Figure 4.11 : Scatter plots showing the relationship between Temperature normalized Mass-weighted Seasonal change (y-axis) in kg/m^2/K and Mass-weighted Mean values (x-axis) in kg/m^2 of mid-latitudinal cloud LIQ mass fraction (*10^2) for 25 CMIP5 models (key in Figure 3.6) in the (a) Total cloud column, (b) High-level clouds (440hPa and above), (c) Mid-level clouds (680 hPa -440 hPa) and (d) Low-level clouds (below 680 hPa). Grey solid line is the linear regression fit. Observed values of Mean and Seasonal change in cloud LIQ are represented by pink crosses. Correlation coefficient values (Black: Pearson; Blue: Spearman) are indicated at the top right corner of each figure. Zero x- and y-axes included as blue dashed lines.

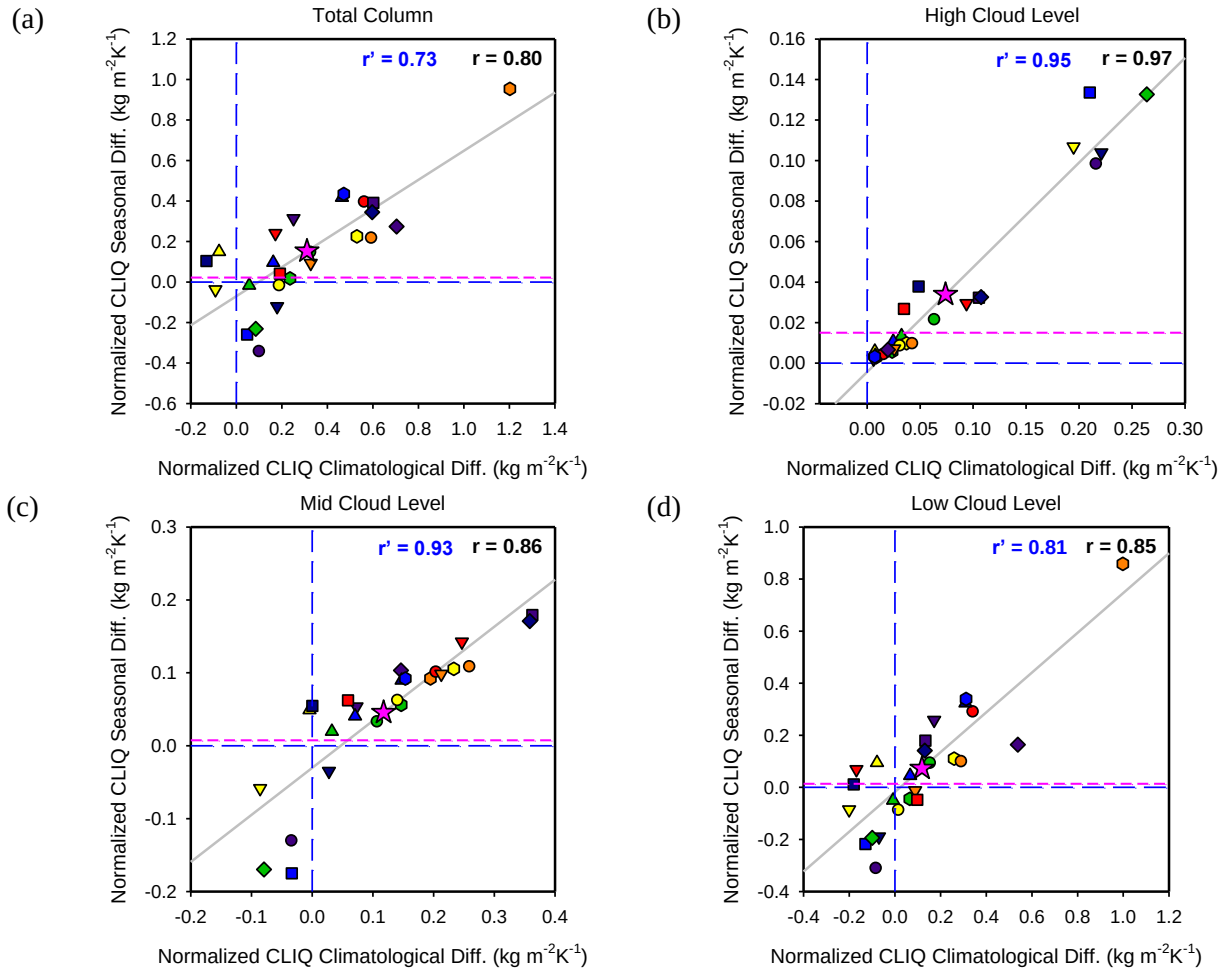

Figure 4.12 : Scatter plots showing the relationship between Mid-latitudinal Temperature normalized Mass-weighted Seasonal change (y-axis) and Climatological difference (x-axis) in kg/m^2/K in cloud LIQ mass fraction (multiplied by 100) for 25 CMIP5 models (key in Figure 3.6) in the (a) Total cloud column, (b) High-level clouds (440hPa and above), (c) Mid-level clouds (680 hPa -440 hPa) and (d) Low-level clouds (below 680 hPa). Grey solid line is the linear regression fit. Observed values of Seasonal change in cloud LIQ are represented by pink horizontal lines. Correlation coefficient values are indicated at the top right corner of each figure (Black: Pearson; Blue: Spearman). Zero x- and y-axes are included as blue dashed lines.

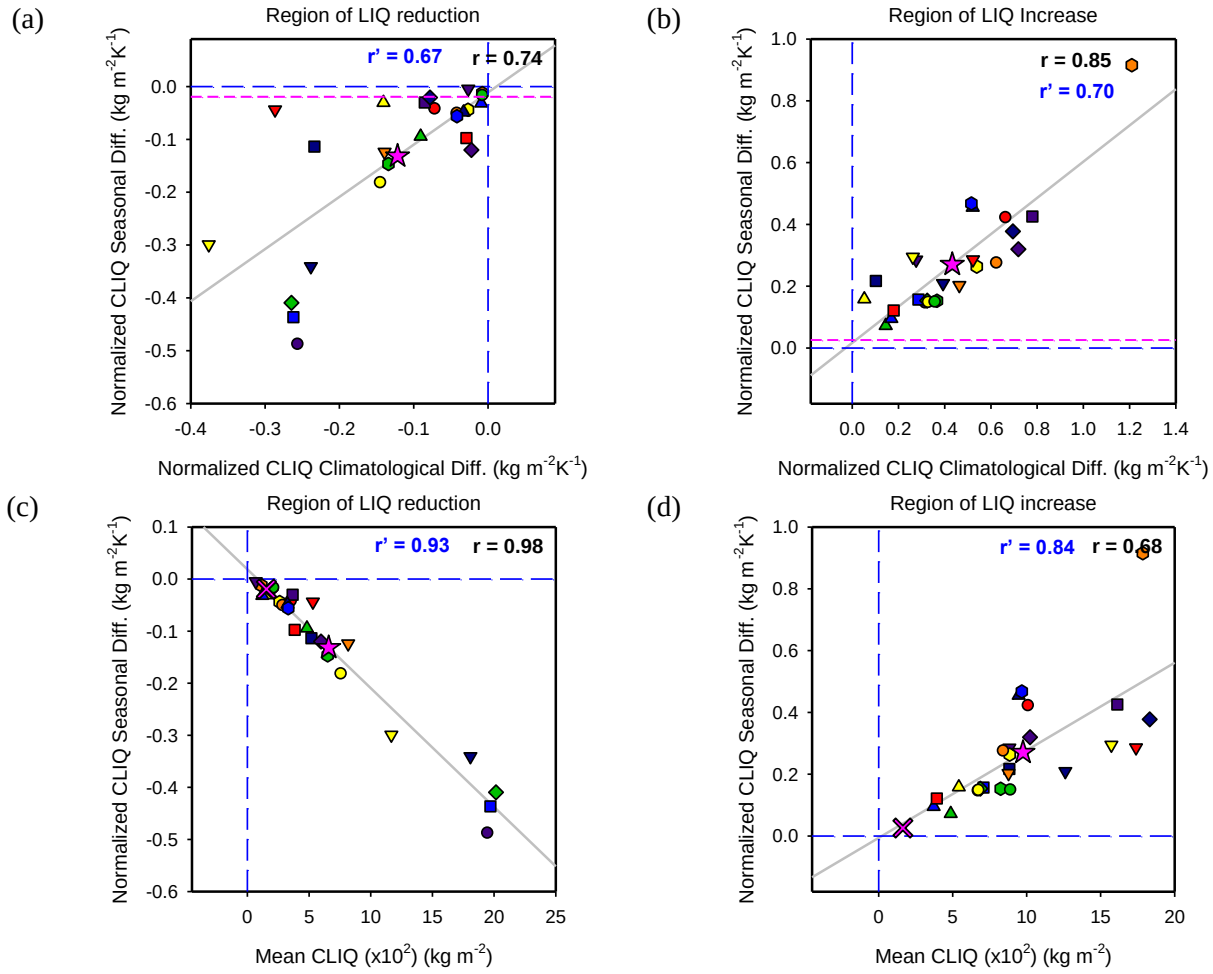

Figure 4.13 : Scatter plots showing the relationship between Temperature normalized Mass-weighted Seasonal change (y-axis) and Climatological difference (x-axis) in kg/m^2/K in mid-latitudinal cloud LIQ mass fraction (multiplied by 100) for 25 CMIP5 models (key in Figure 3.6) in the corresponding layers of (a) Cloud LIQ reduction and (b) Cloud LIQ Increase respectively, and, between Mass-weighted Mean Cloud LIQ mass fraction (x-axis) in kg/m^2 and Seasonal change (y-axis) in the layers of (c) Seasonal Cloud LIQ reduction and (b) Seasonal Cloud LIQ Increase. Grey solid lines represent the linear regression fit. Dashed blue lines indicate the zero x- and y-axes while Correlation coefficients (Black: Pearson; Blue: Spearman) are noted at top right corner in each plot. Observed CLIQ indicated by pink dashed line in (a),(b) and pink cross in (c),(d).

(a)

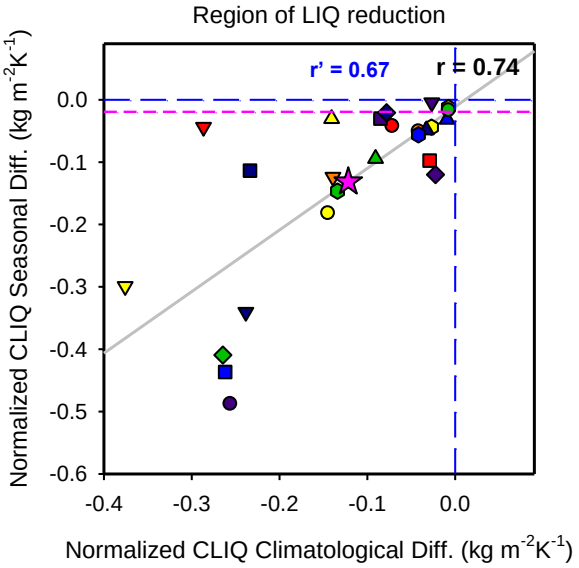

(b)

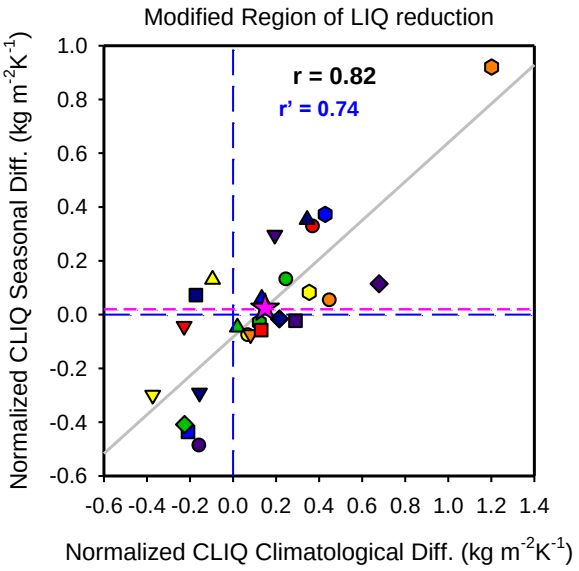

Figure 4.14 : Scatter plots showing the relationship between Temperature normalized Mass-weighted Seasonal change (y-axis) and Climatological difference (x-axis) in kg/m^2/K in mid-latitudinal cloud LIQ mass fraction (multiplied by 100) in the corresponding (a) layers of Cloud LIQ reduction and (b) modified Cloud LIQ reduction with small layer of increase at the bottom. Grey solid lines represent the linear regression fit. Dashed blue lines indicate the zero x- and y-axes. Observed CLIQ indicated by pink dashed line while Correlation coefficients (Black: Pearson; Blue: Spearman) are noted at top right corner in each plot.

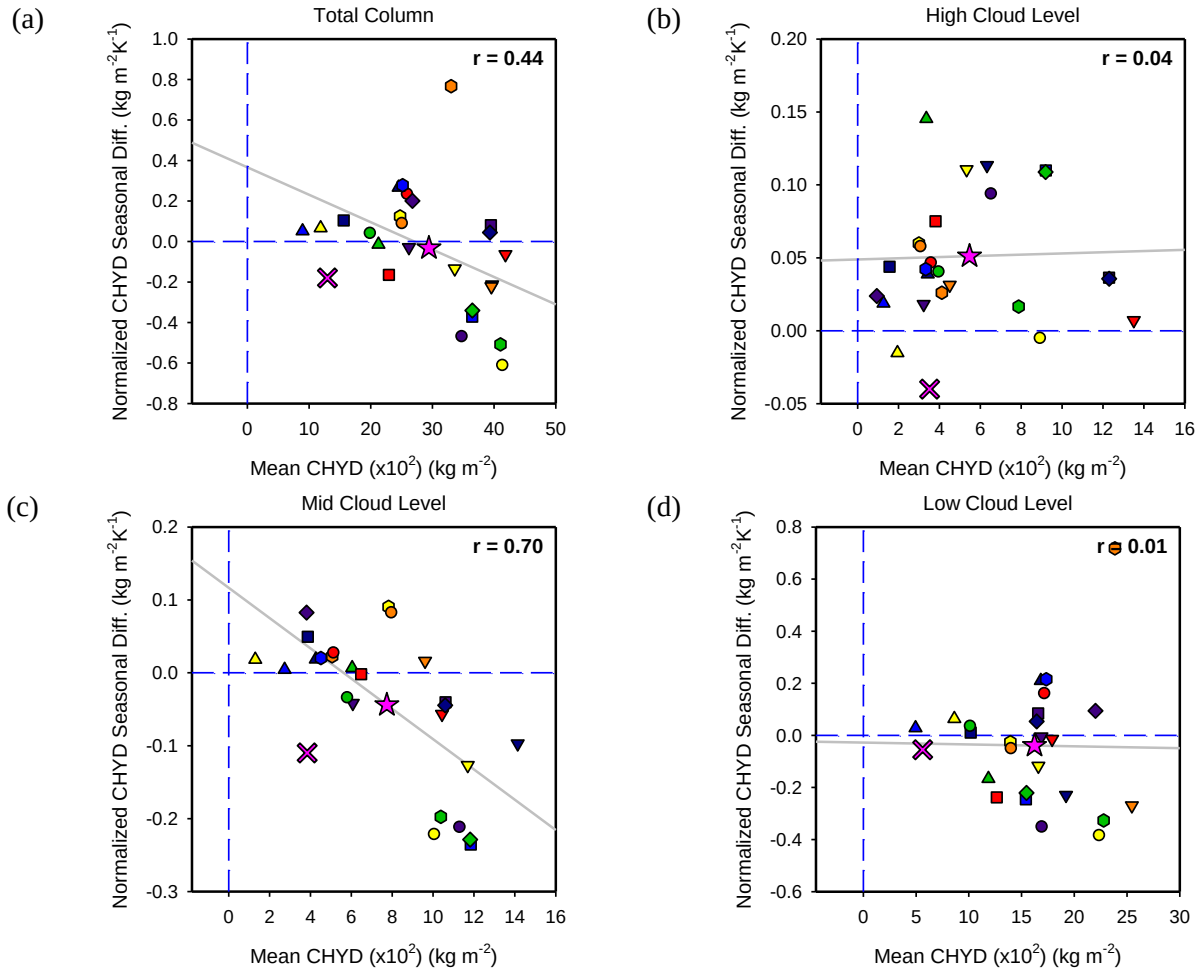

Figure 4.15 : Scatter plots showing the relationship between Temperature normalized Mass-weighted Seasonal change (y-axis) in kg/m^2/K and Mass-weighted Mean values (x-axis) in kg/m^2 of mid-latitudinal cloud HYD mass fraction (*10^2) for 25 CMIP5 models (key in Figure 3.6) in the (a) Total cloud column, (b) High-level clouds (440hPa and above), (c) Mid-level clouds (680 hPa -440 hPa) and (d) Low-level clouds (below 680 hPa). Grey solid line is the linear regression fit. Observed values of Mean and Seasonal change in cloud HYD are represented by pink crosses. Correlation coefficient values are indicated at the top right corner of each figure. Zero x- and y-axes included as blue dashed lines.

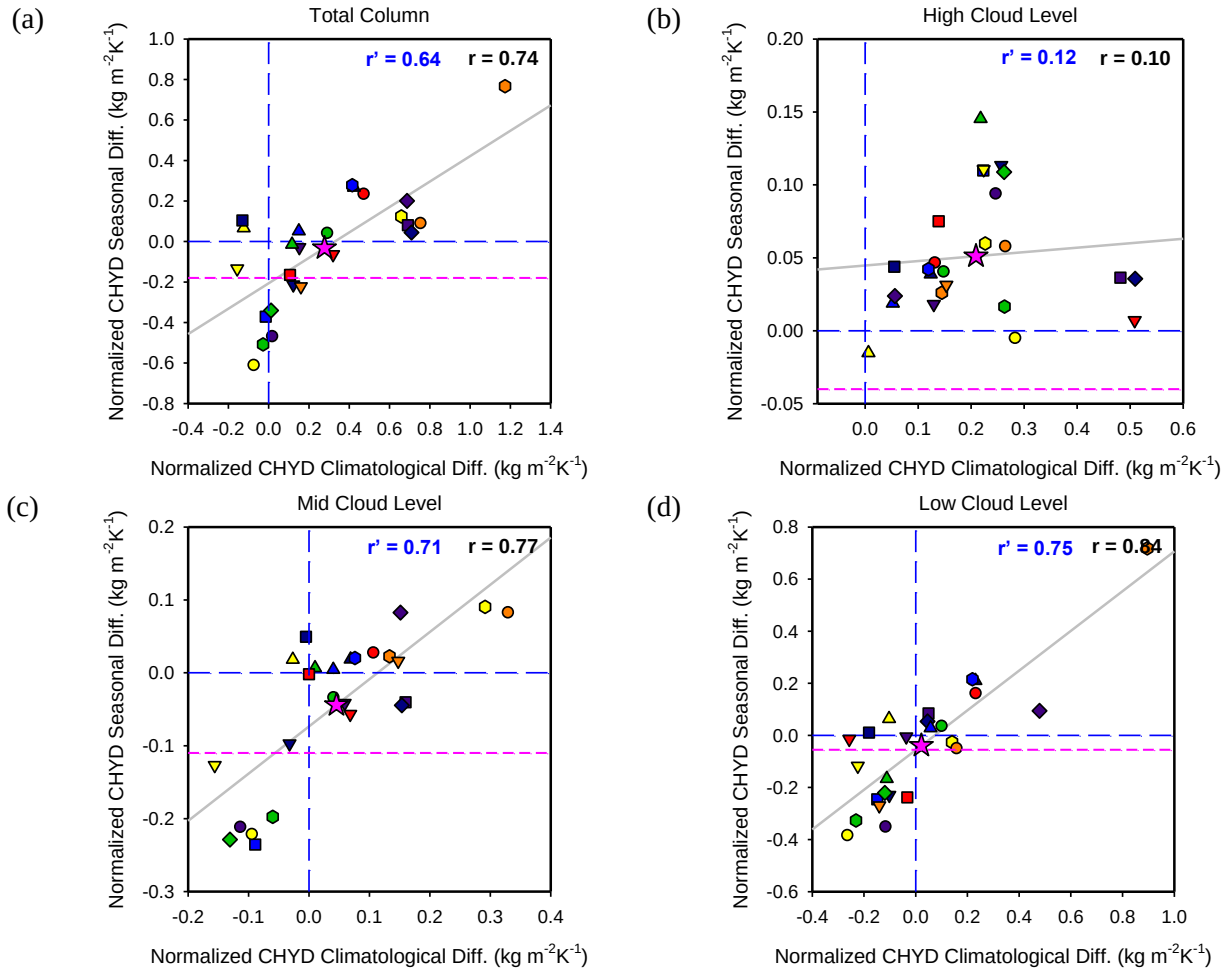

Figure 4.16 : Scatter plots showing the relationship between Mid-latitudinal Temperature normalized Mass-weighted Seasonal change (y-axis) and Climatological difference (x-axis) in kg/m^2/K in cloud HYD mass fraction (multiplied by 100) for 25 CMIP5 models (key in Figure 3.6) in the (a) Total cloud column, (b) High-level clouds (440hPa and above), (c) Mid-level clouds (680 hPa -440 hPa) and (d) Low-level clouds (below 680 hPa). Grey solid line is the linear regression fit. Observed values of Seasonal change in cloud HYD are represented by pink horizontal lines. Correlation coefficient values are indicated at the top right corner of each figure (Black: Pearson; Blue: Spearman). Zero x- and y-axes are included as blue dashed lines

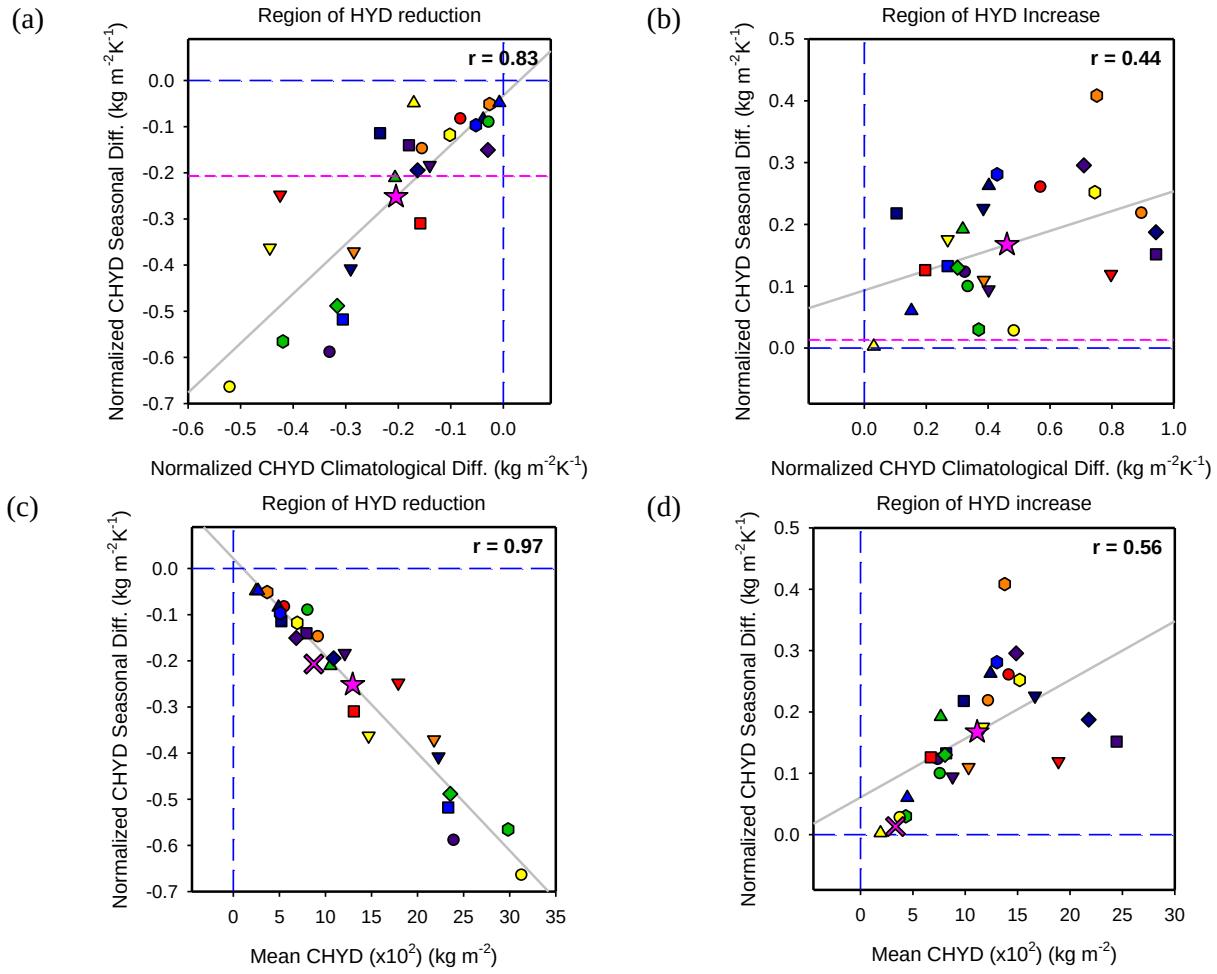

Figure 4.17 : Scatter plots showing the relationship between Temperature normalized Mass-weighted Seasonal change (y-axis) and Climatological difference (x-axis) in kg/m^2/K in mid-latitudinal cloud HYD mass fraction (multiplied by 100) for 25 CMIP5 models (key in Figure 3.6) in the corresponding layers of (a) Cloud HYD reduction and (b) Cloud HYD Increase respectively, and, between Mass-weighted Mean Cloud HYD mass fraction (x-axis) in kg/m^2 and Seasonal change (y-axis) in the layers of (c) Seasonal Cloud HYD reduction and (b) Seasonal Cloud HYD Increase. Grey solid lines represent the linear regression fit. Dashed blue lines indicate the zero x- and y-axes while Correlation coefficients are noted at top right corner in each plot. Observed CHYD indicated by pink dashed line in (a),(b) and pink cross in (c),(d).

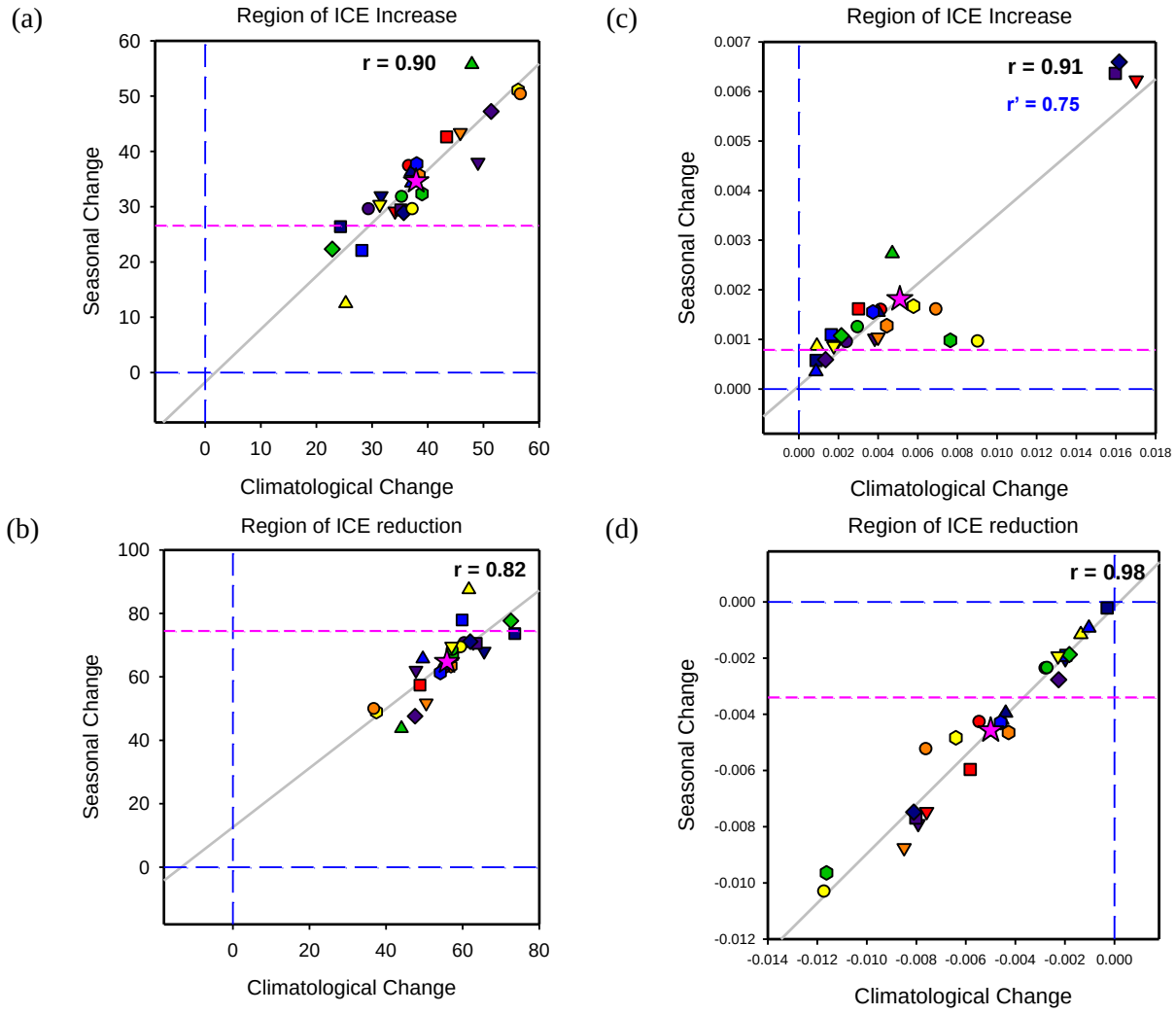

Figure 4.18 : Scatter plots showing the relationship in mid-latitudinal belt between fraction of total number of pressure–latitude grid boxes (expressed in %) with Cloud ICE (a) increase and (b) reduction seasonally (y-axis) and climatologically (x-axis), and average cloud ICE mass fraction (c) increase and (d) reduction in each grid box seasonally (y-axis) and climatologically (x-axis) using 25 CMIP5 models. Solid gray line represents linear regression fit to the data and dashed blue lines indicate the position of zero x-and y-axes. Observation indicated by pink dashed line. Correlation coefficients (Black: Pearson; Blue: Spearman) are noted at top right corner in each plot. Changes in average mass fraction of cloud ICE have been multiplied by 100.

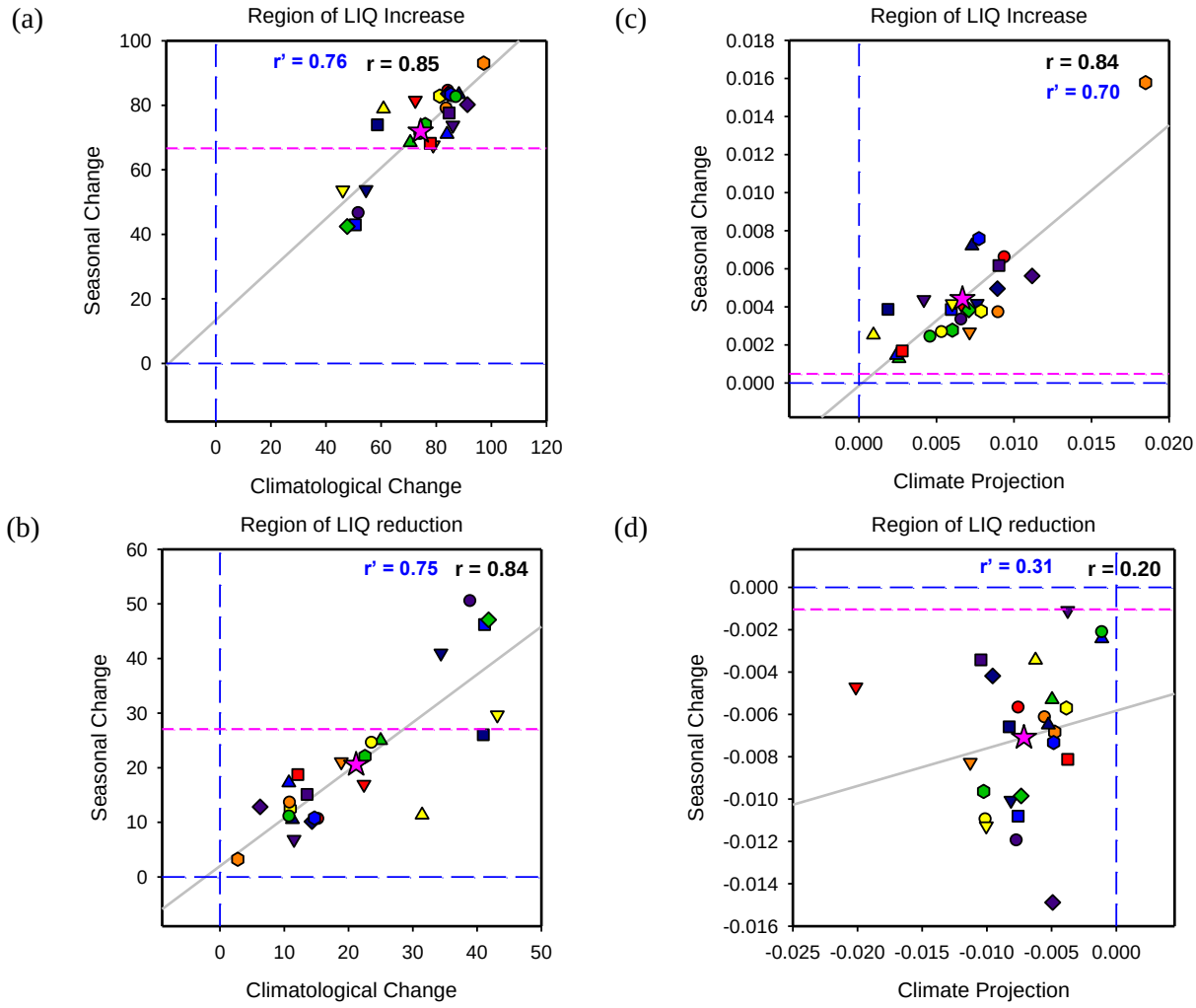

Figure 4.19 : Scatter plots showing the relationship in mid-latitudinal belt between fraction of total number of pressure–latitude grid boxes (expressed in %) with Cloud LIQ (a) increase and (b) reduction seasonally (y-axis) and climatologically (x-axis), and average cloud LIQ mass fraction (c) increase and (d) reduction in each grid box seasonally (y-axis) and climatologically (x-axis) using 25 CMIP5 models. Solid gray line represents linear regression fit to the data and dashed blue lines indicate the position of zero x-and y-axes. Observation indicated by pink dashed line. Correlation coefficients (Black: Pearson; Blue: Spearman) are noted at top right corner in each plot. Changes in average mass fraction of cloud LIQ have been multiplied by 100.

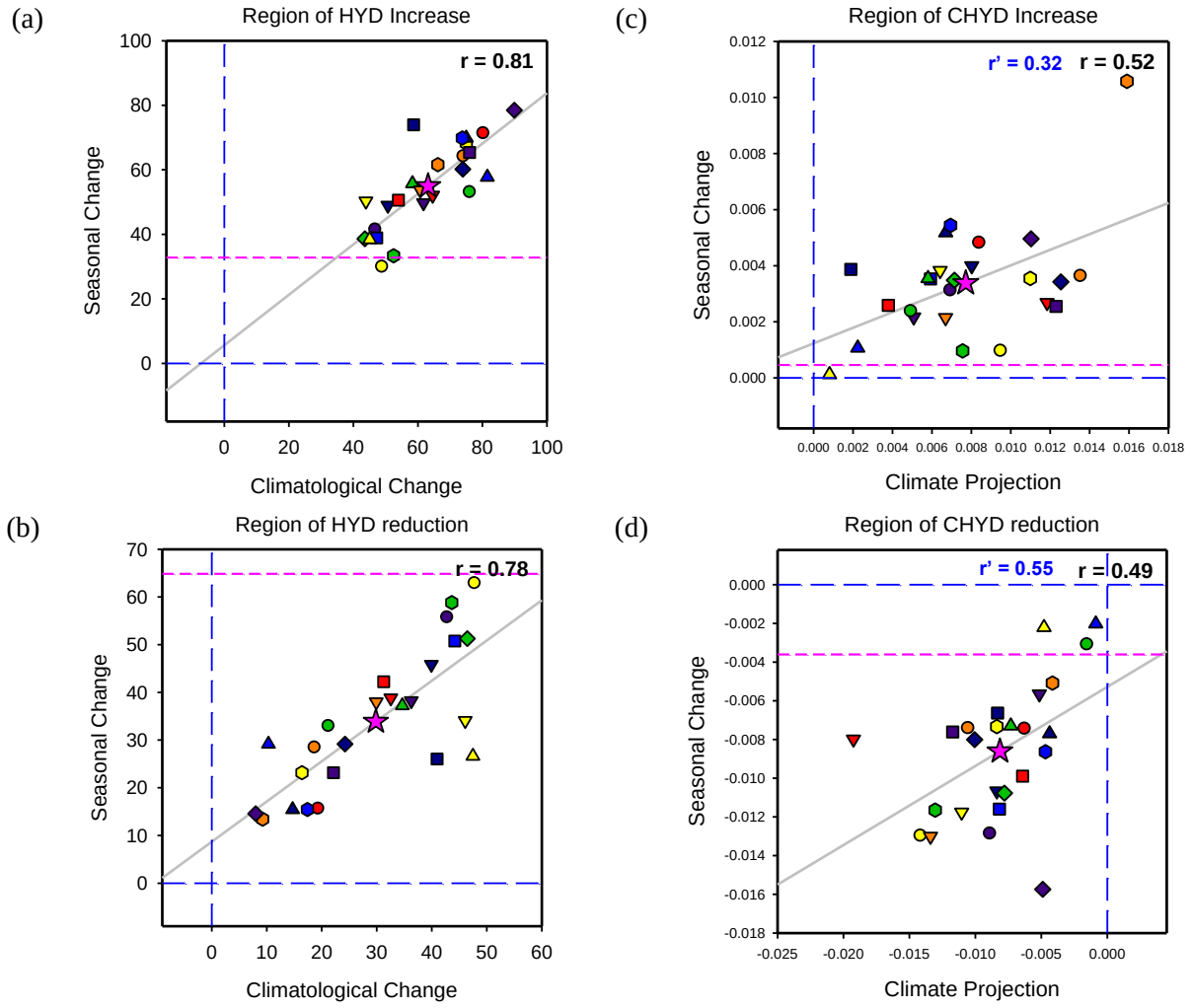

Figure 4.20 : Scatter plots showing the relationship in mid-latitudinal belt between fraction of total number of pressure–latitude grid boxes (expressed in %) with Cloud HYD (a) increase and (b) reduction seasonally (y-axis) and climatologically (x-axis), and average cloud HYD mass fraction (c) increase and (d) reduction in each grid box seasonally (y-axis) and climatologically (x-axis) using 25 CMIP5 models. Solid gray line represents linear regression fit to the data and dashed blue lines indicate the position of zero x-and y-axes. Observation indicated by pink dashed line. Correlation coefficients (Black: Pearson; Blue: Spearman) are noted at top right corner in each plot. Changes in average mass fraction of cloud HYD have been multiplied by 100.

Chapter 5

Inter-Annual Variability in Tropical Clouds and their Relation with Climate Change

To simulate the transition from a cold climate regime to a warmer one, which could serve as a suitable emergent constraint in the tropical belt, a new approach had to be formulated as tropical seasonal variability was ruled out previously. A temporal regime transition, wherein, the difference in clouds between relatively warm and cold years are computed and compared with the projected climate change was thus effected. Correlation between this inter-annual variability of cloud fraction and cloud hydrometeors with their climatological analogue has been established in this chapter. Further, satellite observations of cloud fraction were used to evaluate model biases in regions of high correlation.

5.1. Data and Models

Inter-annual difference in cloud variables (cloud fraction, cloud ice and cloud liquid) have been computed using model data from the historical runs of CMIP5 starting from the year 1980 to 2005. These have been compared with model projected climate change, between the decades 2010 - 2019 and 2090 - 2099. The long-term projected changes in variables have been calculated using RCP8.5 scenario runs. Based on the availability of historical and RCP8.5 data sets, cloud products from 25 models (listed in Table 1) participating in CMIP5 have been used.

Satellite cloud product from ISCCP D2 which was available from July, 1983 to December, 2009 was used for constraining results from models. Surface temperature from ECMWF was used to determine the five warmest and coldest years in the span of 26 years from 1980 to 2005 for

computing observed inter-annual difference. Even though the ISCCP dataset began from 1983, that did not pose a problem as because, the years 1980 – 1982 did not belong to either of the selected warmest or coolest five years.

C3M model data from 2006-2010 was used to prepare mean cloud climatology in the tropical belt for exhibiting the distribution of high and low clouds in different geographical regions.

5.2. Inter-annual variability of clouds and Climate change

For the tropical belt, which was chosen to extend from 30˚S to 30˚N latitudes, inter-annual variability of surface temperature was used to represent a climatic shift from a relatively cold to a warm regime. Starting from the year 1980 to 2005 the annual mean surface temperature in the tropical belt was computed, based on which five of the warmest and five of the coldest years were selected for each model. Since such a long time frame (26 years) in itself might include effects of climate warming, temperature data from each model had to be detrended by removing the linear fit to the temperature time-series from each point. Difference in cloud properties between the selected warm and cold years for each model was then calculated. The cloud properties for each grid box were also detrended to eliminate the possibility of climate warming signatures interfering with the results. The resultant change in cloud response between the warm and the cold years was then compared with long term climatological cloud changes.

Figure 5.1(a) and (b) respectively show the zonally averaged vertical section of ensemble mean inter-annual cloud fraction change and the climatological cloud fraction difference in the tropical belt. The range of temperature change in the case of interannual difference (~0.4K) is much smaller than that for climatological change (~3K on an average) as well as seasonal changes (~10 - 12K) considered in the previous chapter. This is reflected in the order of magnitude of cloud differences resulting from these transitions. Disregarding the actual magnitude of variation, cloud fraction change patterns in Figure 5.1(a) and (b) show noticeable similarities with each other. A strong negative tendency could be seen near the top with the appearance of an eye-like structure capped in both cases by a layer of positive tendency. In addition, a narrow positive column over

the equator is a common feature, although, for the climatological change the positive tendency column gets intercepted by patches of negative tendency.

Relationship between inter-annual and climatological changes in cloud hydrometeors was investigated next. The ensemble mean sections of detrended inter-annual cloud ice and liquid variation and their climate change counterparts are shown in Figure 5.2(a) – (d). Total cloud hydrometeor changes obtained by summing the differences in cloud ice and cloud liquid content are presented in Figure 5.3. The inter-annual and climatological hydrometeor change sections show interesting similarities reflecting almost the same patterns as observed in the case of cloud fraction. The presence of a positive column at the centre with negative tendencies spread out on either sides is seen in both. For the climatological change however, the central positive column is again interspersed by negative patches which is absent in the inter-annual difference profile.

Although the vertical profiles of cloud fraction and cloud hydrometeor differences establish that there are some agreements between the inter-annual variation and long term climate change in these variables a continuous or uniform pattern of variability does not emerge. To support the assumptions of covariability between them, and also obtain a clear perception of the pattern of variance, a correlation contour plot was constructed. In each pressure-latitude grid box, the model spread in inter-annual change in cloud fraction was correlated with the model spread in climatological change. The correlation coefficient from the linear regression fit at each grid was then used to plot the correlation contours in Figure 5.4(a). Regions with significant covariance at the 5% level are indicated using hatched lines in these plots. Unlike the case of seasonal difference, the patterns of covariability although present are quite disorganized. High positive correlation can be seen in most regions above 400hPa pressure level. Positive correlation also exists along a tilted column about the equator and extensive areas of lower subtropical atmosphere. The scattered patches of negative correlation however makes it difficult to eliminate them and delineate a zone of exclusive positive covariability. A similar exercise with total cloud hydrometeor changes produced the correlation contour plot shown in Figure 5.4(b). The climatological and inter-annual cloud hydrometeor differences appear to correlate even better than total cloud fraction as seen from the larger patches of high correlation regions. Above 400 hPa pressure level, the correlations are strongest. Subtropical lower atmospheres particularly in SH show strong relationship as well. The correlation contours demonstrate that inter-annual variability of cloud variables does have

significant relation with the climatological changes, although the patterns of co-variability are not continuous and well defined.

Based on the correlation contours of both cloud fraction and cloud hydrometeors, three different vertical zones enclosing high correlation regions were selected. The first zone included all pressure levels above 400 hPa, the second zone included those layers between 850-600 hPa and the third was a surface layer from 925hPa to ground level. Scatter plots showing the correlations between inter-annual variability and climatological changes in cloud fraction and cloud hydrometeors in these three zones are shown in Figure 5.5. For these scatter plots, the total sum of cloud fraction and cloud hydrometeor change in the selected pressure-latitude grid boxes were used.

The following conclusions were made from this analysis : Inter-annual variability in cloud fractions are well correlated with their climatolgical changes in the mid-atmospheric layers between 850-600 hPa. In this layer both the climate transitions result in cloud reduction which is reported by majority of the models. However, the range of reduction values still shows a wide spread which is also seen in case of climate projections. Strong correlations are also seen between cloud fraction changes in the surface layer (Zone – 3). However, in this case the models show dissent in the sign of cloud change with the ensemble mean predicting cloud reduction in both inter-annual and climatological variations. For cloud hydrometeors, best correlation is also found in the mid-atmospheric layer with the ensemble mean showing small decreases inter-annually and climatologically. The models individually show a wide spread both in magnitude and sign. In Zone-1, above 400 hPa, which is typically the region of high clouds, the correlations are stronger for cloud hydrometeors which increase both inter-annually and climatologically. Cloud fraction shows decrease in these levels as well as the mid-levels with mixed signs near the surface. The presence of strong relationship between inter-annual and climatological changes in clouds, particularly at the mid-atmospheric levels, create the possibility of constraining the large spread in model clouds using observed values which will have implications for the climatological cloud changes in the tropical belts.

5.3. Comparison with Observations

The similarities seen in the vertical difference sections of cloud properties and the qualitative study of their correlation values in the previous sections supports the viability of using interannual difference as a mimic of climatological changes in the tropical belt. The observation dataset, ISCCP, provides total cloud fraction values for the entire atmospheric column rather than a three-dimensional cloud field. Therefore, for this part of the analysis, total cloud product (CLTOT) from the CMIP5 models were used for comparison with observation. Cloud hydrometeor observational data was not available over such a long time range and thus could not be used in investigations of model bias.

Figure 5.6(a) displays the correlation contours of model total cloud product inter-annual variability and climatological change in the tropical belt (30˚N – 30˚S). In this figure, each latitude-longitude grid point represents the correlation coefficient between model spread in values of inter-annual total cloud fraction change and its analogous long term climate change in that grid. Regions with significant correlation above the 5% significance level are identified with hatched lines in the contour maps. From this contour map, several regions of significant positives correlations can be identified, especially in parts of equatorial Pacific and Pacific coast of South America extending into south eastern Pacific Ocean. Next, it was examined if model biases in inter-annual variability of clouds in the observed regions of high co-variability could translate into model projections of long term cloud fraction change. For this, three different regions that exhibited a preponderance of either deep clouds or low clouds and also exhibited significant correlation in Figure 5.6(a) were chosen. These are outlined using black rectangular boxes in the correlation map. Figure 5.6(b) and (c) show the geographical distribution of climatological mean low and high clouds that were used to select the regions of interest analyzed in this section. Region-1 (3˚S – 1.5˚N; 102˚E – 112˚E) is the deep convection region of tropical west Pacific showing dominant presence of high clouds. Region-2 (0.5˚N – 10˚N; 240˚E – 280˚E), in east equatorial Pacific is a region showing high co-variability and exhibits presence of low clouds overlaid with high clouds. Region-3 (30˚S – 15.5˚S; 278˚E – 290˚E) in south east Pacific has an abundance of low clouds.

Within each of these regions the mean cloud fraction difference is computed for inter-annual (x-axis) and climatological (y-axis) changes and a scatter plot showing the interrelationship

between the two is obtained. The corresponding scatter plots for Regions-1, 2 and 3 are shown in Figure 5.7(a), (b) and (c) respectively. ISCCP observational value of total cloud inter-annual variation is shows in these plots using a pink vertical line. Correlation coefficients for each scatter plot are indicated at the top left hand corner.

In the deep cloud regions, (Region-1 and 2) ensemble mean inter-annual cloud changes are of opposite sign. While the west pacific region sees a decrease in total clouds, the east pacific region exhibits cloud increase. In both these cases however, the model mean under-predicts the change in clouds inter-annually by almost the same margin. In Region-1, majority of the models indicate cloud reduction both in the short term and into the future. The inter-annual reduction in observation exceeds the model mean but lies within the range of model simulations. Based on the relationship between the two, climatological reduction in clouds in these regions is also under-predicted by the model mean in this region. In the case of Region-2, models simulate increase in clouds both inter-annually and climatologically. Majority of the models and their mean however fall short of the observed inter-annual variability. Using the strong relationship between inter-annual changes and climate projection in this region, the models are found to underperform in terms of their projected deep cloud increases.

In Region-3, which is mostly a low cloud region, the models show a dissent in the sign of inter-annual cloud change. This is translated into the projected cloud changes as well which shows a large spread in model values. The model mean and the observed cloud changes concur in the magnitude and sign (cloud increase) of change although individual models show such a wide spread. The observation indicates that the low cloud changes in these regions are small and positive as opposed to the large cloud increases and reduction seen in many of the models. The projected change in low clouds is also small and positive based on the interrelationship between inter-annual variations and long term climate change.

A related study of inter-annual variability between the years before and after volcanic eruption of Mt Pinatubo in 1991 was also carried out. Difference in cloud amount between the years 1985-1990, representing warmer regime, and the years 1992-1993, representing colder years due to aerosol loading from the volcanic emissions, was computed. The zonally averaged vertical section of this inter-annual variability is shown in Figure 5.8. Although the profile shows some

similarities with long term climatological cloud changes, analysis using scatter plots did not reveal the presence of strong relationships between the two.

5.4. Summary

In this chapter, a relationship between tropical inter-annual variations in clouds and cloud hydrometeors and their corresponding climatological changes were established. Analysis of CMIP5 model results together with ISCCP observations led to the following important findings:

1) Investigation of the vertical section of cloud changes revealed the presence of strong correlations in selected high, mid and near surface pressure belts. Cloud fraction shows reduction in both the middle and upper atmospheres inter-annually as well as climatologically. The amount of reduction exhibits a large spread among the models inter-annually that translates into their projected changes. Model cloud hydrometeors show increase in upper layers and reduction in mid-layers in both the short term and long term changes. These strong interrelationships exhibit the possibility of observationally constraining the projected cloud changes in climate models.

2) Using ISCCP total column cloud observations, model performance in simulating inter-annual cloud changes was evaluated in two different deep convective cloud regions and a region with low level clouds. In both the deep cloud regions, the model mean underestimates cloud changes compared to observation. Projected cloud climate changes in these areas are thus expected to be aligned with those models that are more sensitive to warming. In the low cloud region, the ensemble model mean agrees well with observed changes and may be used to constrain the projected low cloud change to small positive values, but large differences are found among the models for both interannual and climatological variations with opposite signs.

Figures

(a)

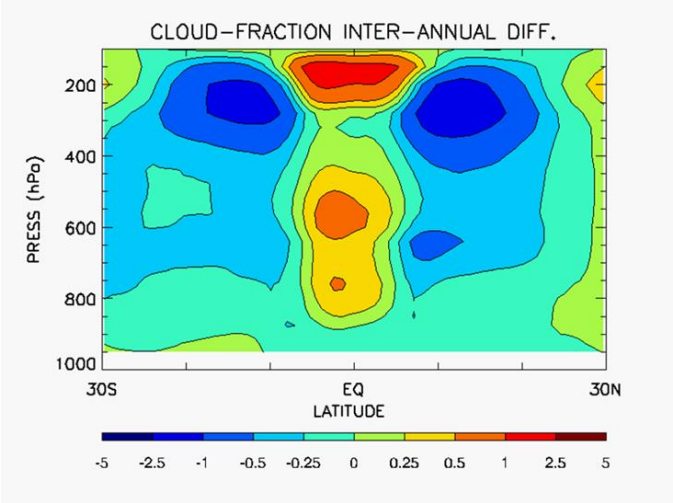

(b)

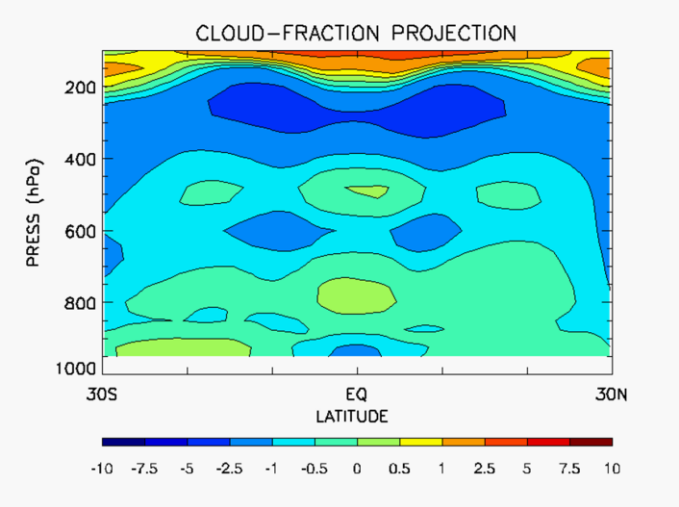

Figure 5.1 Ensemble mean zonally averaged pressure-latitude sections of (a) Inter-Annual difference in Cloud Fraction (%) and (b) Climatological difference in Cloud Fraction (%) in the tropical belt between 30˚S to 30˚N latitudes.

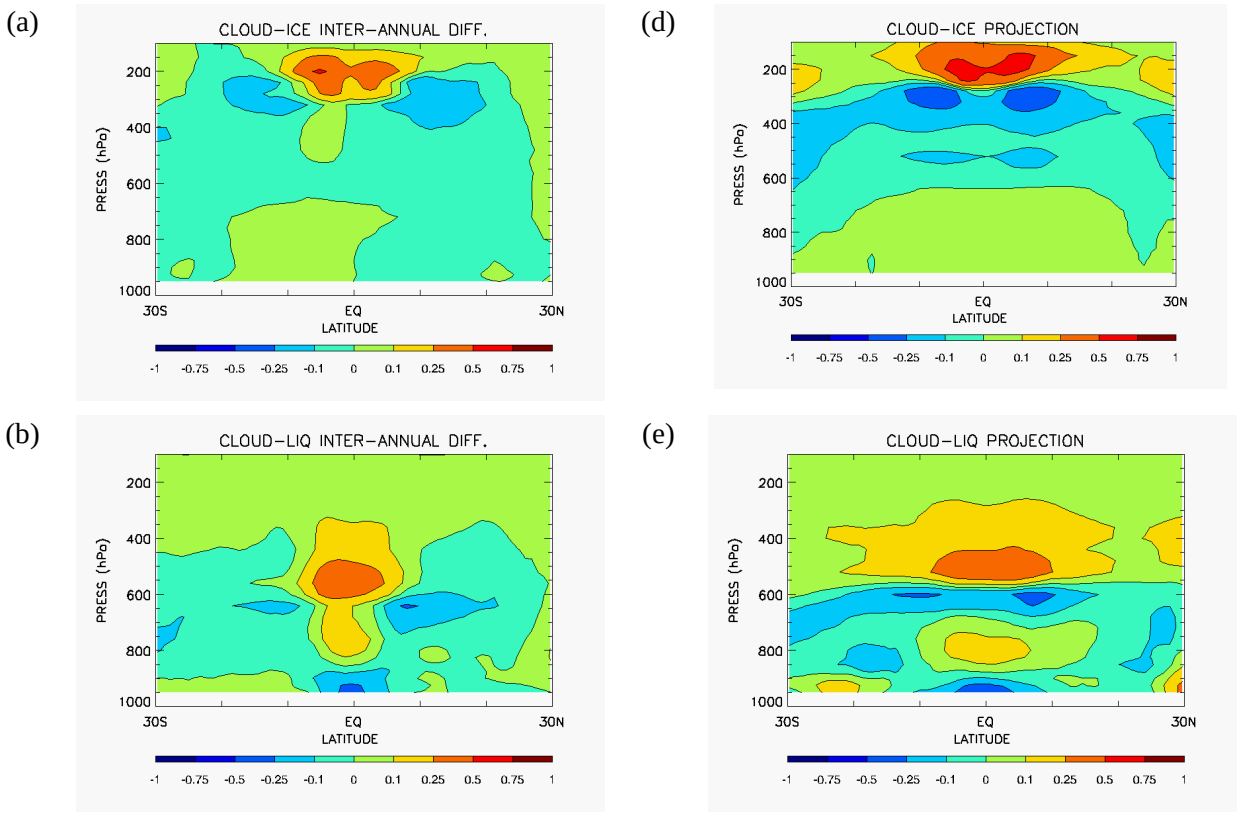

Figure 5.2 : Ensemble mean zonally averaged pressure-latitude sections of (a) Inter-annual difference and (b) Climatological difference in Cloud ice content (mass fraction in air multiplied by 100) and (c) Inter-annual and (d) Climatological difference in Cloud water content (mass fraction in air multiplied by 100) in the tropical belt between 30˚S to 30˚N latitudes.

(a)

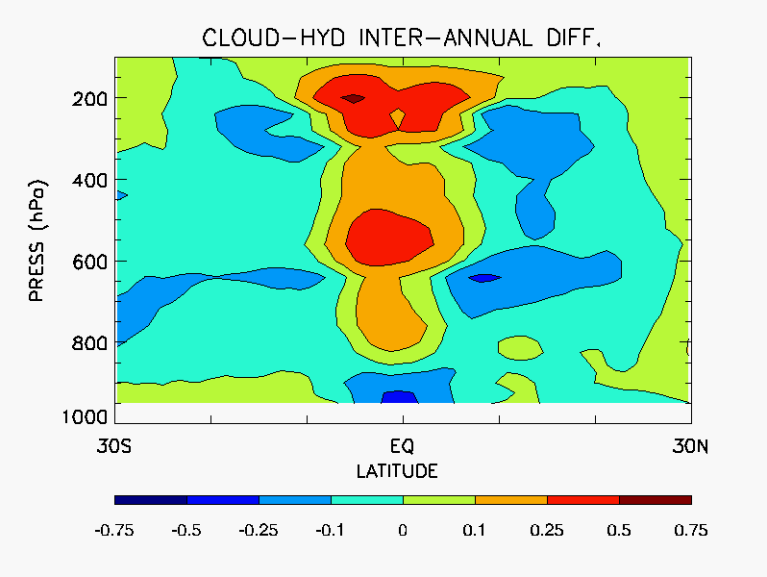

(b)

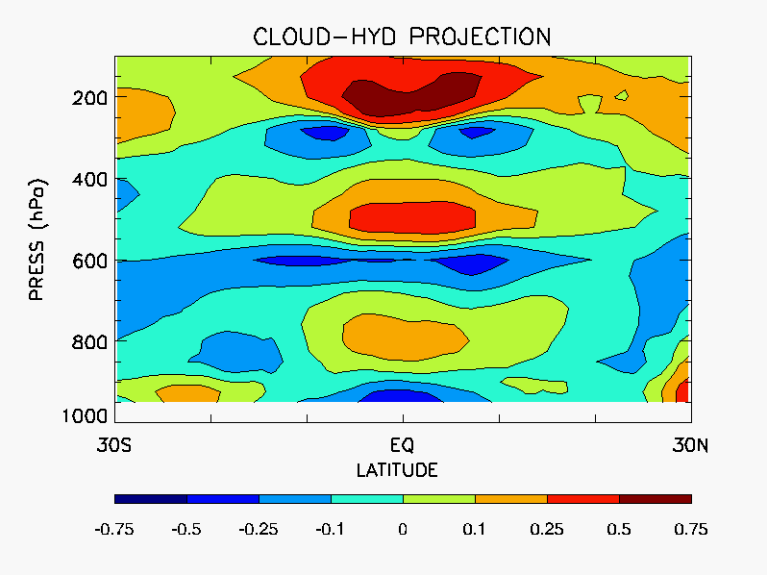

Figure 5.3 : Ensemble mean zonally averaged pressure-latitude section of (a) Inter-annual difference and (b) Climatological difference in Cloud Hydrometeor content (mass fraction in air multiplied by 100) in the tropical belt between 30˚S to 30˚N latitudes.

(a)

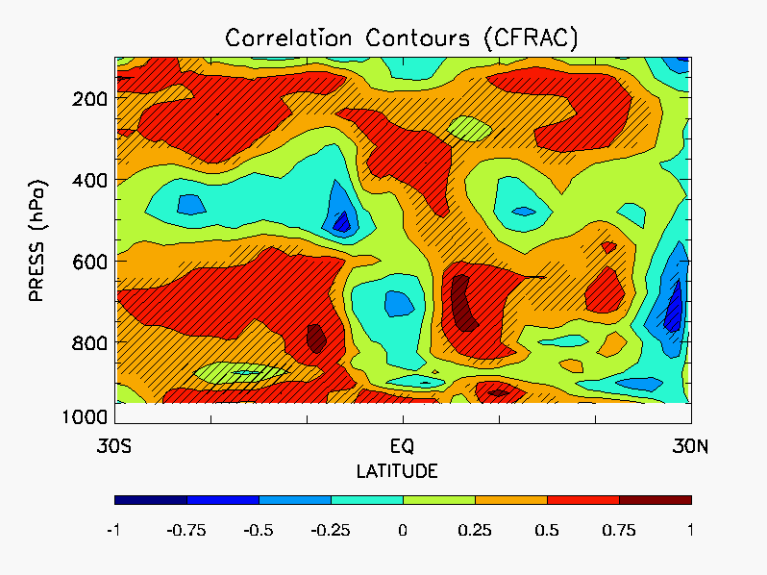

(b)

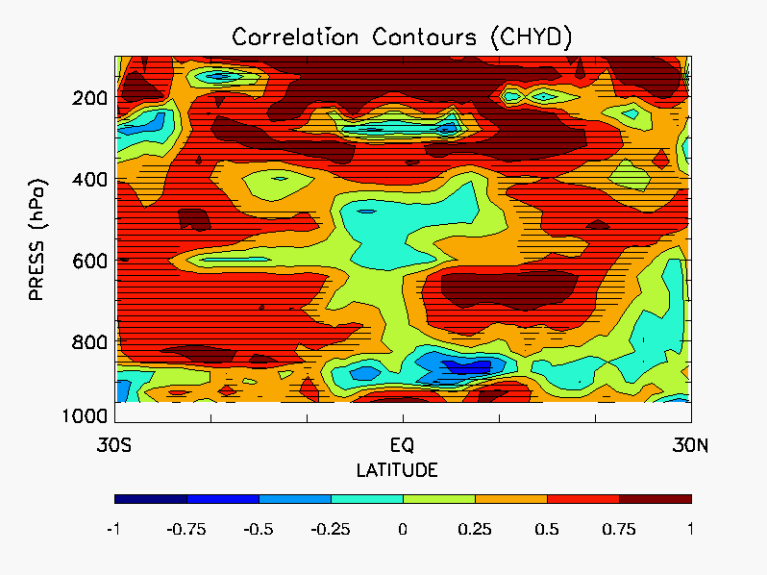

Figure 5.4 : Correlation contours representing the correlation coefficient between the values of Inter-annual difference and Climatological difference at each pressure-latitude grid point in (a) Cloud Fraction and (b) Cloud Hydrometeors for 25 CMIP5 models. Hatched lines indicate regions of significant correlation (5% level)

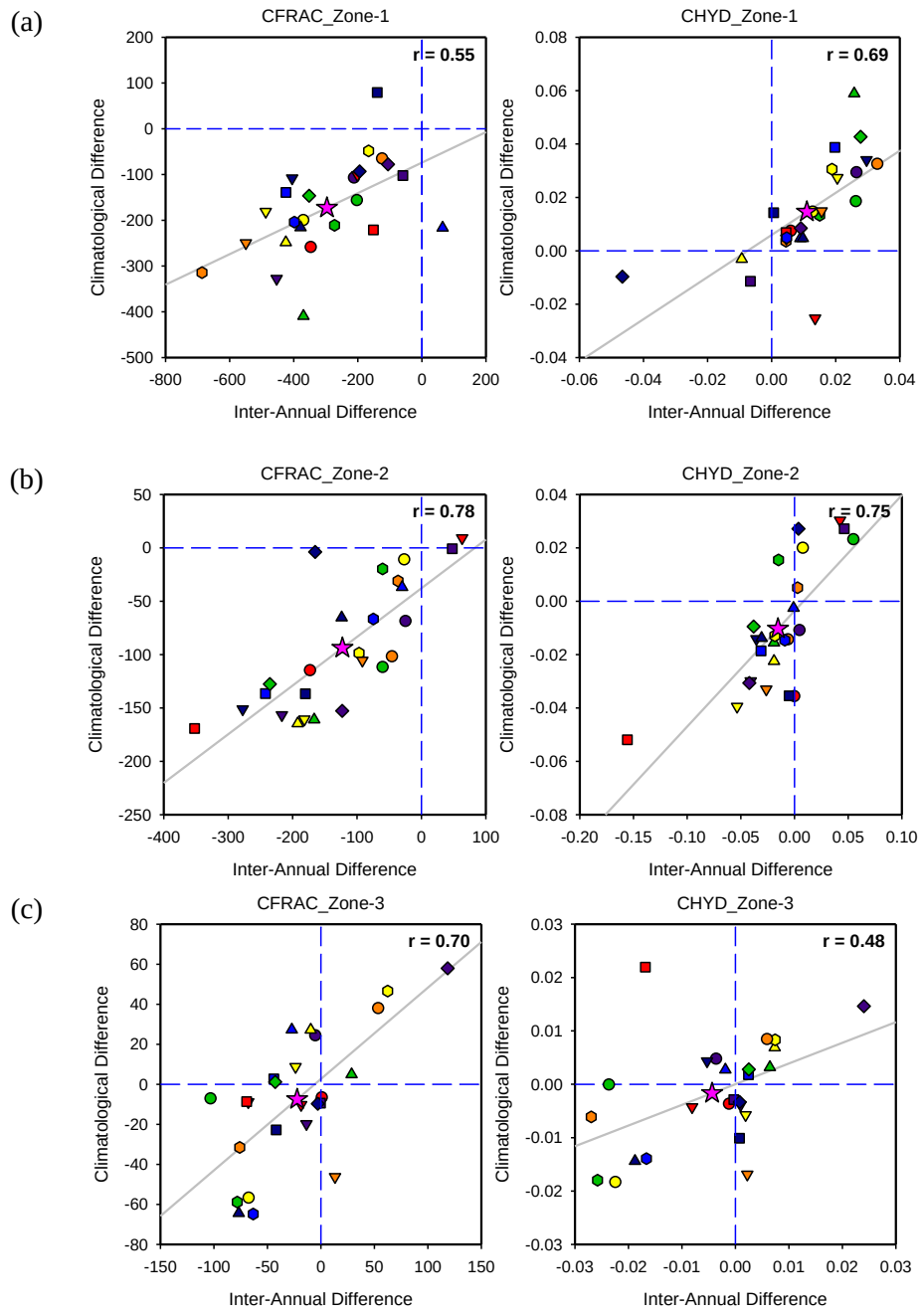

Figure 5.5 : Scatter plots showing the relationship between Inter-annual Change (x-axis) and Climatological difference (y-axis) in cloud fraction for 25 CMIP5 models (listed with their symbols later in Figure 5-7) summed over (a) Zone-1 (above 400hPa), (b) Zone-2 (between 850-600hPa) and (c) Zone-3 (below 925 hPa). Grey solid line is the linear regression fit. Zero x- and y-axes are included as blue dashed lines

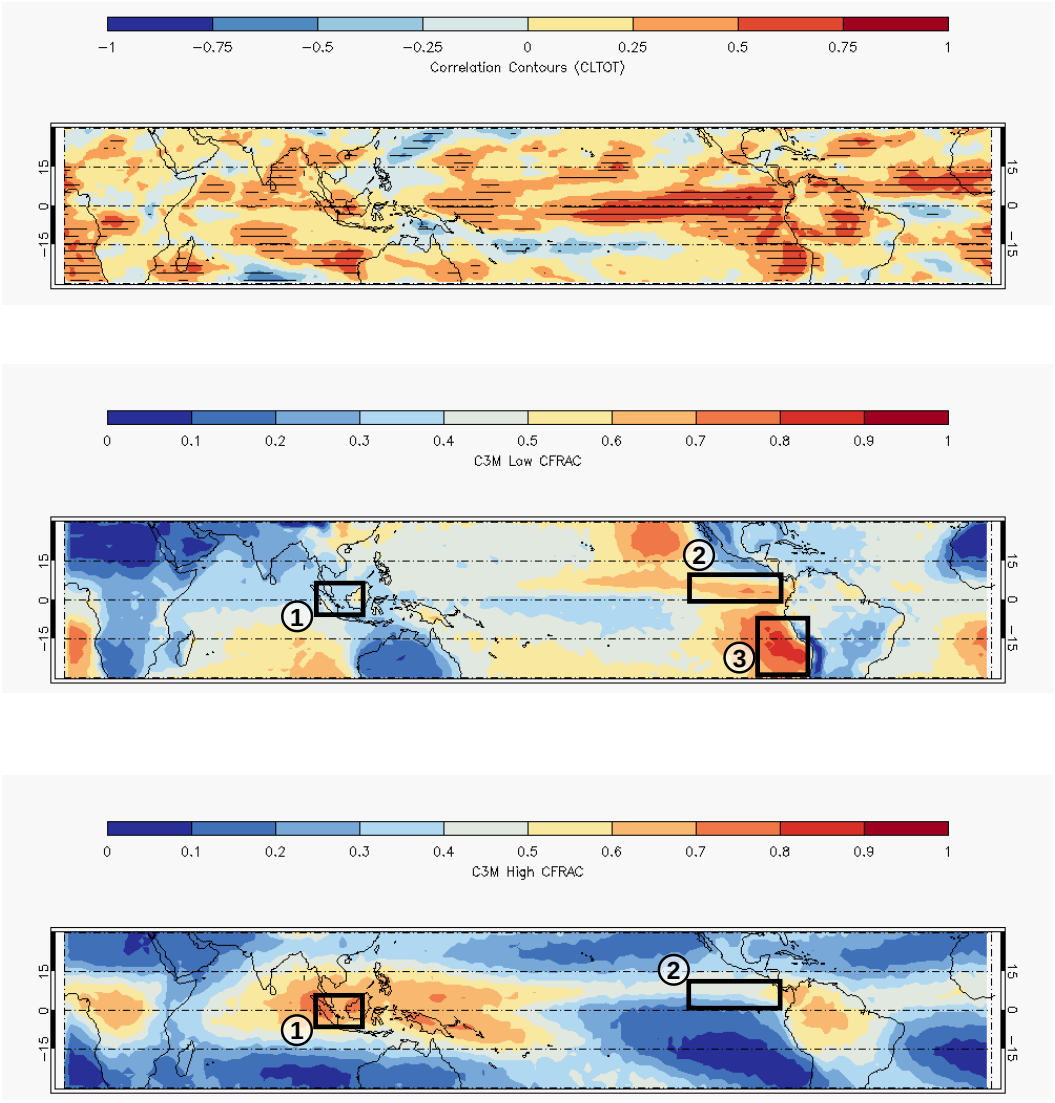

Figure 5.6 : (a) Correlation map constructed from correlation coefficients between model spread in Total Cloud Inter-annual and Climatological changes. Hatched lines indicate regions of significant correlation (5% level). Mean climatology of (b) Low and (c) High level clouds from C3M observations (2006-2010) in the tropical belt. Rectangular boxes indicate the location of Region-1, 2 and 3 discussed in the text and are marked here as ① ② ③

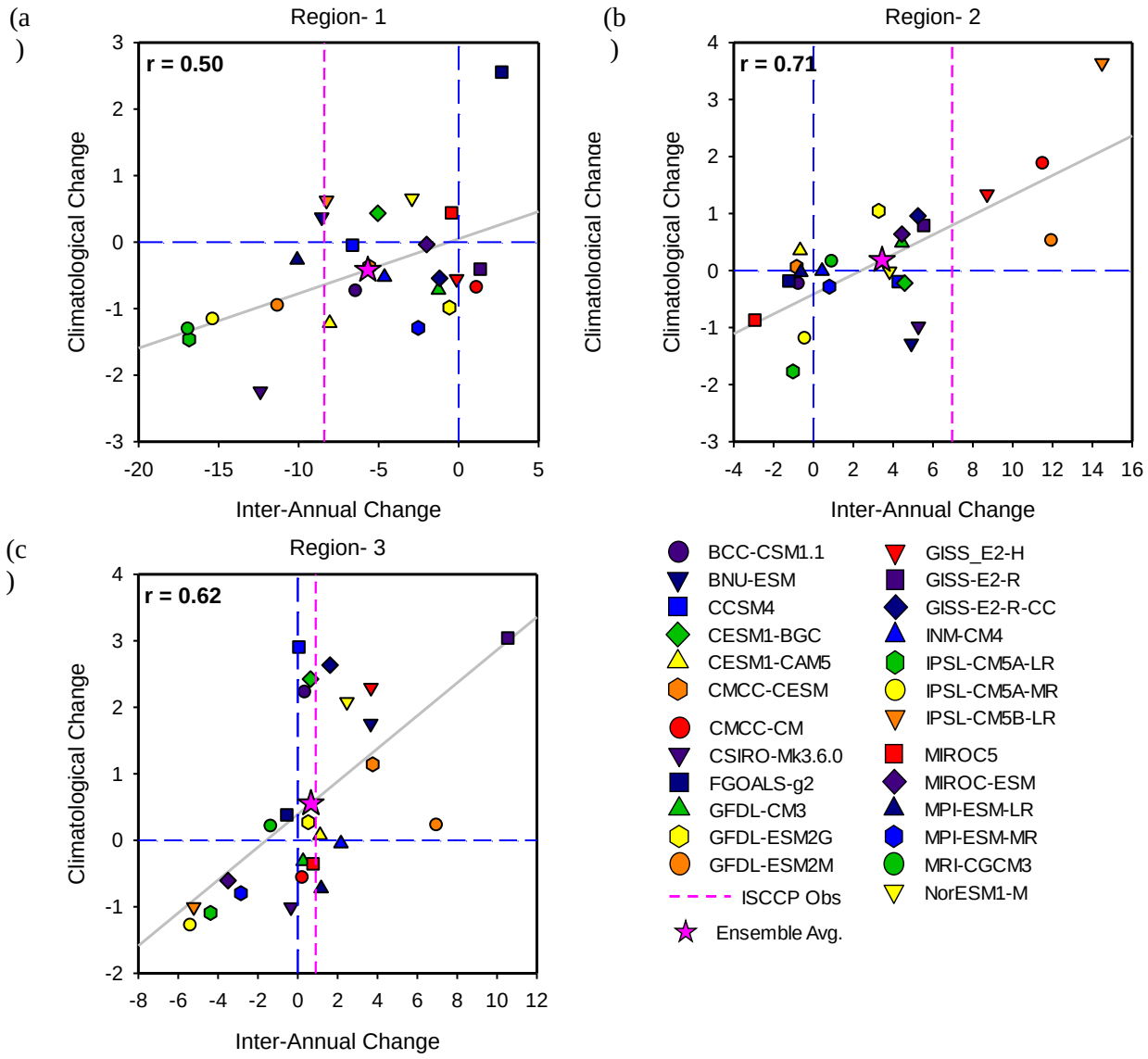

Figure 5.7 : Scatter plots showing the relationship between Inter-annual (x-axis) and Climatological difference (y-axis) in total cloud fraction for 25 CMIP5 models in (a) Region-1 (3˚S – 1.5˚N; 102˚E – 112˚E), (b) Region-2 (0.5˚N – 10˚N; 240˚E – 280˚E) and (c) Region-3 (30˚S – 15.5˚S; 278˚E – 290˚E) Grey solid line is the linear regression fit. Observed values of Inter-annual total cloud change from ISCCP represented by pink horizontal lines. Correlation coefficient values indicated at the top left corner of each figure.

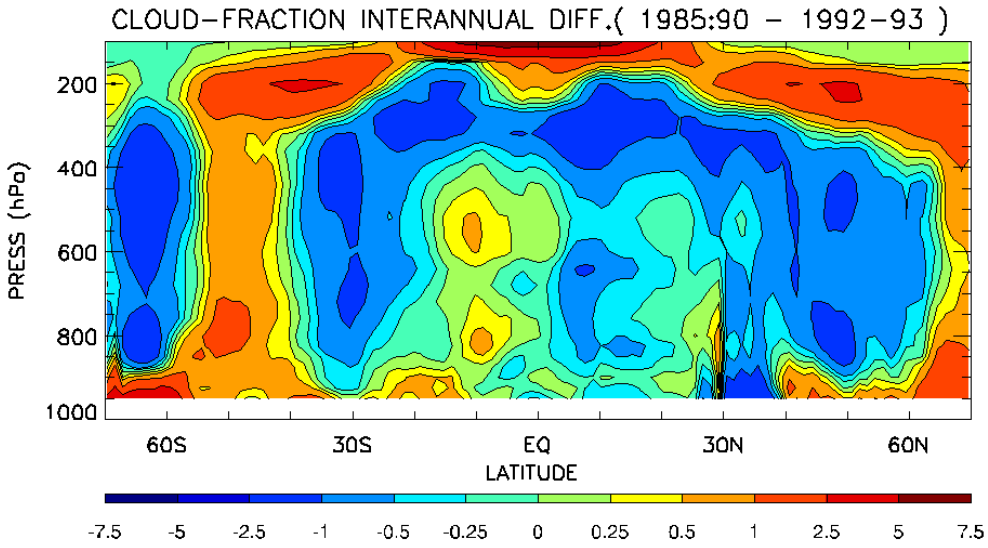

Figure 5.8 : Ensemble mean zonally averaged pressure-latitude section of Inter-Annual difference in Cloud Fraction (%) between years before and after Mt. Pinatubo eruption in 1991.

Chapter 6

Constraining Mid-Latitude Cloud Radiative Forcing Change in CMIP5 models

Climate models exhibit a large divergence in their predictions of long term climate changes due to global warming. The principal cause behind this disagreement is the spread in model cloud radiative response. Encouraged by the presence of strong relationship between the short term and long term variations of clouds and their hydrometeor content in the mid-latitudinal belt, the possibility of establishing similar patterns of co-variability between cloud radiative properties was investigated. In this chapter, seasonal and climatological differences in mid-latitudinal short wave, long wave and net cloud radiative forcing are examined for the presence of correlations. A study of the interrelationship between changes in radiative forcing due to exclusively low-, mid- and high-level cloud presence has also been attempted using CESM1_0_4 model runs.

6.1. Data and Models

Short-wave and long-wave cloud radiative forcing at the top of the atmosphere (TOA) for 16 CMIP5 models (listed in Table 3) were computed using radiative flux data from their RCP8.5 runs. Computation of seasonal differences between warm and cold seasons was restricted to the years 2006-2010 (same as for cloud fraction and hydrometeors for continuity) while climatological differences were calculated between the future decade, 2090-99, and the present, 2010-2019.

Net balanced TOA observational fluxes from the CERES EBAF-TOA product were used for comparative studies of seasonal radiative forcing differences between 2006-2010. This data was available as a part of Obs4MIPS dataset.

The CESM 1_0_4 model was used to conduct offline radiation experiments (Neale et al., November 2012). Using single day runs, the profiles of cloud fraction, cloud ice and cloud liquid content from the monthly averaged CMIP5 output of various models were used as input. The resultant radiative flux output was recorded and analyzed as monthly mean radiation data corresponding to the input cloud distribution. This methodology was used to generate 10 years of present climate (2010-19) data, 10 years of future climate (2090-99) data and 4 years of data from 2006 to 2010 for the computation of seasonal differences for the same set of 16 CMIP5 models. All GCM runs were forced by using climatological SST and sea ice values.

6.2. Seasonal and Climatological changes in CRF

Cloud radiative forcing (CRF) at the top of the atmosphere (TOA) simply represents the difference in net radiative heating at the TOA between clear sky and cloudy conditions (Ramanathan et al., 1989). In other words, it is the effect that the presence of clouds has, on the radiative heating of the atmosphere. For computation of changes in net cloud radiative forcing (in W/m^2) both between seasons and between decades of time, the following relationship adapted from (Cess et al., 1997) has been used,

$$\Delta CRF = (\Delta\alpha_c - \Delta\alpha)S + (\Delta F_c - \Delta F).$$

Here, Δ represents the difference between two temporal regimes (warm and cold months for seasonal and future and present decades for climatological) in albedo (α) and outgoing longwave radiation (F) at the TOA while S stands for incoming solar radiation. The subscript c indicates clear sky values to distinguish from their cloudy counterparts. The first term in this expression represents change in short wave cloud radiative forcing (SWCRF) while the second term represents long wave cloud radiative forcing (LWCRF) change. The advantage of using this equation for SWCRF calculations is that it does not incorporate the contribution from changes in solar insolation which has no significance in investigations of cloud radiative properties.

For computation of seasonal difference in SWCRF the above expression was modified as,

$$\left[(\alpha_{cJJA}-\alpha_{cDJF})-(\alpha_{JJA}-\alpha_{DJF})\right]S_{(JJA+DJF)/2},$$

computed by using mean values over three months for each year and then averaged over four years. For the climatological difference, the following form of the relation was used on monthly values averaged over ten years,

$$\left[(\alpha_{cFuture}-\alpha_{c\mathrm{Present}})-(\alpha_{Future}-\alpha_{\mathrm{Present}})\right]S_{(Future+\mathrm{Present})/2}.$$

Pairs of dataset, each representing the seasonal and climatological differences in SWCRF, LWCRF and NetCRF were thus computed for each of the 16 CMIP5 models.

Figure 6.1(a)-(c) show the seasonal variation of SWCRF, NetCRF, and LWCRF respectively from the Obs4MIPS observations. The corresponding ensemble mean seasonal variation from the models are shown in Figure 6.1(d)-(f). Overall the model mean captures the features in the observation well. However, for both SWCRF and LWCRF in SH, the models overestimate CRF changes. This is more extensive for SWCRF. On the other hand, the observed CRF increases seen in the NH ocean basins are under-predicted by model means. When the seasonal changes are summed over in both the latitudinal belts, these errors compensate each other so that the model mean appears to differ only slightly from the observed changes. Model mean NetCRF values continue to show overestimation of increase in the SH mid-latitudinal belt and slight under-prediction in the NH reflecting the features of SWCRF and LWCRF change patterns. An important question that arises at this point is that what are the implications of these biases to the projected cloud forcing changes in the future climate.

To investigate the presence of a relationship between seasonal and climatological changes in CRF, correlation maps were constructed on two-dimensional latitude-longitude grids as shown in Figure 6.2 (a)-(c). Each grid point on these maps represent the degree of correlation between the spread of seasonal difference and climatological difference values among various models within that grid. Regions of significant correlations at 5% significance level are indicated with hatched lines. Correlations are seen to be the strongest for LWCRF in Figure 6.2(b). Particularly strong positive correlations are seen all over the SH oceans in the 30°- 60°latitude belt. In the same latitudinal belt in NH, strong correlations are only present above ocean basins in the regions of

storm track clouds. Similar patterns of co-variability are also seen for SWCRF in Figure 6.2(a) with a reduced intensity. Correlations for NetCRF are somewhat weaker than either SWCRF or LWCRF, but still significant in middle latitudes. The conclusions from this figure are true to our expectations of finding the presence of interrelationship between seasonal and climatological CRF changes in the mid-latitudinal belt.

CRF values in the NH and SH mid-latitudinal belts are averaged using cosine of latitude as weights and then added together with reversed sign for seasonal SH differences. The scatter-plot showing correlations between seasonal and climatological differences in SWCRF, LWCRF and NetCRF are shown in Figure 6.3(a)-(c). Observed seasonal change in CRF from CERES data is represented in these figures using a cyan vertical line. Correlations are computed using both Pearson and Spearman's correlation coefficients. Correlation is strongest for LWCRF as was also seen from the correlation maps although the relationship is also quite strong in case of SWCRF. The net-CRF however does not exhibit any relationship.

In terms of the model performance as compared to observations, the ensemble model mean matches the observed sign as well as magnitude of change in all cases. This is mainly due to the compensating nature of biases seen before in the CRF maps. For SWCRF (Figure 6.3(a)) majority of the models and the observation predict small seasonal decrease while six out of sixteen models predict very large increases This was seen in the SH mid-latitudinal belts in the model mean CRF maps in Figure 6.1. The two IPSL models included in this study simulate maximum increase in SWCRF both seasonally and climatologically. Decrease in SWCRF in the long term is predicted only by five models (BNU-ESM; CSIRO-Mk3; GISS-R; INMCM4 and MRI-CGCM3). All others predict increasing SWCRF in the future although the magnitude by which they do so varies greatly. A majority of the models also predict large LWCRF decreases seasonally and climatologically.

Based on the seasonal observation the ensemble model mean projections should provide a good estimate of long term increases of about 1.0 W/m2 in SWCRF, a positive cloud feedback. The ensemble model mean and the observed LWCRF are closer to each other in sign and magnitude and they indicate a long term decrease of 1.5 W/m2, a negative cloud feedback. The models continue to simulate a range of values for the seasonal and consequently climatological CRF changes.

Correlation between seasonal and climatological NetCRF changes are not very strong because of the cancellations between SWCRF and LWCRF, and the observation indicates decrease both seasonally and climatologically. The sign of the change is captured by most of the models except four including the IPSL models, likely due to large increases in SWCRF.

In summary, there is a good correlation between the seasonal variation with climatological variation in mid-latitude LWCRF and SWCRF. The ensemble mean simulated the observed seasonal variation well, but the individual models differ greatly among themselves.

6.3. Offline radiation model runs with prescribed clouds

In this section, an attempt was made to determine the origin of the observed model spread in CRF values by separating the contribution to TOA CRF from low-, mid- and high- level clouds. The CESM model version 1_0_4 was used to conduct daily runs by specifying the cloud fraction and hydrometeor distribution that would be used to carry out computations in the radiation module. The radiative response so generated as a result of this exercise was assumed to correspond to the CMIP5 cloud profiles that was used as input. In principle, by changing the type of cloud profile that was prescribed to the model, a complementary radiation response to it could be generated. By using this framework of experiments, radiative effects of low-, mid- and high-level clouds could thus be separated out. Using such a methodology had its own set of shortcomings. For example, the temperature and water vapor profiles were kept unchanged without any adjustments consistent with the prescribed cloud profiles. This could particularly have an impact on the LWCRF values. Further, clouds with large vertical extent were cut-off artificially into low-, mid- and high clouds and treated separately for their radiation response which would be different than treating the entire cloud as a whole. Also different models have their own radiation modules, while by using this method, radiative response for different model clouds were subjected to the same RRTMG radiation computations. In spite of the various deficiencies the results from the offline radiation runs were quite encouraging. Based on the evaluation of offline-module performance as compared to the original CMIP5 radiation data it appeared that the model runs were able to capture the essentials of inter-model variation reasonably well. The bar plots in Figure 6.4(a) represent the correlation coefficients between the two sets of radiation data for climatological and seasonal

changes in SWCRF, LWCRF and NetCRF. Climatological differences in radiative forcing are quite well represented by the prescribed cloud CESM model runs based on the correlation values. Their performance in case of seasonal changes in SWCRF are slightly unmatched. The net effect of SW and LW radiation as represented by NetCRF values show some difference between CMIP5 model output and offline radiation module outputs. Nevertheless, the inter-model spread, which is what is sought to be studied using this methodology, is still captured reasonably well even for NetCRF differences. This relative spread of models about their ensemble mean as the standard (in absence of observations), in projecting climatological NetCRF change using CMIP5 and offline CESM model runs are shown using Taylor diagram (Taylor, 2000) in Figure 6.4(b) and (c) respectively. It may be pointed here that relative positions of models with respect to each other and their mean remain approximately the same in both cases as indicated by the colored circles in both the plots.

Based on the overall agreement in behavior between fluxes from CMIP5 output and those from prescribed cloud CESM model runs, next, the radiative fluxes from CESM runs prescribed with only low-, mid- and high-level clouds were generated. The cloud classification scheme was adapted from ISCCP definitions and model clouds from CMIP5 RCP8.5 datasets were processed accordingly to be input into the CESM model. The correlation plots between total cloud column radiative forcing changes from offline radiation runs are shown in Figure 6.5. The SWCRF behavior is well reproduced but there are still issues in the values of LWCRF all of which appear to exhibit a systematic positive bias as compared with CMIP5 radiative forcing changes.

Comparison of SWCRF changes at high, mid and low cloud levels are shown in Figure 6.6. Several features can be noted from these scatter plots. Firstly, there is a reasonable correlation of the seasonal and climatological SWCRF changes for the mid-level clouds and moderate (significant at the 10% level) correlation for high and low level clouds based on the corrective Spearman's rank correlation coefficient. Presence of these relationships between the seasonal and climatological changes suggest that seasonal changes of cloud forcing can be used to infer the cause of the differences among model projections of the future. Secondly, the ensemble mean has a positive climatological change, thus positive feedback, from both low and middle clouds, with mid-cloud contribution even larger than that of low clouds. The SWCRF from high clouds is negative, a negative cloud feedback. These are consistent with the reductions of hydrometeors and

cloud amount in the low and middle troposphere and their increases in the upper troposphere shown in the previous chapters. The third feature is that the ranges of model climatological differences in SWCRF from the three types of clouds are comparable to each other although the seasonal changes show maximum spread in low clouds.

For the LWCRF due to high, mid and low clouds (Figure 6.7), correlations between the seasonal and climatological changes are still strong at all levels. Maximum contribution to model spread in simulating seasonal as well as climatological changes comes from the high clouds. It may be also noted that the negative LWCRF seasonal and climatological change in the total column ensemble mean, a negative feedback, is primarily from the mid-level clouds. Low level clouds also predict decreasing LWCRF climatologically but their seasonal change shows an increase in majority of the models. At the high cloud levels, where cloud fraction and cloud ice showed increases seasonally and climatologically, the LWCRF also exhibits an increase in both the cases in spite of large differences in magnitude of change among models.

The corresponding scatter plots for NetCRF are shown in Figure 6.8. Good correlations are only seen at the mid cloud levels with moderate correlation at the low levels. In these two levels models exhibit increase in NetCRF climatologically contributed equally by the low and mid-level clouds. In the mid-level, compensation due to opposite sign of LWCRF and SWCRF changes render a comparatively smaller inter-model difference in NetCRF. The radiative response of low clouds thus exhibits the largest spread in model values of climatological change. In the high cloud levels, where strong relationship was seen previously between SWCRF and LWCRF changes, the combination of the two no longer show any correlation between short term and long term changes. Thus, the low level clouds and their radiative response can be singled out as the primary contributor to spread in model projections of climate change.

An extension of this study in particular regions of low cloud population may provide more insight into the reasons behind the observed model disagreement.

6.4. Summary

Interrelationship between seasonal and climatological changes in CRF in the mid-latitudinal belt was examined. The following is the summary of the important results emerging from this analysis :

1) Models overestimate both seasonal SWCRF and LWCRF change in SH oceans and underestimate them in the NH ocean basins. This is reflected in the NetCRF change patterns as well. Presence of strong interrelationship between seasonal and climatological changes in CRF suggests that the observed biases are translated onto long term climate changes projected by models in the regions of high co-variability.

2) Models continue to exhibit a larger spread in CRF values about their ensemble mean. Based on the seasonal CRF observations and the above relationship between seasonal and climate changes, approximate ranges of long term SWCRF increase (positive feedback) and LWCRF decrease (negative feedback) can be estimated.

3) Offline radiation runs were used to understand the contribution of individual cloud types to the observed spread in model radiative responses. It was seen that Low and Mid level clouds contribute most to the long term climatological increases in SWCRF (a positive feedback) and decreases in LWCRF (a negative feedback). This is reflective of the nature of cloud and hydrometeor changes observed in these layers previously. All the cloud levels contribute equally to the spread in SWCRF changes, while major contribution to LWCRF change stems from high level cloud and to NetCRF changes from low level clouds.

Table 3: List of CMIP5 models used for CRF analysis

MODEL	**INSTITUTION**
BCC-CSM1.1	Beijing Climate Center, China Meteorological Administration, China
BNU-ESM	College of Global Change and Earth System Science, Beijing Normal University, China
CCSM4	National Center for Atmospheric Research, United States
CESM1-BGC	National Science Foundation, Department of Energy, National Center for Atmospheric Research, United States
CESM1-CAM5	
CSIRO-Mk3.6.0	Commonwealth Scientific and Industrial Research Organisation in collaboration with the Queensland Climate Change Centre of Excellence, Australia
GFDL-CM3	NOAA Geophysical Fluid Dynamics Laboratory, United States
GISS-E2-R	NASA Goddard Institute for Space Studies, United States
INM-CM4	Institute for Numerical Mathematics, Russia
IPSL-CM5A-MR	Institut Pierre-Simon Laplace, France
IPSL-CM5B-LR	
MIROC5	Atmosphere and Ocean Research Institute (The University of Tokyo), National Institute for Environmental Studies, and Japan Agency for Marine-Earth Science and Technology, Japan
MIROC-ESM	Japan Agency for Marine-Earth Science and Technology, Atmosphere and Ocean Research Institute (The University of Tokyo), and National Institute for Environmental Studies, Japan
MPI-ESM-MR	Max Planck Institute for Meteorology, Germany
MRI-CGCM3	Meteorological Research Institute, Japan
NorESM1-M	Norwegian Climate Centre, Norway

Figures

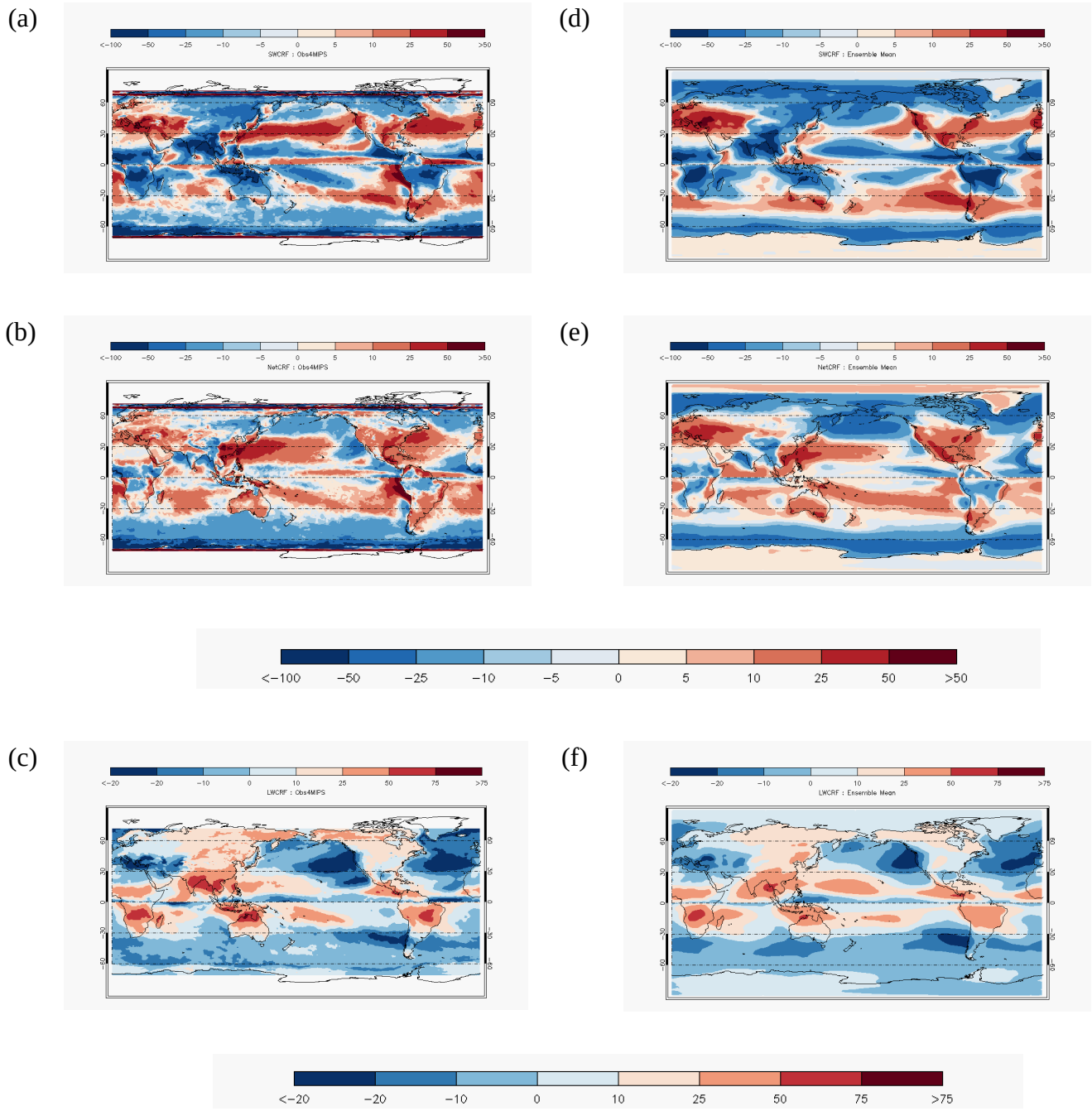

Figure 6.1 : Seasonal variation (JJA-DJF) of (a) SWCRF, (b) NetCRF, and (c) LWCRF from Obs4MIPS observations and (d) SWCRF, (e) NetCRF and (f) LWCRF from ensemble model mean over 16 CMIP5 models.

(a)

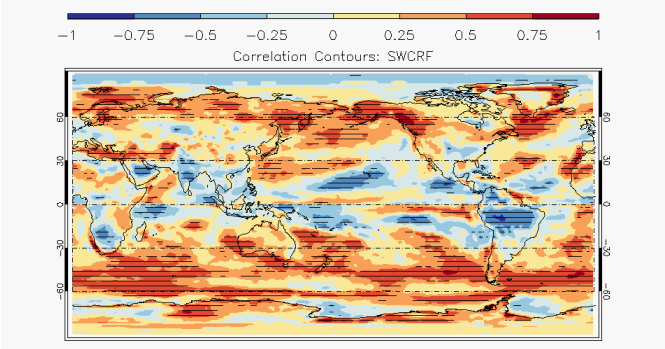

(b)

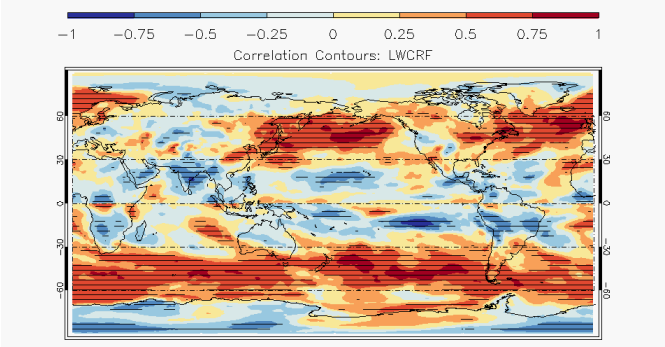

(c)

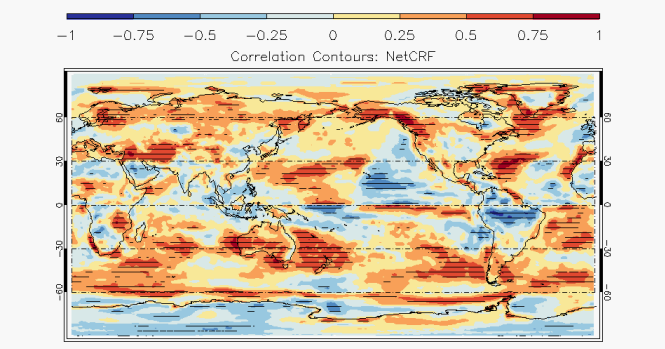

Figure 6.2 : Correlation maps constructed using the values of correlation coefficient, at each Lat-Lon grid point, between CMIP5 model spread in Seasonal (JJA-DJF) and Climatological Differences in (a) SWCRF, (b) LWCRF and (c) NetCRF). Hatched lines indicate regions of significant Correlation.

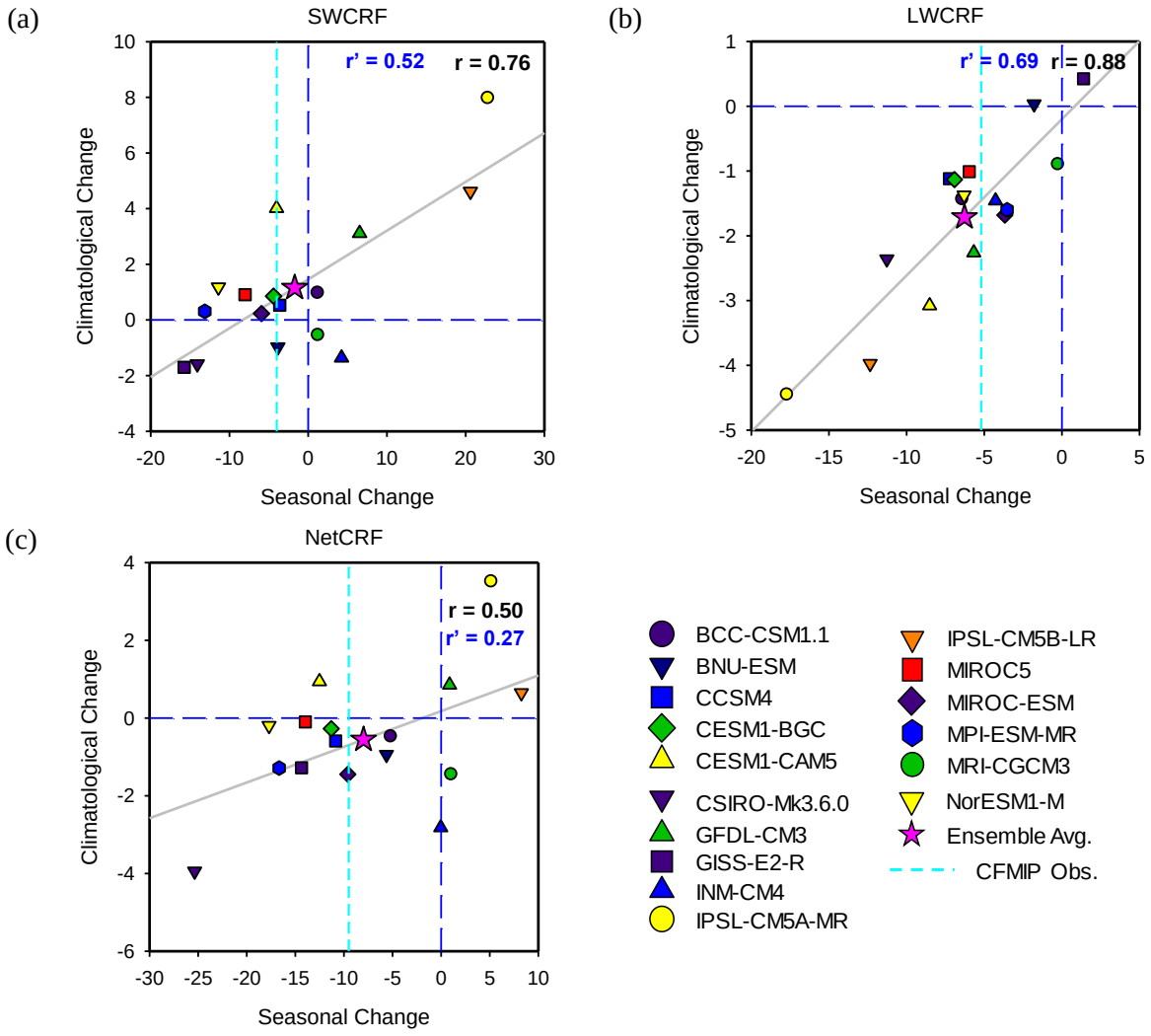

Figure 6.3 : Scatter plots showing the relationship between Seasonal change (x-axis) and Climatological difference (y-axis) in mid-latitudinal (a) SWCRF, (b) LWCRF and (c) NetCRF in 16 CMIP5 models (listed in the key). Grey solid line is the linear regression fit. Observed values of Seasonal changes in CRF are represented by cyan vertical lines. Correlation coefficient values (Black: Pearson; Blue: Spearman) are indicated at the top right corner of each figure. Zero x- and y-axes are included as blue dashed lines.

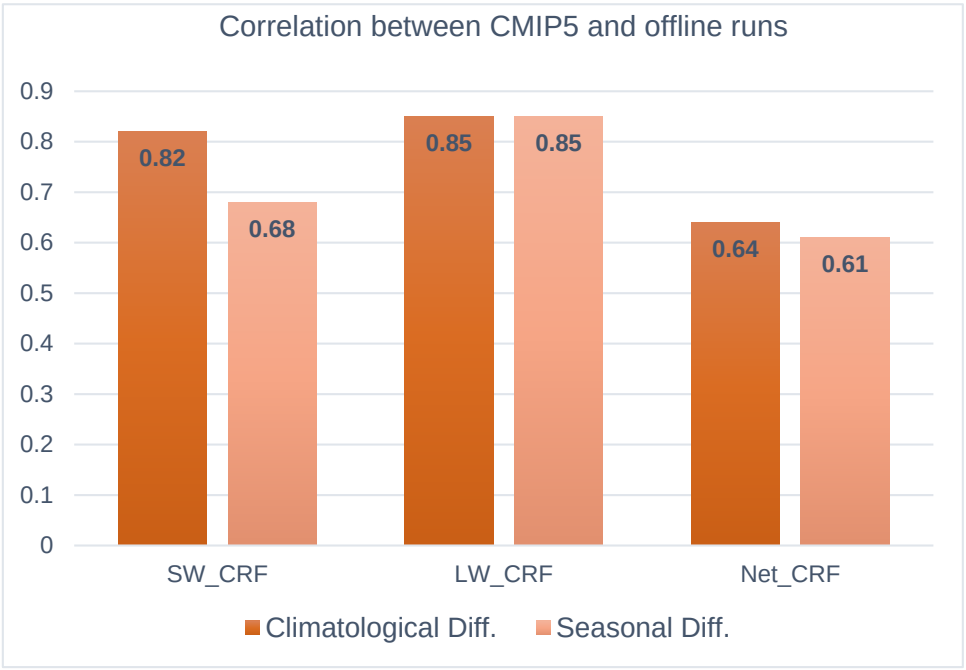

(a)

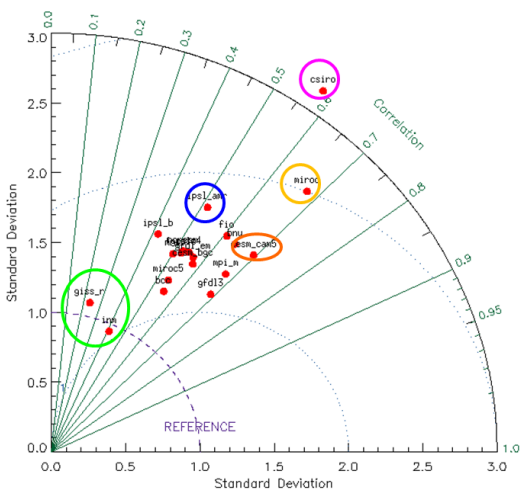

(b)

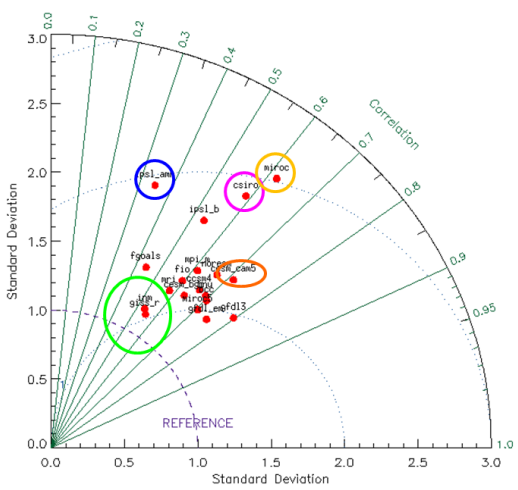

Figure 6.4 : (a) Summary of the correlations between CMIP5 output and prescribed CESM model run output Seasonal and Climatological differences in SWCRF, LWCRF and NetCRF. Taylor diagram (Taylor, 2000) exhibiting (a) CMIP5 and (b) prescribed CESM-run model spread in climatological projection of change in NetCRF with the ensemble mean values as Reference.

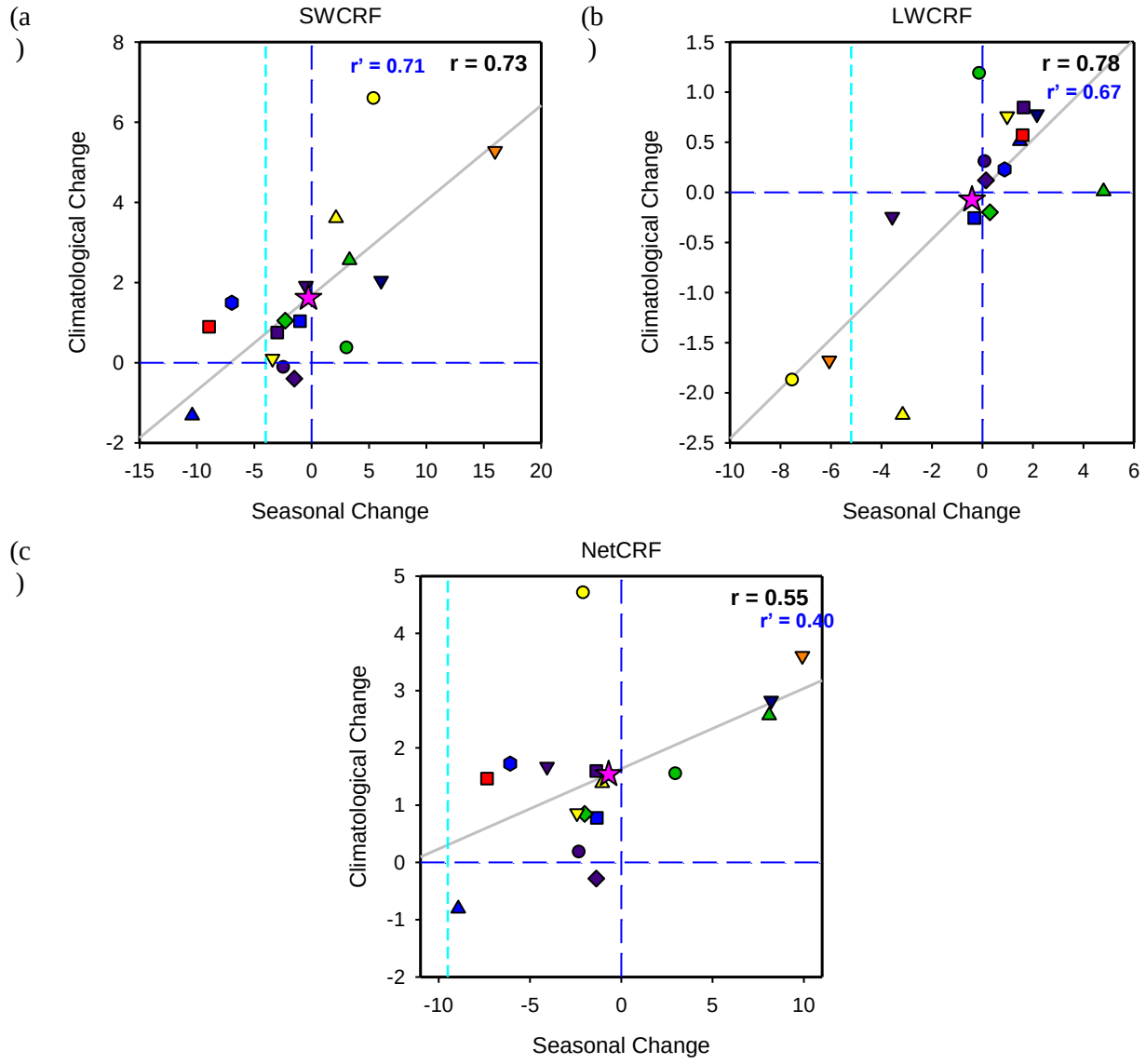

Figure 6.5 : Scatter plots showing the relationship between Seasonal change (x-axis) and Climatological difference (y-axis) in mid-latitudinal (a) SWCRF, (b) LWCRF and (c) NetCRF due to total column clouds in 16 CMIP5 models (key in Figure 6.3) from the prescribed CESM runs. Grey solid line is the linear regression fit. Observed values of Seasonal changes in CRF are represented by cyan vertical lines. Correlation coefficient values (Black: Pearson; Blue: Spearman) are noted at the top right corner of each figure. Zero x- and y-axes are included as blue dashed lines.

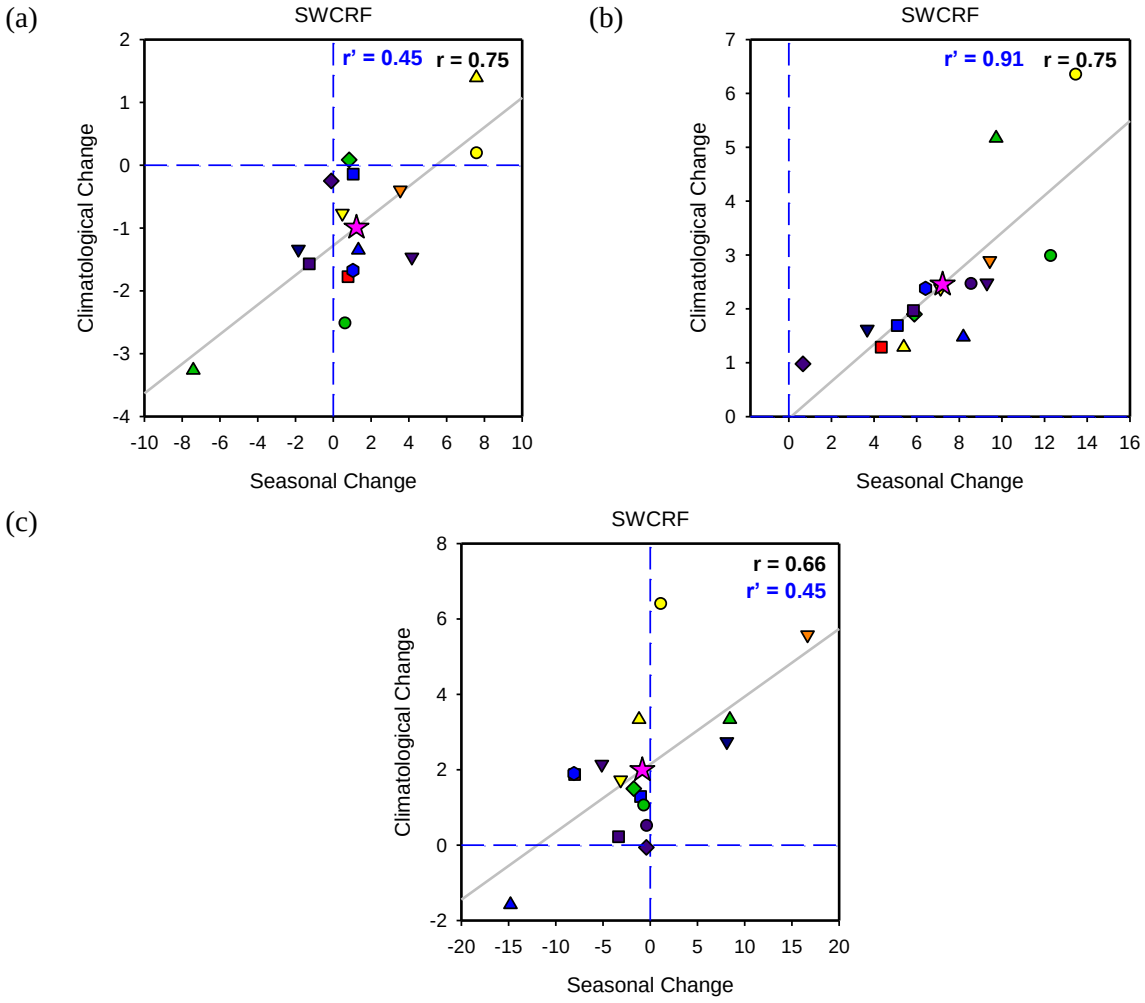

Figure 6.6 : Scatter plots showing the relationship between Seasonal change (x-axis) and Climatological difference (y-axis) in mid-latitudinal SWCRF due to clouds at (a) High- , (b) Mid- and (c) Low-levels in 16 CMIP5 models (key in Figure 6.3) from the prescribed CESM runs. Grey solid line is the linear regression fit. Correlation coefficient values (Black: Pearson; Blue: Spearman) are noted at the top right corner of each figure. Zero x- and y-axes are included as blue dashed lines.

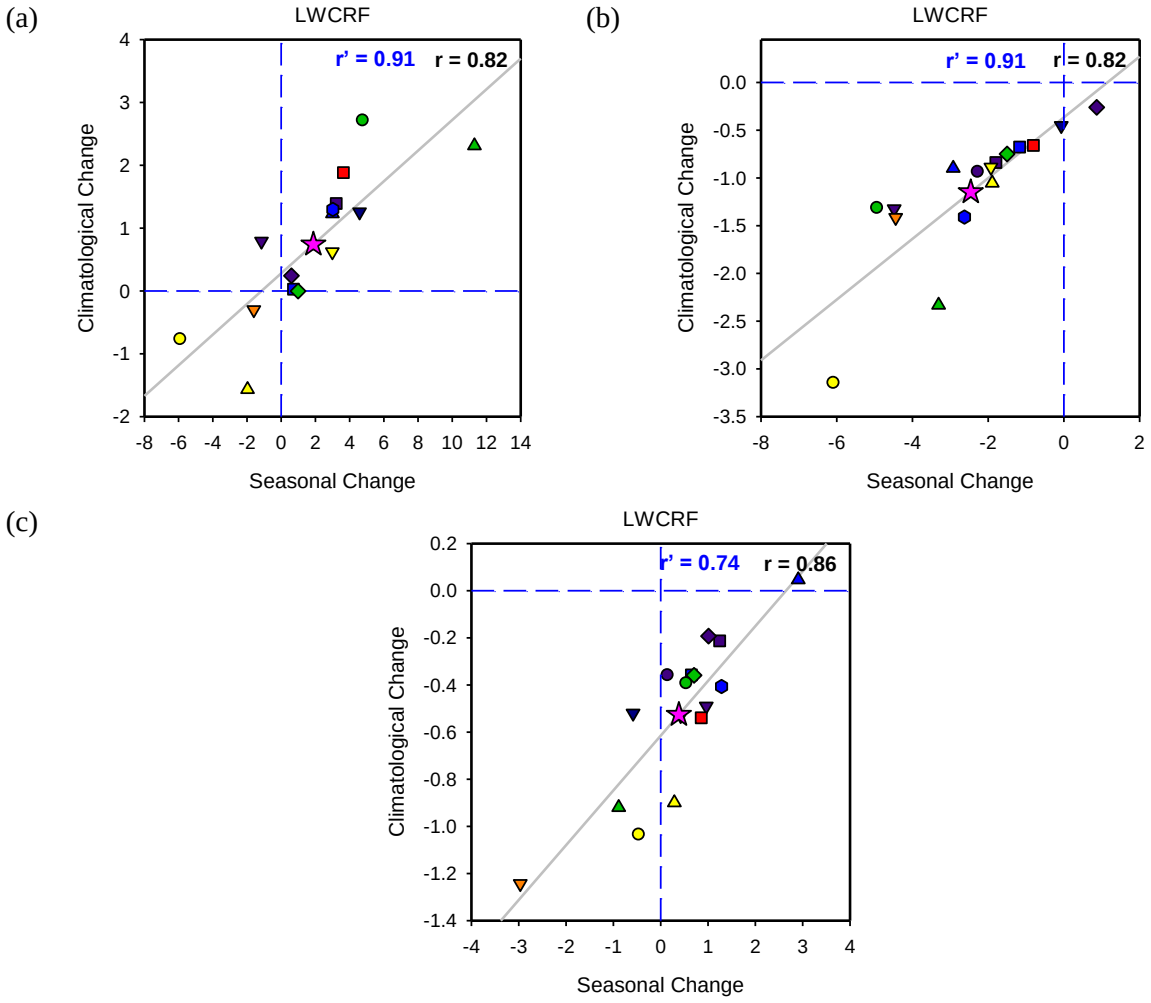

Figure 6.7 : Scatter plots showing the relationship between Seasonal change (x-axis) and Climatological difference (y-axis) in mid-latitudinal LWCRF due to clouds at (a) High- , (b) Mid- and (c) Low-levels in 16 CMIP5 models (key in Figure 6.3) from the prescribed CESM runs. Grey solid line is the linear regression fit. Correlation coefficient values (Black: Pearson; Blue: Spearman) are noted at the top right corner of each figure. Zero x- and y-axes are included as blue dashed lines.

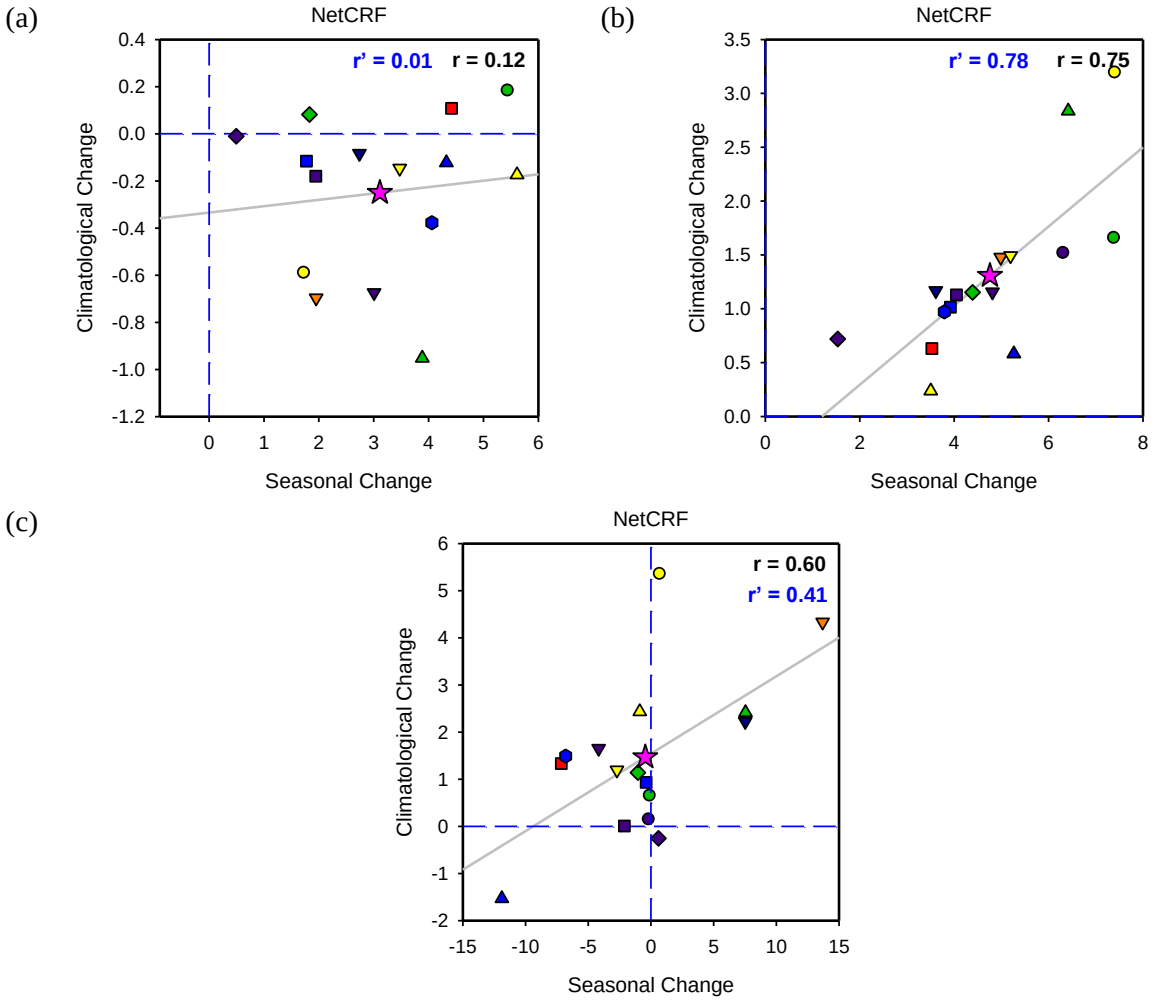

Figure 6.8 : Scatter plots showing the relationship between Seasonal change (x-axis) and Climatological difference (y-axis) in mid-latitudinal NetCRF due to clouds at (a) High- , (b) Mid- and (c) Low-levels in 16 CMIP5 models (key in Figure 6.3) from the prescribed CESM runs. Grey solid line is the linear regression fit. Correlation coefficient values (Black: Pearson; Blue: Spearman) are noted at the top right corner of each figure. Zero x- and y-axes are included as blue dashed lines.

Chapter 7

Conclusions and Future Work

7.1. Conclusions

This dissertation attempted to establish a relationship between short term climate variability in the present with its long term climate change analogue and utilize the presence of such a correlation to observationally constrain the future climate prediction in GCM's. By examining the pattern of changes in cloud fraction and cloud hydrometeors in various latitudinal belts both seasonally and inter-annually, and comparing them with their corresponding climatological evolution, various significant relationships emerged. Where available, observational data were used to determine model biases in simulation of short term variability in present day climate. Based on the present and future climate interrelationship, these biases were then used to confine the spread in model projections of future cloud changes to a smaller range.

A summary of the important conclusions from this study is presented below:

1. Seasonal changes in cloud fraction were compared with their long-term climatological changes using data from 25 CMIP5 models. Strong correlations were found to exist between the two in the mid-latitudinal belts. Co-variability between mean cloud fractions and their seasonal changes were also investigated and their relationship was found to be strong only in specific pressure levels. Splitting the total atmospheric column into low, mid and high level clouds enabled identification of low and mid cloud layers as regions of strong seasonal-climatological correlation. In the high cloud layers, disagreement in the sign of change in cloud fractions was likely responsible for weak correlations and warranted the need to partition the total atmospheric column into separate cloud reduction and cloud growth regions. This revealed that

the observed interrelationship was restricted to the cloud decrease regions only. A comparison of model mean cloud amount and their seasonal variability with satellite observations revealed an under prediction of model mean clouds and an over prediction of their seasonal reduction. Based on the strong correlation between the two phenomenon, it was concluded that the seasonal cloud reduction overestimation translated into an over prediction of mid-latitudinal model cloud reduction in the future climate scenario. Independent analyses of SH and NH indicated that most of the overestimation in cloud reduction originated in SH with a large spread in magnitude of simulated decrease among models.

2. The seasonal and climatological changes in mid-latitudinal cloud hydrometeors were also examined for the presence of correlations using cloud ice and cloud liquid content data from CMIP5 models.

   For the total column ice, correlations were seen in case of mean cloud ice amount and their seasonal variations but between seasonal and climatological changes the relationship appeared to be weak. This was due to the reversal in sign of change in the upper atmosphere which necessitated a division of the atmospheric column into separate regions based on cloud ice increase or decrease. Significant correlations were observed between mean and seasonal changes as well as seasonal and climatological changes in cloud ice both in the reduction as well as growth regions. Using C3M observations of cloud ice it was found that although the ensemble model mean prognosis od cloud ice reduction compared well with observation in most cases, models themselves forecast a large range of values. This implied that model mean projections of long term reduction in cloud ice content were reasonable in spite of the large spread about the mean. In the cloud ice increase regions, models exhibited overestimation of ice increase which gets transmitted to their projected long term changes.

   Unlike cloud ice, mean cloud liquid content did not correlate well with their seasonal changes. However, their seasonal-climatological change correlations were quite strong for the total column as well as low-, mid- and high-cloud levels. Compared to observation, model estimations of cloud liquid water were found to be largely overestimated as were their seasonal changes. Separation into cloud liquid reduction and growth regimes revealed an over-sensitivity in models in terms of simulating both larger reduction and larger increase in contrast

with observed changes. It was concluded based on the findings that climate models projected larger cloud hydrometeor changes, both decrease at lower levels and increase at higher levels in a warmer climate. The presence of a narrow band of cloud increase near the surface, undetected in satellite observations, was found to compensate for large cloud reduction in the layers above when combined together.

3. Mean tropical surface temperature values were used to select a set of warm and cold years and the variations in cloud amount and cloud hydrometeors between them and their climatological counterparts were examined in the tropical belt. Patterns of co-variability between inter-annual and long term climate change were established using CMIP5 model simulations. Particularly high correlations were detected among clouds in three different vertical layers: high (above 400hPa), mid (between 850-600 hPa) and near surface (below 925hPa). Seasonal reduction of cloud fraction in middle and higher levels translated to projected cloud decrease in these layers climatologically. Cloud hydrometeors on the other hand showed increases in upper layer and reduction below. Two dimensional latitude-longitude correlation maps between inter-annual and climatological changes in cloud fraction were constructed for total column clouds. Using ISCCP total cloud observational changes, model biases in cloud changes were evaluated in regions of high correlation. This revealed an under prediction of cloud changes in the tropics by the model mean in regions of deep convective clouds. In regions of low cloud population, the model mean was found to agree with observations although models themselves showed a range of cloud changes. Based on the interrelationship between the short term variability with the long term changes in cloud fraction, these biases carry over to the future projection of cloud changes in the tropical belt.

4. Cloud Radiative Forcing in the mid-latitudinal belt were also examined for presence of interrelationship between their seasonal and climatological variability. Strong relationship was exhibited by the changes in SWCRF and LWCRF which were used to constrain model spread in their climatological projections. Using radiative flux observations from Obs4MIPS, long term increases of about 1.0 W/m2 in SWCRF, thus constituting a positive cloud feedback, and decreases in LWCRF of 1.5 W/m2, constituting negative cloud feedback were established. The projected NetCRF was also found to be increasing climatologically.

Offline radiation runs of CESM model were also used to separate the radiative effects of low, mid and high level clouds and determine the source of the spread in model simulations of change in CRF. They revealed that the low and mid-level clouds primarily contributed to the SWCRF increase and LWCRF decrease in the long term. High-level cloud radiative response was found to be opposite to that in the lower levels and in general contributed less to the total column responses. Combination of opposite signs of LWCRF and SWCRF changes likely contributed to the large spread in NetCRF in low clouds which gets translated onto their projected changes as well.

5. Based on the analysis of seasonal and climatological variability in cloud fraction, cloud hydrometeors and CRF in the mid-latitudinal belt the following unified message emerges: Seasonally, clouds show a reduction in the lower and mid-levels which is strongly correlated with similar reductions seen in long term cloud changes. However, models tend to overestimate the magnitude of this reduction. The ice and liquid content in these lower clouds also show a similar decrease accompanied by increasing ice and liquid in upper clouds. Models show a tendency to over predict both the increase in ice and liquid and the decrease in water content in the respective levels. These cloud changes find reflection in the pattern of mid-latitudinal CRF changes generated using offline runs. Complementary to the reduction in cloud amount and cloud hydrometeors in the lower and mid-levels of the atmosphere, seasonal and climatological increase in SWCRF (a positive cloud feedback) and decrease in LWCRF (a negative feedback) are observed. The over prediction of cloud changes carries over to the radiative response of the models with most of them predicting larger SWCRF increases and LWCRF decreases. Further, the over prediction as well as model spread in values are found to originate from the SH mid-latitudinal belt.

It is within the span of last few years that the idea of Emergent Constraint has gained momentum very rapidly. Many of the reported studies on Emergent constraints have demonstrated a direct statistical relationship between ECS and some present day base climate mean value or some form of its short term variability. However, as has been argued by many (Fasullo et al., 2015; Klein and Hall, 2015), a quantity like ECS has multiple independent factors that influence it, like the different feedbacks and forcing. Each of these contributing factors have their own model spread

which makes it challenging to establish a robust relationship. Compensating errors in different feedbacks could lead to the identification of certain groups of models to be better predictors of long term climate changes when they may not be truly realistic. Thus, it is more appropriate to restrict emergent constraint relationships to individual processes or specific feedback contributors. Therefore, in this study only the relationship between seasonal changes in cloud amount, cloud hydrometeor content and their radiative effects with their respective long term transformations have been investigated. Correlating these with climate sensitivity may be attempted in the future with the objective of only constraining the part of sensitivity that is contributed by cloud feedbacks.

The strong relationship demonstrated by seasonal and climatological variability in mid-latitudinal cloud properties likely has its physical basis in the poleward migration of mid-latitude storm track regions with warming. Signatures of storm track broadening and shifting towards the equator in colder seasons had already been noticed in the past (Trenberth, 1991). Similar trends of poleward migration of storm track in the long term due to climate warming was also seen in GCM simulations (Yin, 2005). Although models continued to exhibit a change in storm track activity due to climate change, observational basis to this was only found recently (Bender et al., 2012) by analyzing changes in ISCCP cloud amount between 1983 and 2008, representing a period of increasing greenhouse warming. This shift in mid-latitudinal storm track activity may be linked with the reduction in cloud amount in the 30˚ - 60˚ latitudinal belt as seen in this study. Cloud feedback from the storm track regions affect global cloud feedbacks independent of the contribution from tropical cloud changes and can still be considered to impact the global climate sensitivity independently thus emerging as a useful constraint for model projections.

7.2. Future work

The analysis and experiments carried out as a part of this dissertation have managed to address some of the key questions that are part of the larger challenge of constraining future climate projections by GCMs. Two issues that are relevant to this research and require prompt consideration will be pursued next. These are briefly described below:

1. Developing better observational constraints in the tropical belt: A different representation of short term variability in tropics using a spatial regime change will be pursued. In this method, difference in cloud variables would be computed between bins of warm and cold SST grid points to represent progression into a warmer climate. This approach makes it suitable to use 3-Dimensional C3M satellite dataset for observational constraining. Adapting Bony et al.'s (Bony et al., 2004) approach of separating the dynamical and thermo-dynamical contribution to change in cloud patterns, grid points in tropical belt could also be separated into different vertical velocity clusters. Some preliminary analysis along these directions gave encouraging results shown in Figure 7.1. Focusing on the tropical belt between 20°N to 20°S latitudes, for each CMIP5 model, the surface temperature at each grid point within that belt was averaged. Next the grid points were binned on the basis of their temperature values into different boxes. Further, for each surface temperature bin the grid boxes were further distributed into various omega bins. Following this process of two dimensional binning a segregation of hot and cold grid areas for different dynamical regimes were obtained. Based on the cloud type, grid points belonging to the relevant omega ranges could be selected and the cloud difference between clusters of warm and cold points used for correlation studies with climatological change. In Figure 7.1 the relevant plots from initial analysis of high level clouds is presented. Omega value in the 850-500hPa pressure band and the surface temperature are used to obtain the cloud distribution shown in Figure 7.1(a) and (b) for ensemble model mean and observation respectively. Model values of climatological change in high level cloud fraction are then correlated with the difference in cloud values in temperature bins 290-295K and 295-300K for omega range -50 to -30 hPa/day. The correlation scatter plot is shown in Figure 7.1(c).

2. Locating and understanding the regional contributions to model spread in cloud radiative response: Using the correlation contour plot in Figure 7.2, where each grid point represents the correlation between model spread in global CRF projections and model spread in CRF climate projections at that grid point, the regions contributing most to the observed model spread in predicting long term CRF changes can be isolated. An independent study in these isolated regions has been planned to better understand the processes that lead to model disagreement. EOF analysis to determine common patterns of variance of CRF has also been outlined with the aim of getting more insight into inter model differences. An example of the results from

the early phases of this study is shown in Figure 7.3. Here, the first EOF mode of Net CRF variance among the models is shown this figure. Along with identifying the regions of maximum inter model variability, it also exhibits signs of opposite patterns of change in the lower and higher latitudes.

Apart from these specific projects, the future plans also include using model simulations to carry out sensitivity studies. By changing model parameterizations and running them to produce long term simulations, the seasonal and climatological correlations found to exist in this study may be evaluated further. Eventually, the overarching goal of this study would be to relate the observed mean cloud and seasonal variabilities with cloud feedback in models. Efforts to relating that with long term cloud and radiative feedback changes would greatly benefit the entire climate science community in their endeavor to unite model estimations of climate sensitivity.

Figures

(a)

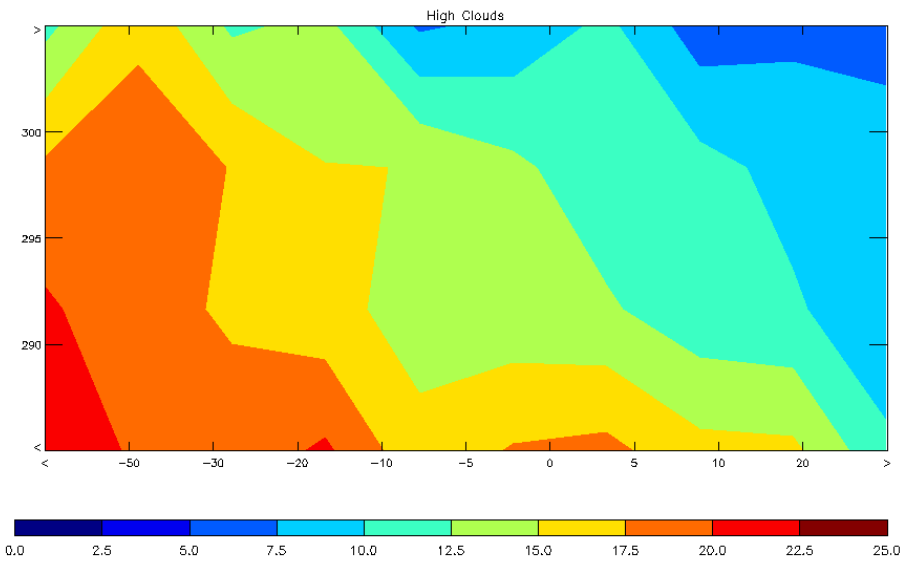

(b)

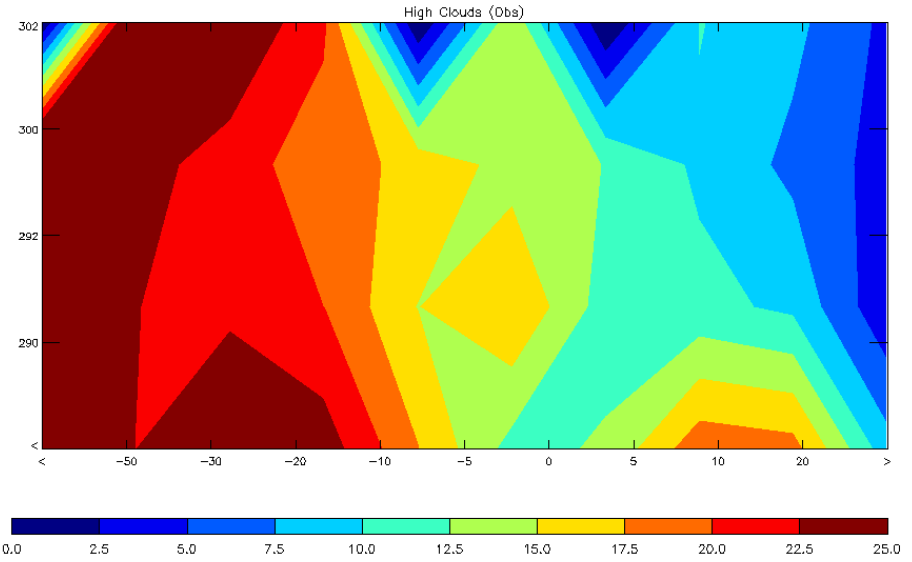

Figure 7.1 : Distribution of high Cloud fraction as a function of surface tempertaure (y-axis) and vertical velocity in the 850-500 hPa pressure level (x-axis) in the (a) ensemble model mean of CMIP5 models and (b) C3M observations.

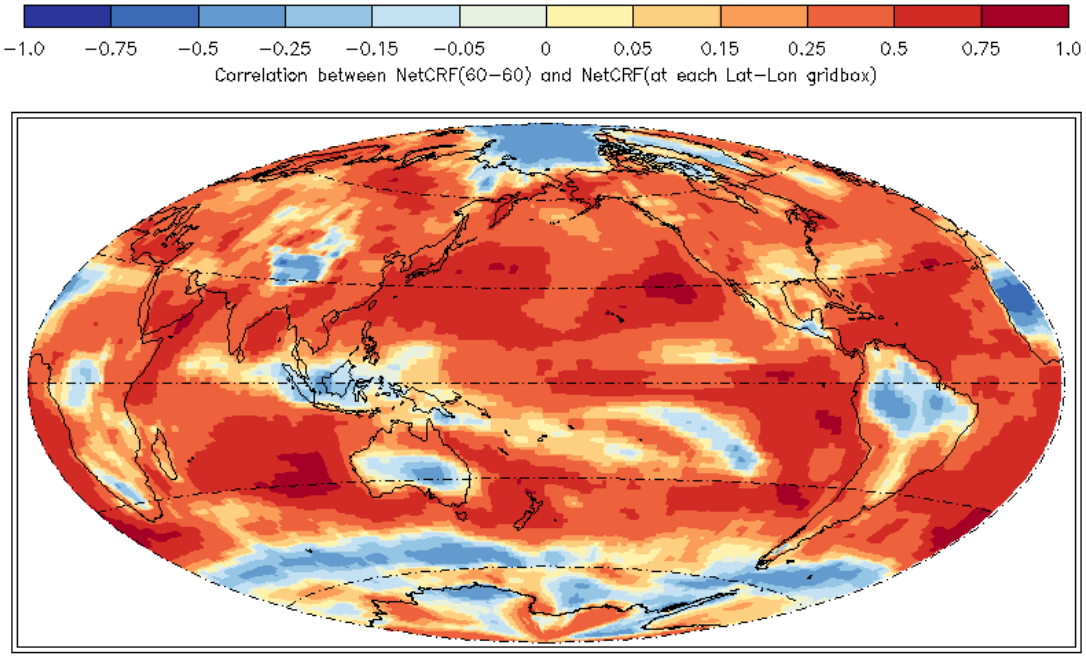

Figure 7.2 : Correlation map showing the contribution of model spread at each lat-lon grid point to the total model spread in NetCRF between 60^{o}N - 60^{o}S latitudes.

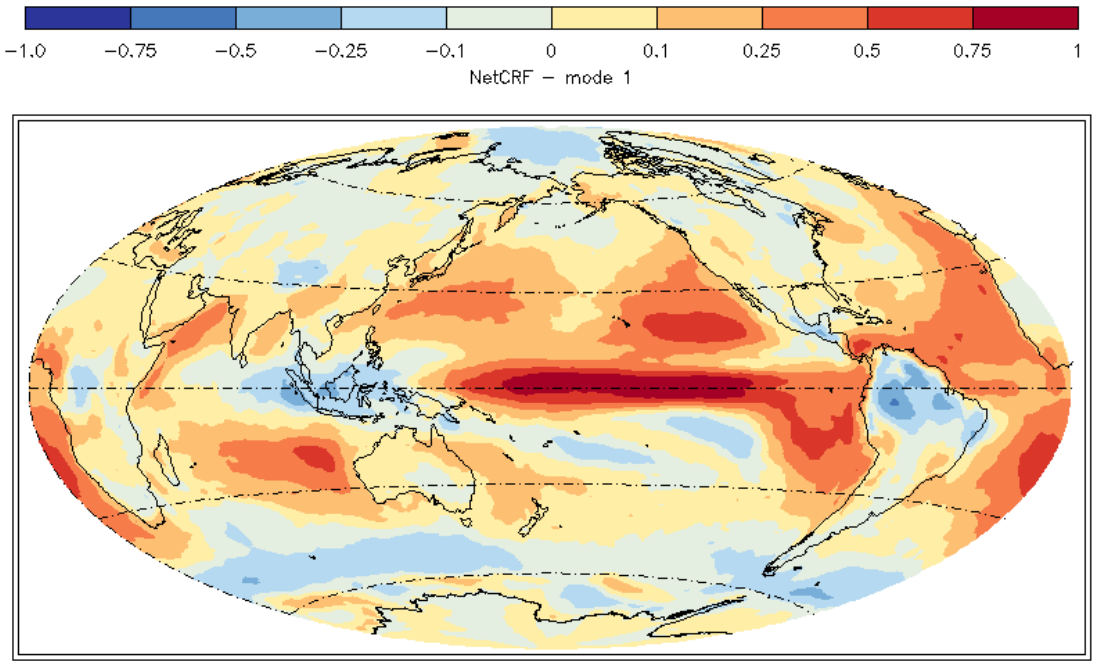

Figure 7.3 : Correlation map showing the contribution of model spread at each lat-lon grid point to the total model spread in NetCRF between 60^{o}N - 60^{o}S latitudes.

References

Andrews, T., J. M. Gregory, M. J. Webb and K. E. Taylor (2012). "Forcing, feedbacks and climate sensitivity in CMIP5 coupled atmosphere-ocean climate models." Geophysical Research Letters 39.

Bender, F.-M., V. Ramanathan and G. Tselioudis (2012). "Changes in extratropical storm track cloudiness 1983–2008: observational support for a poleward shift." Climate Dynamics 38(9-10): 2037-2053.

Boe, J., A. Hall and X. Qu (2009). "September sea-ice cover in the Arctic Ocean projected to vanish by 2100." Nature Geosci 2(5): 341-343.

Bony, S., R. Colman, V. M. Kattsov, R. P. Allan, C. S. Bretherton, J.-L. Dufresne, A. Hall, S. Hallegatte, M. M. Holland, W. Ingram, D. A. Randall, B. J. Soden, G. Tselioudis and M. J. Webb (2006). "How Well Do We Understand and Evaluate Climate Change Feedback Processes?" Journal of Climate 19(15): 3445-3482.

Bony, S. and J.-L. Dufresne (2005). "Marine boundary layer clouds at the heart of tropical cloud feedback uncertainties in climate models." Geophysical Research Letters 32(20): L20806.

Bony, S., J.-L. Dufresne, H. Le Treut, J.-J. Morcrette and C. Senior (2004). "On dynamic and thermodynamic components of cloud changes." Climate Dynamics 22(2-3): 71-86.

Bracegirdle, T. and D. Stephenson (2012). "Higher precision estimates of regional polar warming by ensemble regression of climate model projections." Climate Dynamics 39(12): 2805-2821.

Bracegirdle, T. J., D. B. Stephenson, J. Turner and T. Phillips (2015). "The importance of sea-ice area biases in 21st century multi-model projections of Antarctic temperature and precipitation." Geophysical Research Letters

Caldwell, P. M., C. S. Bretherton, M. D. Zelinka, S. A. Klein, B. D. Santer and B. M. Sanderson (2014). "Statistical significance of climate sensitivity predictors obtained by data mining." Geophysical Research Letters 41(5): 1803-1808.

Cesana, G. and H. Chepfer (2013). "Evaluation of the cloud thermodynamic phase in a climate model using CALIPSO-GOCCP." Journal of Geophysical Research: Atmospheres 118(14): 7922-7937.

Cess, R., M. Zhang, G. Potter, V. Alekseev, H. Barker, S. Bony, R. Colman, D. Dazlich, A. DelGenio and M. Deque (1997). "Comparison of the seasonal change in cloud-radiative forcing from atmospheric general circulation models and satellite observations." Journal of Geophysical Research-Atmospheres 102: 16593-16603.

Cess, R. D., G. L. Potter, J. P. Blanchet, G. J. Boer, A. D. Delgenio, M. Deque, V. Dymnikov, V. Galin, W. L. Gates, S. J. Ghan, J. T. Kiehl, A. A. Lacis, H. Letreut, Z. X. Li, X. Z. Liang, B. J. Mcavaney, V. P. Meleshko, J. F. B. Mitchell, J. J. Morcrette, D. A. Randall, L. Rikus, E. Roeckner, J. F. Royer, U. Schlese, D. A. Sheinin, A. Slingo, A. P. Sokolov, K. E. Taylor, W. M. Washington, R. T. Wetherald, I. Yagai and M. H. Zhang (1990). "Intercomparison and Interpretation of Climate Feedback Processes in 19 Atmospheric General-Circulation Models." Journal of Geophysical Research-Atmospheres 95(D10): 16601-16615.

CESS, R. D., G. L. POTTER, J. P. BLANCHET, G. J. BOER, S. J. GHAN, J. T. KIEHL, H. LE TREUT, Z.-X. LI, X.-Z. LIANG, J. F. B. MITCHELL, J.-J. MORCRETTE, D. A. RANDALL, M. R. RICHES, E. ROECKNER, U. SCHLESE, A. SLINGO, K. E. TAYLOR, W. M. WASHINGTON, R. T. WETHERALD and I. YAGAI (1989). "Interpretation of Cloud-Climate Feedback as Produced by 14 Atmospheric General Circulation Models." Science 245(4917): 513-516.

Cox, P. M., D. Pearson, B. B. Booth, P. Friedlingstein, C. Huntingford, C. D. Jones and C. M. Luke (2013). "Sensitivity of tropical carbon to climate change constrained by carbon dioxide variability." Nature 494(7437): 341-344.

Dessler, A. E. (2010). "A Determination of the Cloud Feedback from Climate Variations over the Past Decade." Science 330(6010): 1523-1527.

Dufresne, J.-L. and S. Bony (2008). "An Assessment of the Primary Sources of Spread of Global Warming Estimates from Coupled Atmosphere–Ocean Models." Journal of Climate 21(19): 5135-5144.

Fasullo, J. T., B. M. Sanderson and K. E. Trenberth (2015). "Recent Progress in Constraining Climate Sensitivity With Model Ensembles." Current Climate Change Reports 1(4): 268-275.

Fasullo, J. T. and K. E. Trenberth (2012). "A Less Cloudy Future: The Role of Subtropical Subsidence in Climate Sensitivity." Science 338(6108): 792-794.

Flato, G., J. Marotzke, B. Abiodun, P. Braconnot, S. C. Chou, W. Collins, P. Cox, F. Driouech, S. Emori, V. Eyring, C. Forest, P. Gleckler, E. Guilyardi, C. Jakob, V. Kattsov, C. Reason and M. Rummukainen (2013). Evaluation of Climate Models. Climate Change 2013: The Physical Science Basis. Contribution of Working Group I to the Fifth Assessment Report of the Intergovernmental Panel on Climate Change. T. F. Stocker, D. Qin, G.-K. Plattner et al. Cambridge, United Kingdom and New York, NY, USA, Cambridge University Press.

Hall, A. and X. Qu (2006). "Using the current seasonal cycle to constrain snow albedo feedback in future climate change." Geophysical Research Letters 33(3): L03502.

Huber, M., I. Mahlstein, M. Wild, J. Fasullo and R. Knutti (2010). "Constraints on Climate Sensitivity from Radiation Patterns in Climate Models." Journal of Climate 24(4): 1034-1052.

Klein, S. and A. Hall (2015). "Emergent Constraints for Cloud Feedbacks." Current Climate Change Reports 1(4): 276-287.

Knutti, R., G. A. Meehl, M. R. Allen and D. A. Stainforth (2006). "Constraining Climate Sensitivity from the Seasonal Cycle in Surface Temperature." Journal of Climate 19(17): 4224-4233.

Le Treut, H., R. Somerville, U. Cubasch, Y. Ding, C. Mauritzen, A. Mokssit, T. Peterson and M. Prather (2007). Historical Overview of Climate Change. Climate Change 2007: The Physical Science Basis. Contribution of Working Group I to the Fourth Assessment Report of the Intergovernmental Panel on Climate Change. S. Solomon, D. Qin, M. Manning et al. Cambridge, United Kingdom and New York, NY, USA, Cambridge University Press.

Neale, R. B., C.-C. Chen, A. Gettelman, P. H. Lauritzen, S. Park, D. L. Williamson, A. J. Conley, R. Garcia, D. Kinnison, J.-F. Lamarque, D. Marsh, M. Mills, A. K. Smith, S. Tilmes, F. Vitt, H. Morrison, P. Cameron-Smith, W. D. Collins, M. J. Lacono, R. C. Easter, X. Liu, S. G. Ghan, P. J. Rasch and M. A. Taylor (November 2012). Description of the NCAR Community Atmosphere Model (CAM 5.0). NCAR Technical Note

O 'Gorman, P. A. (2012). "Sensitivity of tropical precipitation extremes to climate change." Nature Geosci 5(10): 697-700.

Ramanathan, V., R. D. Cess, E. F. Harrison, P. Minnis, B. R. Barkstrom, E. Ahmad and D. Hartmann (1989). "Cloud-Radiative Forcing and Climate: Results from the Earth Radiation Budget Experiment." Science 243(4887): 57-63.

Randall, D. A., R. A. Wood, S. Bony, R. Colman, T. Fichefet, J. Fyfe, V. Kattsov, A. Pitman, J. Shukla, J. Srinivasan, R. J. Stouffer, A. Sumi and K. E. Taylor (2007). Cilmate Models and Their Evaluation. Climate Change 2007: The Physical Science Basis. Contribution of Working Group I to the Fourth Assessment Report of the Intergovernmental Panel on Climate Change. S. Solomon, D. Qin, M. Manning et al. Cambridge, United Kingdom and New York, USA, Cambridge University Press.

Schmidt, G. A., J. D. Annan, P. J. Bartlein, B. I. Cook, E. Guilyardi, J. C. Hargreaves, S. P. Harrison, M. Kageyama, A. N. LeGrande, B. Konecky, S. Lovejoy, M. E. Mann, V. Masson-Delmotte, C. Risi, D. Thompson, A. Timmermann, L. B. Tremblay and P. Yiou (2013). "Using paleo-climate comparisons to constrain future projections in CMIP5." Clim. Past Discuss. 9(1): 775-835.

Shell, K. M. (2012). "Constraining Cloud Feedbacks." Science 338(6108): 755-756.

Sherwood, S. C., S. Bony and J.-L. Dufresne (2014). "Spread in model climate sensitivity traced to atmospheric convective mixing." Nature 505(7481): 37-42.

Soden, B. J. and I. M. Held (2006). "An Assessment of Climate Feedbacks in Coupled Ocean–Atmosphere Models." Journal of Climate 19(14): 3354-3360.

Stevens, B. and S. Bony (2013). "What Are Climate Models Missing?" Science 340(6136): 1053-1054.

Su, H., J. H. Jiang, C. Zhai, T. J. Shen, J. D. Neelin, G. L. Stephens and Y. L. Yung (2014). "Weakening and strengthening structures in the Hadley Circulation change under global warming and implications for cloud response and climate sensitivity." Journal of Geophysical Research: Atmospheres 119(10): 2014JD021642.

Taylor, K. E. (2000). Summarizing multiple aspects of model performance in a single diagram, Program for Climate Model Diagnosis and Intercomparison, Lawrence Livermore National Laboratory, University of California.

Tian, B. (2015). "Spread of model climate sensitivity linked to double-Intertropical Convergence Zone bias." Geophysical Research Letters 42(10): 4133-4141.

Tomassini, L., A. Voigt and B. Stevens (2014). "On the connection between tropical circulation, convective mixing, and climate sensitivity." Quarterly Journal of the Royal Meteorological Society

Trenberth, K. E. (1991). "Storm Tracks in the Southern Hemisphere." Journal of the Atmospheric Sciences 48(19): 2159-2178.

Tsushima, Y., M. Ringer, T. Koshiro, H. Kawai, R. Roehrig, J. Cole, M. Watanabe, T. Yokohata, A. Bodas-Salcedo, K. Williams and M. Webb (2015). "Robustness, uncertainties, and emergent constraints in the radiative responses of stratocumulus cloud regimes to future warming." Climate Dynamics: 1-15.

Volodin, E. M. (2008). "Relation between temperature sensitivity to doubled carbon dioxide and the distribution of clouds in current climate models." Izvestiya, Atmospheric and Oceanic Physics 44(3): 288-299.

Webb, M. J., C. A. Senior, D. M. H. Sexton, W. J. Ingram, K. D. Williams, M. A. Ringer, B. J. McAvaney, R. Colman, B. J. Soden, R. Gudgel, T. Knutson, S. Emori, T. Ogura, Y. Tsushima, N. Andronova, B. Li, I. Musat, S. Bony and K. E. Taylor (2006). "On the contribution of local feedback mechanisms to the range of climate sensitivity in two GCM ensembles." Climate Dynamics 27(1): 17-38.

Wenzel, S., P. M. Cox, V. Eyring and P. Friedlingstein (2014). "Emergent constraints on climate-carbon cycle feedbacks in the CMIP5 Earth system models." Journal of Geophysical Research: Biogeosciences 119(5): 2013JG002591.

Yin, J. H. (2005). "A consistent poleward shift of the storm tracks in simulations of 21st century climate." Geophysical Research Letters 32(18)

Zelinka, M. D., S. A. Klein and D. L. Hartmann (2011). "Computing and Partitioning Cloud Feedbacks Using Cloud Property Histograms. Part II: Attribution to Changes in Cloud Amount, Altitude, and Optical Depth." Journal of Climate 25(11): 3736-3754.

Zhai, C., J. H. Jiang and H. Su (2015). "Long-term cloud change imprinted in seasonal cloud variation: More evidence of high climate sensitivity." Geophysical Research Letters 42(20): 8729-8737.

Zhang, M. H., W. Y. Lin, S. A. Klein, J. T. Bacmeister, S. Bony, R. T. Cederwall, A. D. Del Genio, J. J. Hack, N. G. Loeb, U. Lohmann, P. Minnis, I. Musat, R. Pincus, P. Stier, M. J. Suarez, M. J. Webb, J. B. Wu, S. C. Xie, M. S. Yao and J. H. Zhang (2005). "Comparing clouds and their seasonal variations in 10 atmospheric general circulation models with satellite measurements." Journal of Geophysical Research: Atmospheres 110(D15)